Role of Endothelial Cell CD36 in Atherosclerosis and Fatty Acid Metabolism

by

Umar Rauf Rekhi

A thesis submitted in partial fulfillment of the requirements for the degree of

Doctor of Philosophy

Medical Sciences – Periodontology
University of Alberta

Abstract

Background and Objective

High-fat Western diets have been linked to the dysregulation of fatty acids (FA) and glucose intake in tissues, resulting in adverse metabolic outcomes such as obesity, insulin resistance, and atherosclerosis. There is a pressing need for new therapeutic approaches to address the challenges posed by this epidemic. This research focuses on the regulation of FA entry into tissues at the endothelial cell (EC) interface, an area that has been understudied but holds potential for identifying novel therapeutic targets. The dysfunctional endothelium, characterized by activation, pro-inflammatory nature, and pro-thrombotic properties, plays a critical role in initiating atherosclerosis and is linked to thrombotic events, myocardial infarction, stroke, and insulin resistance. Dyslipidemia from high-fat diets (HFDs) is a major contributor to endothelial dysfunction. CD36, acting as a receptor for pathological ligands from HFDs and participating in FA uptake, is hypothesized to contribute to EC dysfunction. The primary objective of this study is to investigate the role of EC CD36 in the metabolic changes associated with HFDs. Specifically, the study aims to understand how EC CD36 contributes to fatty acid uptake, systemic metabolism, and the development of atherosclerosis.

Hypothesis

We hypothesize that CD36 is a major EC receptor of FAs and proinflammatory atherogenic ligands, and that loss of EC CD36 will result in a metabolic phenotype and differences in atherosclerosis that correlate with changes in inflammation and FA uptake.

Materials and Methods

We generated EC CD36 knockout (EC CD36 KO) mice using cre-lox technology and a specific cre-promoter (Tie2e cre) that spares CD36 in hematopoietic cells. These mice were fed various diets and crossed with low-density lipoprotein receptor knockout (LDLR KO) mice for evaluating atherosclerosis. EC CD36 KO/LDLR KO and fl/fl CD36/LDLR KO control mice, aged six to eight weeks, were fed a high-fat, high-cholesterol diet for 3, 6, and 16 weeks for atherosclerosis assessments, with separate cohorts of male and female mice examined at each time point. Measurements of fasting glucose and weights were taken before euthanasia; at 3 and 6 weeks. Plasma samples were analyzed for 3-nitrotyrosine (3-NT), triglycerides (TG), total and free cholesterol levels, glucose tolerance test (GTT), and fast protein liquid chromatography (FPLC). At 16 weeks, aorta morphometry was performed on isolated aortas. To investigate the impact of EC CD36 loss on metabolism, four-week-old fl/fl CD36 and EC CD36 KO mice were monitored in metabolic cages after being fed a normal chow (NC) diet. The Comprehensive Laboratory Animal Monitoring System (CLAMS) was employed for indirect calorimetry. After 4 weeks, fasting glucose and weights were measured before euthanasia. Plasma was isolated for untargeted metabolomics by chemical isotope labeling liquid chromatography mass spectrometry, and blood was subjected to flow cytometry. Additionally, we explored the effect of EC CD36 loss in a diabetogenic scenario, with mice fed ingredient-matched diets containing 10% and 45% fat for 12 weeks. GTT was performed at the 8-week time point, and after 12 weeks, mice were sacrificed, and blood was drawn for plasma extraction to conduct TG, cholesterol assays, and FPLC.

Results

The results indicate that EC CD36 KO and EC CD36 KO/LDLR KO mice exhibit metabolic changes, suggesting an uncompensated role for EC CD36 in FA uptake. Notably, the

mice lacking EC CD36 expression showed increased glucose clearance across various diets. Male EC CD36 KO mice displayed increased carbohydrate utilization and decreased energy expenditure, as observed through indirect calorimetry. Furthermore, female EC CD36 KO/LDLR KO mice demonstrated reduced atherosclerosis. Metabolomics profiling uncovered altered plasma levels of acetylcarnitine, phenylalanyl-glutamine, threonine, xanthurenic acid and menaquinol in EC CD36 KO mice compared to control mice, providing insights into the intricate metabolic consequences of EC CD36 deficiency.

Conclusion

In conclusion, the data support a significant role for EC CD36 in systemic metabolism and reveal sex-specific impacts on atherosclerosis and energy substrate use. The findings suggest that targeting EC CD36 could be a promising avenue for therapeutic interventions aimed at addressing the metabolic consequences of HFDs. The study offers valuable insights that could enhance our comprehension of how EC CD36 deficiency contributes to endothelial dysfunction, leading to atherosclerosis and metabolic dysregulation induced by HFDs. This research lays the groundwork for future investigations in this crucial domain of cardiovascular health.

Preface

This thesis represents original work by Umar Rauf Rekhi. Approval for all procedures was obtained from the Animal Care and Use Committee (ACUC) at the University of Alberta (AUP # 0001953, 0570). The study design, planning, and experiment development were done in collaboration with Dr. Maria Febbraio. Dr. Febbraio created the EC CD36 KO mouse model employed in this research. Animal experiments were conducted in collaboration with Dr. Febbraio, Dr. Maria Alexiou, and Dr. Mohamed Omar. Dr. Mohamed Omar and I performed the morphometric analysis of aortas, while all activity assays were executed by me. Dr. Maria Alexiou scanned mice heads for micro-CT analysis, and Dr. Raisa Catunda, along with Dr. Aaron Fong, helped with micro-CT analysis and data interpretation using a protocol developed by Dr. Raisa Catunda. Dr. Monica Sharma aided in the SEAP assay and image formatting for the study titled "Impact of a CD36 inhibitor on *Porphyromonas gingivalis*-mediated atherosclerosis." Time to thrombosis and hemoglobin assay is an unpublished data and were performed by Dr. Mohamed Omar, and Dual-Energy X-ray absorptiometry was conducted by Dr. Linnet Immaraj. The indirect calorimetry experiment was carried out in collaboration with Dr. Febbraio and Amy Barr. The flow cytometry experiment was conducted by Cole Delyea, a student in Dr. Shokrollah Elahi's lab. The results chapters include two previously published papers. Lipoprotein analyses were performed by the Lipidomics Core Facility part of the Faculty of Medicine and Dentistry at the University of Alberta, Edmonton, Canada. Untargeted metabolomics by chemical isotope labeling liquid chromatography mass spectrometry using 4 channels analysis, were carried out at The Metabolomics Innovation Centre, University of Alberta, Edmonton, Canada, and data extraction was based on the report provided by the metabolomics core.

Chapter 3 of this thesis has been published and the authors are Rekhi UR, Omar M, Alexiou M, Delyea C, Immaraj L, Elahi S, Febbraio M, titled as "Endothelial Cell CD36 Reduces Atherosclerosis and Controls Systemic Metabolism" on Front Cardiovasc Med. 2021 Nov 23;8:768481.

Chapter 4 of this thesis has been published and the authors are Rekhi UR, Catunda RQ, Alexiou M, Sharma M, Fong A, Febbraio M, titled as "Impact of a CD36 inhibitor on *Porphyromonas gingivalis* mediated atherosclerosis" on Arch Oral Biol. 2021 Jun;126:105129.

Dedication

I extend my heartfelt gratitude and dedication for this dissertation to my parents, Professor Abdul Rauf and Hafeez Rekhi, whose unwavering support and continuous prayers has been the cornerstone of all my academic endeavors and achievements. A special acknowledgment goes to my incredible wife, Sehrish, and to my beloved children, Haiqa and Taha for their continuing patience throughout this journey. Finally, I dedicate this work to my sister, Sara, and my entire extended family living in Pakistan.

Acknowledgements

I would like to express my deepest gratitude and appreciation to my mentor and supervisor, Dr. Maria Febbraio, for her outstanding guidance, unwavering support, and encouragement during my doctoral pursuit. As a clinical student initially lacking lab experience, Dr. Febbraio's commendable patience was instrumental in my development. Over the seven years, her dedicated supervision not only helped me overcome professional challenges but also fostered intellectual growth, confidence, and curiosity. This achievement stands as a testament to her precious guidance, and I am extremely thankful for the significant impact she has had on both my academic and personal development. Additionally, I want to express my appreciation and thanks to my committee member and former Periodontology Program Director, Dr. Monica Gibson, whose invaluable input and counseling together with her tireless and sincere support greatly contributed to my shaping into a better Periodontist. I also wish to extend my thanks for the assistance and valuable insights provided by my committee member, Dr. Ava Chow in the realization of my research project leading to the successful completion of this project. Furthermore, I would like to express my gratitude to my arm's length and external examiner, Dr. Khaled Altabtbaei and Dr. Priya Raman for their time and valuable input. A special thank you goes to Dr. Maria Alexiou for her guidance from the inception of my lab training and for imparting foundational concepts with amazing patience throughout my learning process. My heartfelt thanks also go to fellow lab members and friends viz., Dr. Raisa Catunda, Dr. Mohamed Omar, Karen Ho, Dr. Konrad Lehmann, Dr. Linnet Immaraj, Dr. Yuli Berlin-Broner, Dr. Monica Sharma, Dr. Wasif Qayyum, Danielle Clark, and Julia Piche for their determined support. It was an amazing experience and a pleasure working with them throughout my studies. Finally, I extend my thanks to all the funding sources, including the: Heart & Stroke Foundation of Canada Grant in Aid (MF), Canada Foundation for Innovation, Alberta Enterprise and Advanced Education and University of Alberta, Faculty of Medicine & Dentistry Motyl graduate Studentship in Cardiac Sciences (URR).

Table of Contents

List of Tables

List of Figures

List of Abbreviations

ABC – Alveolar bone crest

ADMA – Asymmetric dimethylarginine

AMPK - Adenosine Monophosphate-Activated Protein Kinase

Apo - Apolipoprotein

bp – base pair

BMDM – Bone Marrow-Derived Macrophages

CAD – Coronary artery disease

CEJ - Cementoenamel junction

CD36 - Cluster of differentiation 36

CVD – Cardiovascular disease

DAMPs - Damage- associated molecular patterns

DAG - Diacylglycerol

DMSO – Dimethyl sulfoxide

DMEM - Dulbecco's Modified Eagle Media

EC – Endothelial cell

ED – Endothelial dysfunction

EDTA - Ethylenediaminetetraacetic acid

eNos – Endothelial nitric oxide synthase

FABP – Fatty acid binding protein

FBS – Fetal bovine serum

FATP – Fatty acid transport proteins

FAK - Focal adhesion kinase

FDR – False discovery rate

GPIHBP1 - Glycosylphosphatidylinositol anchored high density lipoprotein binding protein 1

G-CSF - Granulocyte – colony stimulating factor

HFD – High fat diet

ICAM - Intercellular adhesion molecule

IGF - Insulin-like growth factor

IL – Interleukin

IP – Intra-peritoneal

IR – Insulin resistance

Kb – Kilobase

KO – Knock out

LCFA - Long chain fatty acid

LDL – Low-density lipoprotein

LDLR – Low density lipoprotein receptor

LOX-1 - Lectin-like oxidized LDL receptor-1

LPS – Lipopolysaccharide

MECs - Microvascular endothelial cells

MCFA - Medium chain fatty acid

MCP-1 – Monocyte chemoattractant protein -1

M-CSF – Macrophage-colony stimulating factor

Micro-CT - Micro-Computed Tomography

MPO – Myeloperoxidase

NADPH - Nicotinamide adenine dinucleotide phosphate

NHANES 1 - First National Health and Nutrition Examination Survey

OD - Optical density

Ox-LDL - Oxidized-LDL

padj – Adjusted p-value

PAMPs - Pathogen- associated molecular patterns

PBS – Phosphate buffered saline

PCR – Polymerase chain reaction

PECAM-1 - Platelet endothelial cell adhesion molecule 1

PKC - Protein kinase C

Pg - *Porphyromonas gingivalis*

PPARγ - Peroxisome proliferator-activated receptor gamma

PRR – Pattern recognition receptor damage- associated molecular patterns (DAMPs) and pathogen- associated molecular patterns (PAMPs)

ROS – Reactive oxygen species

RNS – Reactive nitrogen species

SEAP - Secretory Alkaline Phosphatase

SCFA - Short chain fatty acid

SHP-2 - Src homology 2–containing phosphotyrosine phosphatase

TG – Triglyceride

TGF-β - Transforming growth factor-β

TIMP - Tissue Inhibitor of Metalloproteinase

TNFα - Tumor necrosis factor α

TLR - Toll-like receptor

TRL – Total root length

VCAM - Vascular cell adhesion molecule

VE-cadherin – Vascular endothelial-cadherin

VEGF – Vascular endothelial growth factor

VEGFR2 – Vascular endothelial growth factor receptor 2

VLDL – Very low-density lipoprotein

WT – Wildtype

Chapter 1 - Introduction

1.1 Cardiovascular Disease

Cardiovascular diseases (CVDs), including coronary heart disease, hypertension, stroke, and some other vascular illnesses are a significant global health issue, characterized by increasing prevalence and associated death and disability rates, resulting in substantial economic implications (1). The two primary causes of death worldwide are heart disease (caused by atherosclerotic plaque formation in coronary arteries) and stroke (2). According to a Global Burden of the Disease study, in 2020, approximately 523 million individuals were affected by CVD, resulting in nearly 19 million deaths. These deaths accounted for approximately 32% of all worldwide deaths, signifying an absolute increase of 18.7% compared to the figures from 2010 (3, 4). On a global scale, there were around 244.1 million individuals worldwide living with ischemic heart disease (IHD) in 2020. This condition was found to be more common in males, with 141.0 million affected, compared to 103.1 million in females (3). This trend persisted despite the widespread availability of lipid-lowering medications such as statins and continuing scientific research aimed at understanding the underlying causes and physiological mechanisms of the disease. Meanwhile, it has been projected that CVD will be responsible for over 23 million deaths worldwide by 2030 (5).

According to Statistics Canada (2021), in the list of leading causes of death, heart disease resulting primarily from atherosclerosis ranks as the second most prevalent cause of mortality following malignancy and is responsible for about 18.5% of the overall deaths recorded within the country. A latest report released in 2017 by the Public Health Agency of Canada regarding the economic implications of diseases, reported that CVD incurred medical expenses and productivity losses amounted to approximately 13.6 billion dollars in 2010. Notably, CVD was responsible for the largest spending on hospitalization and pharmaceuticals among all chronic diseases. These substantial expenses are not exclusive to Canada; they are a global phenomenon, extending to regions like the European Union, where in 2021 the estimated costs are an astounding 282 billion euros (6). According to National Health Interview Survey (NHIS) in the years 2018 to 2019, heart disease incurred an annual cost of approximately $239.9 billion in the United States. This included expenses related to healthcare services, medications, and the economic impact of lost productivity resulting from fatalities. Therefore, the aforementioned statistics emphasize the imperative need

to conduct further research on the underlying mechanisms of the disease to uncover and acquire a deeper understanding of both novel and recognized risk factors.

1.2 Atherosclerosis

Atherosclerosis is a multifactorial inflammatory condition characterized by the deposition of lipid and/or fibrous substances within the intimal layer of arteries, which leads to hardening and loss of elasticity of the arterial walls. Several distinct cell types, such as dendritic cells, neutrophils, B and T lymphocytes, endothelial cells (ECs), vascular smooth muscle cells, and macrophages, play a role in the development and progression of the inflammatory response inside the damaged arterial intima (7). Macrophages play a leading role in the pathogenesis of atherosclerosis. They contribute to the inflammatory response and promote accumulation of cholesterol by internalizing oxidized low density lipoprotein (ox-LDL) through scavenger receptors (SR), foremost among these receptors are CD36, SR-A and lectin-like oxidized LDL receptor-1 (LOX-1) (8, 9). In vitro studies show that CD36 and SR-A are responsible for 75 to 90 percent of modified LDL uptake by macrophages, with other scavenger receptors unable to makeup for their absence (9). These internalized ox-LDL are then trapped in the intimal layer leading to formation of foam cells which are the basic building blocks of atherosclerotic plaque (10, 11).

The atherosclerosis process is triggered by the activation of the endothelium, which is subsequently followed by a series of events. These events involve vessel constriction and the activation of inflammatory pathways, ultimately resulting in the formation of atheroma (lipid-laden plaque), a distinctive feature of established atherosclerosis (12). Plaque formation is characterized by the increased proliferation of fibrous tissues and smooth muscle cells in the arterial walls, resulting in their protrusion and subsequent partial or complete obstruction of blood flow to vital organs such as heart and brain.

1.3 Atherosclerosis Risk Factors

The development of atherosclerosis is a complicated process whereby various risk factors combine to increase the probability of disease onset or exacerbate an existing condition.

Atherosclerosis risk factors encompass various factors such as high-fat diet (HFD), smoking, age, family history, obesity, sedentary lifestyle, hyperlipidemia, and metabolic syndrome components (hypertension, insulin resistance (IR) visceral adiposity, and hypertriglyceridemia), which can eventually lead to diabetes mellitus type II (13-16). Most of these risk factors can be addressed and potentially reversed, and there is evidence to suggest that reversing them can decrease the complications associated with atherosclerosis (17, 18).

Chronic exposure to risk factors associated with atherosclerosis results in a decrease in nitric oxide (NO) production due to elevated oxidative stress, commonly linked to these risk factors (19, 20). This persistent exposure to risk factors and oxidative stress surpasses the vascular endothelium's protective mechanisms, leading to endothelial dysfunction (ED). This, in turn, leads to the loss of endothelial integrity, increased proliferation and migration of smooth muscle cells, as well as enhanced adhesion and migration of leukocytes (21). ED serves as both an initiating event and a significant contributor to the advancement of atherosclerotic cardiovascular disease (22).

1.4 CD36

Cluster of differentiation 36 (CD36), is a multi-ligand integral transmembrane glycoprotein with wide expression and biological functions. It has also been referred to as fatty acid translocase (FAT), the thrombospondin receptor and platelet glycoprotein IV. CD36 is the most commonly used name for this protein. CD36 is an ~88Kd cell surface receptor first reported on human platelets as glycoprotein IV in the late 1970s (23). It is expressed on the surface of various cell types, including microvascular endothelial cells (MECs), monocytes/macrophages, platelets, adipocytes, microglia, hepatocytes, and cardiac and skeletal myocytes. (24-29). CD36 is a member of the class B scavenger receptor family, which also includes lysosomal integral membrane protein II (LIMPII) and scavenger receptor BI (30). These three proteins share a common structure. It’s official name, based on scavenger receptor nomenclature, is scavenger receptor class B member 2 (SR-B2). The synthesis of CD36 occurs on polyribosomes, after which it is moved to the endoplasmic reticulum and Golgi apparatus for additional processing. Finally, CD36 is delivered to the cell membrane by endosomes (31).

1.5 Structure and Ligands of CD36

The CD36 gene is present on chromosome 7 (7q11.2) (32). It comprises a total of 19 exons, and there are a minimum of 20 alternatively spliced transcript variants (33). In humans, this protein's structure consists of a single peptide chain composed of 472 amino acids. It contains two transmembrane domains, two short amino (N)- and carboxyl (C)-terminal cytoplasmic domains, and a large extracellular, heavily glycosylated domain including a hydrophobic region, two phosphorylation sites, ten glycosylation sites and three pairs of disulfide bonds (10, 34-36). These modified sites possess the ability to interact with various extracellular substances, such as ox-LDL and long-chain fatty acids (LCFAs) (37, 38). Both amino and carboxyl termini located in the cytoplasm contain a pair of palmitoylated cysteine residues which play an important role in the anchoring of CD36 in caveolae and lipid rafts (39-41). In addition, the carboxyl terminus has two ubiquitination sites (35). As a scavenger receptor family member, CD36 exhibits a remarkable ability to bind a variety of ligands. These ligands encompass modified and native lipoproteins (42, 43), LCFAs (44), thrombospondin (45), oxidized phospholipids (ox PL) (46), P. falciparum-infected erythrocytes (47), advanced glycation end-products (AGES) (48), amyloid β (49) and apoptotic cells (50).

To better understand the mechanisms supporting CD36 function, we now have a detailed blueprint because of the recent high-resolution, three-dimensional structure of the extracellular domain of CD36 using X-ray crystallography (51). Previously, the CD36 extracellular domain was described as having an oval-shaped structure with an antiparallel β-barrel core, based on a homology model that utilized the crystal structure of LIMP-2 as a reference (52). The hydrophobic cavity created by the β -barrel core runs the entire length of the extracellular domain (52). During this three-dimensional structure determination, it was found that the central cavity had two potential entrances, referred to as "entrance 1" and "entrance 2". Both entrances were subjected to crystallization in the presence of LCFAs, specifically palmitic acid, and stearic acid (51). The interactions involving the LCFAs, and the central cavity are predominantly facilitated by hydrophobic properties between the tail of the FA and the hydrophobic residues that line the cavity, as well as hydrogen bonding present between the carboxylic acid head group of fatty acids (FAs)

and Thr195 (FA binding residue), located inside the hydrophobic cavity of CD36. This aligns with a previous investigation that employed homology modeling to anticipate the presence of a fatty acid binding site on CD36, where Thr195 was identified (53).

The interaction between LCFA and CD36 is associated with intracellular signaling cascades and modifications in lipid metabolism. These changes involve the separation of the Src-family kinase (SFK) Fyn from the CD36 signaling complex and an increase in cytosolic liver kinase B1 levels. This elevation activates the adenosine monophosphate-activated protein kinase (AMPK) pathway, leading to an enhancement in FA oxidation (54). LCFAs serve as ligands for nuclear receptors like peroxisome proliferator-activated receptor (PPAR), which are recognized for their role in promoting the production of proteins related to cellular lipid metabolism. Intriguingly, through this mechanism, CD36 enables the control of its own expression (55, 56). In macrophages, ox LDL stimulates the activation of Toll-like receptors 4-6 (TLR4-TLR6), which is dependent on CD36 leading to subsequent pro-inflammatory signaling through the nuclear factor kappa-light-chain-enhancer of activated B cells (NF-κB) pathway (57). The binding of ox LDL to CD36 triggers the assembly of a protein complex involving the Na+/K+-ATPase and the SFK Lyn. This complex enhances the uptake of ox LDL and contributes to the formation of foam cells within macrophages (58).

1.6 Function of CD36

CD36 is involved in a diverse array of physiological processes, encompassing the phagocytosis of apoptotic cells (50), the endocytic uptake of ox LDL in macrophages, leading to foam cell formation in atherosclerosis (43, 59), and maintaining lipid homeostasis by binding to LCFAs with high affinity, thereby facilitating FA uptake in muscle and adipose tissues (26, 60). It also plays a role in innate immunity as a pattern recognition receptor (PRR) by recognizing specific molecular patterns associated with pathogens (61-63). Furthermore, it is involved in adaptive immunity (64, 65) influences T and B cell metabolism (66, 67) contributes to cancer progression (68) and is linked to metabolic disease (69).

In ECs, CD36 inhibits angiogenesis triggered by growth factors such as fibroblast growth factor 2 (FGF2) and vascular endothelial growth factor (VEGF) while promoting apoptosis (65). In platelets, CD36 stimulates activation, aggregation, and the release of substances (65). Additionally, in sensory cells, CD36 is involved in the cellular responses to dietary fats in the mouth and gastrointestinal tract (65, 70). An important characteristic that sets CD36 apart from other PRRs is its dual role as a signaling receptor in response to damage- associated molecular patterns (DAMPs) and pathogen- associated molecular patterns (PAMPs) and its promotion of LCFA uptake (64).

1.7 Macrophages: Origin and Function

Macrophages represent a prominent subset of immune cells within the human body, originating from bone marrow progenitors and monocytes (71). The macrophages possess several functions and are actively engaged in the physiological and pathological mechanisms of immune response and healing by controlling inflammation and eliminating infection through different processes such as antigen presentation, phagocytosis, and polarization (72). They are extensively involved in the pathogenesis of numerous inflammatory diseases, such as atherosclerosis, asthma, cancer, rheumatoid arthritis, neurodegeneration, and fibrosis (73). The extent of their involvement in these conditions varies significantly and is regulated by numerous factors. In terms of their origin, they can be categorized into resident macrophages derived from the yolk sac and fetal liver, as well as postnatal macrophages derived from circulating monocytes (74, 75).

Atherosclerotic plaques contain both types of macrophage populations, including those originating from infiltrating monocytes and those arising from the proliferation of resident vascular macrophages (76, 77). During adulthood, most tissue-specific macrophages undergo local proliferation and exhibit prolonged lifespans (78). However, in the event of injury, these resident macrophages are augmented by inflammatory monocytes that are recruited from the bone marrow and ultimately become macrophages (74). During the early stages of plaque formation, inflammatory monocytes derived from the bone marrow serve as the predominant source of plaque macrophages. As the disease progresses and the atherosclerotic plaques grow larger renewal of macrophages in established plaques relies on the proliferation of resident macrophages. The

microenvironment within the atherosclerotic plaque plays a critical role in encouraging macrophage proliferation during this stage (76, 79).

1.8 Phenotypes of Macrophages in Atherosclerosis

Extensive research has been conducted in the past decade regarding the heterogeneity of macrophage populations (80). Macrophage CD36 plays a role in the development of atherosclerotic arterial lesions by recognition and internalization of ox LDL, initiating signaling pathways that lead to inflammatory responses. This signaling cascade then results in formation of lipid rich foam cells, the pivotal initial stage of atherosclerosis and ultimately atherosclerotic plaque (9, 81, 82). Macrophages exhibit diverse phenotypic presentations depending upon their surrounding milieu and required functional roles. The heterogeneity of macrophages within atherosclerotic plaques is influenced by the complex microenvironment consisting of modified lipoproteins, inflammatory mediators, necrotic cells, and apoptotic cells. Consequently, these macrophages assume distinct roles in the advancement of atherosclerosis (83). Therefore, in atherosclerotic lesions, currently recognized macrophage subtypes include M1, M2, M (Hb), Mhem, Mox, and M4.

Pro-inflammatory M1 macrophages were found in progressive plaques, whereas M2 macrophages were found in regressing plaques, where they were implicated in tissue healing and remodelling (84). M1 macrophages are stimulated by lipoprotein and lipopolysaccharide (LPS) and undergo differentiation due to interferon-γ (IFN-γ) and TLR signalling (83, 85). They execute their functions by secreting proinflammatory cytokines/chemokines, such as interleukin-1 beta (IL-1β), IL-6, IL-23, tumour necrosis factor -alpha (TNF-α), CXCL9 and, CXCL10, as well as elevated levels of reactive oxygen species (ROS), and NO (83, 86). Conversely, the anti-inflammatory M2 macrophages (87) are activated in response to IL-4 and IL-13 signals. The anti-inflammatory mediators secreted by these macrophages are IL-10, transforming growth factor-beta (TGF-β), IL-1 receptor antagonist (Ra), C-C motif chemokine ligand 17 (CCL17), and CCL22.Thus, these mediators result in an anti-inflammatory response to combat the chronic inflammation induced by the M1 type (88, 89). Studies have shown that M2 phenotype, primarily

consume LCFA as their main source of energy. LCFA uptake in this phenotype is facilitated by CD36, which is highly expressed in M2 macrophages (90-92).

M2 macrophages can be further classified into four subtypes based on distinct *in vitro* stimulation factors: M2a, M2b, M2c, and M2d. The M2a subtype of macrophages, stimulated by IL-4 and IL-13, features abundant glucocorticoid receptors. These macrophages release pro-fibrotic molecules like fibronectin, insulin-like growth factor (IGF), and TGF-β, which contribute to tissue repair (93, 94). M2b subtype of macrophages can be triggered by immune complexes and TLR agonists and they are capable of producing both anti-inflammatory factors like IL-10 and IL-12, and pro-inflammatory factors such as IL-1β, IL-6, and TNF-α (95, 96). The M2c macrophages are activated by glucocorticoids and IL-10, exhibiting potent anti-inflammatory capabilities. They release significant amounts of IL-10 and TGF-β, particularly effective in addressing apoptotic cell responses (97). TLR agonists stimulate adenosine A2A receptors to produce M2d macrophages, the fourth subtype. This macrophage secretes anti-inflammatory cytokines including IL-10 and IL-12 and suppresses pro-inflammatory ones (98). Unlike lipid-core macrophages, M (Hb) and Mhem macrophages are found together in areas of bleeding at sites where new blood vessels are developing or in unstable plaque formations (99). Mox macrophages, which are a proatherogenic subtype triggered by ox PL, provide protection against oxidative stress by upregulating antioxidant enzymes such as heme oxygenase 1, thioredoxin reductase 1, and sulfiredoxin-1, a process mediated by nuclear factor erythroid-derived 2-related factor 2 (100). M4 macrophages, activated by C-X-C motif ligand 4 (CXCL4), mainly exhibit CD68, S100A8, and matrix metalloproteinase 7 (MMP-7) in the arterial adventitia and intima. These macrophages also express pro-inflammatory factors like MMP-12, IL-6, and TNF-α and are present in human lesions (101, 102). Furthermore, CXCL-4-induced inflammation exacerbates atherosclerosis by inhibiting CD163 (103), highlighting the pro-atherogenic nature of this macrophage subtype (101, 104).

1.9 FAs

FAs are carboxylic acids having a hydrocarbon chain (H-C) and a terminal hydroxyl (OH) group. They are highly diverse and are classified based on the length of the carbon chain and the number of double bonds. Short-chain fatty acids (SCFA) have 1-6 carbon aliphatic tails; medium-

chain fatty acids (MCFA) have 7-12 carbon aliphatic tails; LCFAs have 13 to 20 carbon aliphatic tails; and very long- chain fatty acids (VLCFA) have aliphatic tails longer than 20 carbons (105, 106). FAs can also be classified into three categories based on the presence of double bonds: saturated (no double bonds), unsaturated (one double bond), and polyunsaturated (multiple double bonds).

LCFAs are the building blocks for phospholipids which form the structural components of biological membranes and play an essential role in membrane function. They are crucial for systemic energy metabolism, where efficient ATP generation through mitochondrial β-oxidation supports the energy needs of metabolically active tissues such as skeletal muscle, brown fat and the heart. Additionally, the esterification of FAs into triglycerides (TGs) provides a means to store energy in adipose tissue and various other tissues (107-109). In mammalian cells, LCFAs, including palmitic acid and oleic acid, constitute the predominant types of FAs (106). In addition to being produced by the body, palmitic acid can be obtained from meat, dairy products, and palm oil. Its homeostatic imbalance has been associated with the occurrence of conditions such as atherosclerosis, metabolic disorders, cancer, and neurological diseases (110).

1.10 LCFA Uptake and Utilization

LCFAs in the blood can be found either as unesterified free fatty acids (FFAs) attached to albumin or as constituents of lipoproteins in the form of TG and phospholipids. Variability in cellular uptake and utilization of FAs during shifts in energy metabolism plays a crucial role in preserving homeostasis, by directing FAs to particular tissues (111, 112). During periods of fasting or exercise, the muscles and heart exhibit an increased dependence on FA intake as glucose availability decreases. This adaptation allows glucose preservation for tissues that rely on it e.g., brain and red blood cells. Conversely, when feeding increases the availability of glucose, the use of glucose by the muscles and heart increases, and a greater proportion of FAs are stored in the adipose tissue (112, 113). This indicates that the uptake of FAs by tissues is controlled locally, enabling rapid adaptations in response to fluctuations in fuel availability.

FA uptake in tissues primarily occurs at the capillary level, commencing with their transfer across MECs. To facilitate this process, high-affinity FA receptors present on the surface of MECs play an important role, because they are responsible for FA recognition. These receptors collaborate with intracellular fatty acid-binding proteins and fatty acyl-CoA ligases to enhance the accumulation of lipids (114-116). The liberation of FAs from lipoproteins is facilitated by intravascular lipoprotein lipase (LpL), in conjunction with its glycosylphosphatidylinositol anchored high density lipoprotein binding protein 1 (GPIHBP1) located in ECs (117).

1.11 FA Transport Mechanisms

In general, two types of mechanisms are involved in the transport of FA across the EC membrane. These are: simple diffusion and saturable transport processes. The passive diffusion mechanism relies on intracellular metabolic activity, which generates a concentration gradient across the cell membrane, facilitating uptake in a downhill manner. In contrast, the saturable process is controlled by the presence of specific proteins expressed on the cell membrane.

1.12 Flip- Flop Model of FA Transport

Movement of FAs through the lipid bilayer had long been considered to occur via passive diffusion or flip-flop (118). The flip-flop model for transporting FFAs across the plasma membrane is divided into three sequential steps: first, the binding or adsorption of the FA to the membrane; second, the translocation process known as "flip-flop" across the membrane; and finally, the release or desorption of the FA into the cytosol (118, 119). The endothelium serves as the initial barrier encountered during the transport of FAs. Therefore, the possible mechanisms for the transport of FA across the endothelium include the following sequential steps: initially, FAs can move through the spaces between adjacent endothelial cells. Subsequently, they may undergo lateral movement within the phospholipid bilayer cell membrane. Lastly, FAs are passively diffused across the luminal membrane, into the cytoplasm of the EC, and then across the abluminal membrane on the opposite side (120).

While FAs can passively diffuse across membranes through a "flip-flop" mechanism, it has become evident that the uptake of LCFAs, which are the predominant FAs in our diet, is facilitated by transporters. This facilitated uptake is essential to ensure an efficiently regulated supply of FAs to tissues and to prevent their inappropriate delivery (121, 122). The concept of protein-mediated FA uptake has been a subject of debate because, generally, it was considered unnecessary, primarily because of the rapidity of FAs flip-flopping from the outer leaflet to the inner leaflet (123). The step that might limit the rate of FA uptake into cells appears to involve the transition from the lipid bilayer into the cytosol.

1.13 Protein-Mediated FA Transport Across ECs

A substantial body of evidence is available that provides strong support for the role of proteins in facilitating the uptake of FAs (124-127). Several proteins found in or associated with the cell membrane, including the widely studied CD36, plasma membrane-associated fatty acid-binding protein (FABPpm), family of fatty acid transport proteins (FATP1–6), caveolin 1, palmitoylation regulated caveolar endocytosis, long-chain fatty acyl coenzyme A (CoA) synthetase (ACSL), have been suggested to play a role in cellular FA transport (125, 128-132). These proteins have the capacity to operate at various stages of the uptake process, which includes both the transfer across the cell membrane and channeling of FAs within the cell. The key element in protein-mediated FA uptake, however, lies in its capacity for regulation. Regarding the protein-mediated trafficking of LCFAs, our focus will be on CD36, which holds significant relevance for this project.

1.14 EC CD36 Regulates FA Uptake

Extensive research conducted in both human and animal models supports a key role of CD36 in the transport of FAs (129, 133-137). The glycoprotein CD36, was first determined to be a transporter of FAs on isolated rat adipocytes by affinity labeling. This labeling was achieved using a reactive compound derived from oleic acid known as sulfo-N-succinimidyl oleate, which

is impermeable to the membrane (138). Further research revealed that during the differentiation of preadipocytes, CD36 expression increased and contributed to the enhanced cellular uptake of LCFAs (26). Through the utilization of tissue-specific knockout mouse models, a recent study unveiled the involvement of CD36 in both ECs and adipocytes in controlling the storage and release of LCFA within adipose tissue. This work also showcased the contribution of CD36 in ECs and adipocytes to the enhancement of tumor growth and the development of chemoresistance, facilitated by the presence of LCFA derived from adipose tissue. Apart from the FAs that circulate bound to albumin, CD36 facilitates the transfer of FAs released by LpL from very low-density lipoproteins (VLDL) (139). However, uptake of FAs resulting from chylomicron hydrolysis occurs independently of CD36 (140, 141). Consistent with its role in FA uptake, increased serum fasting levels of unesterified free FAs have been observed in CD36 KO mice, along with reduced uptake of the LCFAs oleate and palmitate into isolated adipocytes (133).

The molecular events involved in the transport of FA into ECs have been under study for decades, but they are still under debate. The regulation of LCFAs uptake by ECs has received less attention, because most of the research has focused on specific cell types within organs (such as cardiomyocytes, skeletal myocytes, and adipocytes) rather than the ECs themselves (31, 113, 142). In terms of the molecular mechanism of FA uptake, one hypothesis, supported by crystal structure data (52) is that on the extracellular side CD36 serves as a receptor of FAs enabling their distribution and transport to the outer layer of the plasma membrane. Following this, the FA movement across the membrane occurs through passive diffusion without any involvement of a protein mediator. Nonetheless, on the inner membrane surface CD36 assists in the detachment of FAs and their subsequent attachment to cytoplasmic fatty acid-binding protein (FABPc) or ACLS, leading to a unidirectional flow of FA as both proteins trap FAs inside the cell (143-146). In this context, CD36 may be crucial for assembling an FA "transport channel" through protein-protein interactions, potentially within caveolae or lipid rafts, as suggested by previous research (40, 147, 148). Furthermore, caveolae are associated with both signaling processes and the endocytosis of pathogens (149). Thus, FA uptake is governed by a molecular process that encompasses both passive diffusion, occurring within the membrane s lipid bilayer, and protein-mediated diffusion, which entails the capture and release of FAs by the membrane. CD36 present on the membrane, leads to a substantial increase in the overall rate of FA uptake (146).

Recent studies have highlighted the importance of CD36 acylation, glycosylation, and their respective reversals in governing the uptake of extracellular FAs in ECs and adipocytes. These modifications are crucial in regulating the uptake of FA and the caveolae associated movement of CD36 to and from lipid droplets within adipocytes, particularly in the context of lipolysis. (130, 150). These findings underscore the critical role of CD36 palmitoylation-mediated endocytosis in facilitating its function as a bidirectional LCFA transporter between ECs and adipocytes (130). Caveolae in adipocytes have been associated with the uptake of FAs, and it has been reported that FAs can initiate the process of caveolae endocytosis in these cells (41, 130). Another latest study regarding the uptake of FAs by EC CD36 demonstrated that the interaction of FAs with CD36 on the ECs apical membrane initiates a coordinated process involving CD36 and Src, resulting in the endocytosis of FAs. This process occurs through the budding of caveolae which then form intracellular vesicles. These vesicles are released at the basolateral membrane, resembling small extracellular exosomes (sEVs), which act as transporters, facilitating the transfer of FAs to tissue cells (151).

ECs, acting as metabolic regulators, oversee the transcytosis, which involves the transport of macromolecules enclosed within lipid bilayers across the interior of the cell, particularly for FAs. When EC FA transport becomes disrupted, it can exacerbate IR, a condition that plays a central role in various pathological processes (116, 152). CD36 exhibits high levels of expression in capillary ECs, contributing to the gene expression pattern that characterizes how microvascular cells manage lipids (116, 153, 154). Substantial evidence obtained from the targeted deletion of EC CD36 and various transcription factors specific to ECs reinforces the notion that the endothelium acts as a gatekeeper in the uptake of FAs by tissues (114, 153, 155). Mice with the absence of CD36 specifically in ECs exhibit compromised uptake of FAs in adipose tissue, heart, skeletal muscle (116) and gastric mucosa (109). These mice also replicate the elevated levels of plasma FAs and improved glucose clearance observed in mice with a complete CD36 gene deletion (116). Furthermore, deletion of CD36 in ECs of mice leads to a decrease in the mobilization of LCFA from white adipose tissue and their bioavailability to cancer cells (150).

The first link between CD36 and the regulation of LCFAs uptake in ECs was established in an EC-specific peroxisome proliferator-activated receptor gamma KO (PPARγ KO) mouse model. In this model, there is a significant reduction in CD36 expression specifically in ECs which

closely mimics the metabolic characteristics observed in the global CD36 KO mouse (133, 155). This encompasses an elevated reliance of the heart on glucose, protection against IR, and alterations in plasma FAs and VLDL triglyceride levels. These findings suggest that ECs significantly regulate metabolism without compensation. Several recent reports have confirmed the early findings on CD36 KO and PPARγ KO mice, as well as the significance of EC CD36 in regulating LCFAs transport. Using a tissue-specific null model, a recent study demonstrated the critical role of EC CD36 in facilitating the optimum LCFAs uptake by cardiomyocytes from the blood (116). Additionally, this study revealed that CD36 KO in ECs resulted in enhanced glucose tolerance and improved insulin sensitivity. Moreover, there was an increase in glucose uptake during fasting in the cardiac muscle, which aligns with findings previously observed in mice with cardiomyocyte specific CD36 deletion (116, 156). Son *et al*, also showed that in contrast to the control mice, the hearts of EC CD36 KO mice do not exhibit lipid droplet accumulation in response to fasting. CD36 deletion in cardiomyocytes also decreases lipid droplet formation, indicating that CD36 influences lipid uptake in both cardiomyocytes and ECs (116).

The heart is the body's largest consumer of FAs, and studies involving CD36-deficient mice and humans have demonstrated reduced FA uptake in the heart along with elevated glucose uptake (134, 137, 157). CD36 appears to play the primary role in facilitating FA uptake in cardiac tissues. In individuals who possess different single-nucleotide polymorphisms (SNPs) in the CD36 gene, FA uptake by the myocardium was found to be significantly diminished or absent *in vivo* (158, 159). This was observed in both humans and mice with tissue specific CD36 deletion. Also, these mice exhibited a substantial decrease in cardiac FA uptake, both *in vivo* and *in vitro* (113, 160). Transcriptome analysis of cardiac EC revealed that, in comparison with ECs from other organs, cardiac ECs exhibited the highest expression of the gene encoding FA binding protein 4 (FABP4) and other downstream targets of PPAR signaling, including CD36 (161).

A study conducted by Jabs *et al.* showed that endothelial-specific Notch signaling is a novel regulator that plays a significant role in modulating FA uptake proteins, such as CD36 and FABP4, in addition to regulating repair pathways and cellular interactions. CD36 is also involved in albumin transcytosis across dermal ECs both *in vitro* and in endothelial-specific deletion of CD36 in mice. Decreased dermal fat and reduced albumin traffic were observed in these mice, which indicates that albumin transcytosis may regulate FA delivery from the circulation to tissues (162).

This presents a secondary mechanism through which CD36 enables the transport of FAs into tissues, hence controlling the plasma FA levels and influencing insulin signalling (162). Impaired uptake of LCFA by ECs is a key factor in the development of EC IR and dysfunction serving as an important initiating event in atherosclerosis (152).

1.15 Endothelial Dysfunction (ED)

The endothelium is a monolayer of ECs that lines the inner surface of blood vessels, creating an interface between the circulating blood or lymph within the vessel lumen and the vessel wall. The endothelium is a discerning and metabolically active barrier that serves as a vital organ in the preservation of vascular equilibrium. It achieves this by delicately regulating the equilibrium between vasoconstriction and vasodilation (163).

ED represents a transition in the characteristics of the endothelium toward a phenotype marked by impaired vasodilation, elevated ROS, and depletion of NO bioavailability leading to a proinflammatory and prothrombotic state. Vasodilation primarily occurs through the mediation of factors such as NO, endothelium-derived hyperpolarizing factor, and prostacyclin. Conversely, vasoconstriction is primarily driven by factors such as endothelin-1 (ET-1), thromboxane A2, angiotensin II, and prostaglandin H2 (164). Within this group of factors, NO is widely recognised as the most potent endogenous vasodilator produced in the body and an important ED marker (165). Moreover, NO contributes to the preservation of vascular wall homeostasis by exerting inhibitory effects on platelet aggregation, oxidative stress, inflammation, smooth muscle cell migration and proliferation, and leukocyte adhesion (166). ED has been linked to most atherosclerosis risk factors, including diabetes, dyslipidemia, smoking, hypertension, obesity, and aging (165, 167-172). Among several complex mechanisms, oxidative stress is considered to be the most prevailing mechanism involved in the development of ED in connection with the aforementioned risk factors (172, 173).

Hyperglycemia results in the formation of advanced glycation end products (AGEs) via non-enzymatic glycation of proteins and lipids. (174). The accumulation of AGEs in the blood vessels leads to structural changes in the endothelium and basement membrane, thus impairing

NO function and contributing significantly to ED. Furthermore, AGEs bind to surface receptors found on various cell types, including monocytes, macrophages, and vascular smooth muscle cells. This interaction leads to an intensifying inflammatory response, increased vascular permeability, and the promotion of oxidative stress (175, 176).

Increased LDL cholesterol levels and decreased high-density lipoprotein (HDL) cholesterol levels are both independently connected to ED (177). Elevated levels of cholesterol are linked to impaired endothelial vasodilation in both coronary and peripheral blood vessels (178). Conversely, dyslipidemia induces the oxidative stress by elevating the production of reactive species, resulting in decreased NO availability (179). This reduced NO availability, in turn, promotes the oxidation of LDL and contributes to ED (180).

The pathophysiological processes underlying atherosclerosis start with dysfunctional endothelium and are driven by a sequence of intra- and intercellular signaling events that influence the behavior of vascular cells (12, 19). The vascular endothelium experiences both tangential forces, such as shear stress, and circumferential forces, as in pulsatile stretch, generated by blood flow (181, 182). The mechanical force induced by fluid shear stress is detected by mechanosensors which include platelet endothelial cell adhesion molecule (PECAM), vascular endothelial growth factor receptor 2 (VEGFR2), vascular endothelial (VE)–cadherin and other components present on ECs. These mechanosensors initiate biochemical signals via mechanotransduction, which in turn influence critical cellular processes in response to variations in the vascular surroundings, including proliferation and turnover (181-183).

1.16 Initiation of Atherosclerosis

During the initial stages of atherosclerosis, the endothelium undergoes a shift from a dormant state to an activated state in response to proatherogenic triggers. These triggers encompass ox LDL, proinflammatory cytokines, and disturbed blood flow patterns (184). Dyslipidemia from high-fat diets (HFDs) leads to the establishment of dysfunctional endothelium (185), with significant implications for the regulation of thrombosis, homeostasis (19), local vascular tone, and development of inflammation inside the arterial wall, which may result in atherogenesis (186,

187). Mechanisms contributing to ED induced by dyslipidemia include: (1) oxidation of LDL (188), (2) increased nicotinamide adenine dinucleotide phosphate (NADPH) oxidase activity, oxidative stress, and super oxide anion (O2-) production, and (3) elevated plasma concentrations of asymmetric dimethylarginine (ADMA) (189). ADMA functions as an endogenous endothelial nitric oxide synthase (eNOS) inhibitor, competing with L-arginine for the same eNOS binding site. Consequently, this competition leads to eNOS uncoupling, elevation in O2- generation, and subsequently reduced NO production (180).

One of the key risk factors involved in the onset of ED is reduced shear stress due to turbulent blood flow as a result of hyperlipidemia (12, 190). Turbulent flow of blood is prevalent at arterial bifurcations and branch points, where increased arterial curvature leads to flow separation and early atherosclerosis lesions are localized to these high curvature areas (12, 191). Turbulent blood flow triggers the upregulation of hypoxia-inducible factor 1α and NF-κB, leading to inflammation, proliferation, and activation of ECs (192). ECs in an activated state facilitate the recruitment of neutrophils and monocytes into the intima by increasing permeability to macromolecules such as lipoproteins and increased expression of proinflammatory cytokines and chemokines (164, 193).

The initial step in the recruitment of monocytes involves the capture and rolling of monocytes on the endothelium, primarily facilitated by adhesion molecules called P or E-selectin (194, 195). This is followed by a decrease in rolling activity and firm adherence of monocytes to the endothelium. The attachment process is regulated by the interaction between monocyte integrins and the intercellular adhesion molecule 1 (ICAM-1) and vascular cell adhesion molecule 1 (VCAM-1) molecules on ECs, as shown in Figure 1 (195-197). Next, the monocytes transmigrate by crossing the EC barrier into arterial intimal space and the most frequent chemokine mediating this migration process is monocyte chemoattractant protein-1 (MCP-1) (198). The primary sources of MCP-1 expression are ECs, smooth muscle cells, and monocytes and macrophages residing in the intima. Following a proinflammatory stimulus such as hyperlipidemia or tissue damage, MCP-1 expression is elevated, promoting the transendothelial migration of circulating monocytes from the bloodstream into the subendothelial space (199). The atherosclerotic process initiates as blood-borne monocytes migrate into the arterial intima, where, in the presence of growth factors like macrophage-colony stimulating factor (M-CSF), they undergo differentiation into macrophages

that can be polarized to the M1 or M2 phenotype (200, 201). In individuals with hyperlipidemia, elevated LDL infiltrates in the arterial wall where they interact with the subendothelial proteoglycans in the matrix, resulting in their retention and chemical modification, such as oxidation. The interaction between proteoglycans and LDL leads to alterations in LDL structure, influencing both the conformation of apoB100 and the lipid composition. As a result, binding of LDL to proteoglycans renders LDL more prone to oxidation and aggregation (202). Also, through an oxidative mechanism involving superoxide production, glucose increases LDL lipid peroxidation. This suggests that the chronic hyperglycemia in diabetes may also accelerate lipoprotein oxidation (203).

1.17 Oxidative Conversion of LDL into the Atherogenic form and Foam Cell Formation

LDL undergoes oxidation through the action of several enzyme systems, including xanthine oxidase, NADPH oxidase, lipoxygenase, and myeloperoxidase (MPO). MPO is a heme protein found in abundance and is released by monocytes, neutrophils, and macrophages (204). This enzyme system is involved in atherosclerosis and is considered to be more physiopathologically relevant for LDL oxidation (205). It produces a range of cytotoxic oxidants and radical species, including hypochlorous acid (HOCl) and nitrogen dioxide (NO_2) by using hydrogen peroxide (H_2O_2) (206-208). Furthermore, NO gives rise to nitrating oxidants at locations associated with vascular pathology (209, 210). Lipid peroxidation within LDL is the result of nitration of the tyrosyl residue in apo lipoprotein B-100 which occurs when LDL is exposed to reactive nitrogen species (RNS) produced either by monocytes or by MPO enzyme (211, 212). The activation of monocytes in the presence of physiological levels of nitrite (NO_2–), a prominent NO metabolism byproduct, leads to LDL modification. This modification, facilitated by MPO dependent enzyme system, transforms the LDL particle into NO_2-LDL (212) a high-affinity ligand for CD36, which mediates their uptake by macrophages (81).

Another mechanism that contributes to the promotion of foam cell formation involves infection mediated by *Porphyromonas gingivalis* (*Pg*). *Pg* is a gram-negative anaerobic keystone pathogen involved in the pathogenesis of periodontal disease (PD) in humans which has been shown to have an association between PD and several systemic conditions including

atherosclerosis (213-215). Prior work by Brown *et al*. demonstrated that the induction of PD via oral infection with *Pg* led to an increase in atherosclerosis lesion burden in an LDLR KO mouse model of atherosclerosis and that the absence of CD36 protects against *Pg*- mediated accelerated atherosclerosis in these mice (CD36 KO/LDLR KO) (216). According to this study CD36 cooperates with TLR 2 resulting in the activation of the inflammasome in response to *Pg*LPS stimulation. This activation subsequently led to the synthesis, processing, and systemic release of IL-1β, leading to enhanced lipid uptake by macrophage CD36 (216). IL-1β is an important proinflammatory cytokine that is implicated in both the host's response to oral cavity microbes and the progression of atherosclerosis (217, 218). Furthermore, this study suggested that *Pg*LPS-induced CD36/SR-B2-TLR2 signaling pathway which led to IL-1 β production and encouraged cell pyroptosis. Conversely, ox-LDL inhibited IL-1β generation and prevented cell pyroptosis through a mechanism dependent on CD36/SR-B2.Therefore, when macrophages within the vascular wall encounter systemic IL-1β, other proinflammatory cytokines and oxidative stress, this triggers the localized release of IL-1β promoting greater uptake of lipids, foam cell formation, and the advancement of atherosclerotic lesions. Simultaneously, foam cells in the vessel wall persist due to the suppression of pyroptosis increasing plaque development (216). In another study it was shown that *Pg* activates the ERK/NF-κB pathway, which subsequently triggers the activation of the CD36 promoter, resulting in an elevated expression of CD36 in macrophages and, consequently, an enhanced uptake of lipids (219).

As mentioned above and depicted in Figure 1, when monocytes and LDL migrate into the subendothelial space the oxidized LDL interacts with and is internalized by the macrophage scavenger receptor, CD36 (43, 81). Once ox LDL is taken up by macrophage CD36, it serves as a source of distinctive oxidized lipids, acting as ligands for the nuclear transcription factor PPAR-γ leading to increased CD36 expression. The upregulation of CD36 facilitates enhanced LDL uptake, hence maintaining a positive feedback loop that leads to the accumulation of LDL cholesterol within macrophages leading to formation of lipid-laden foam cells, an initiating atherosclerosis event (63, 82).

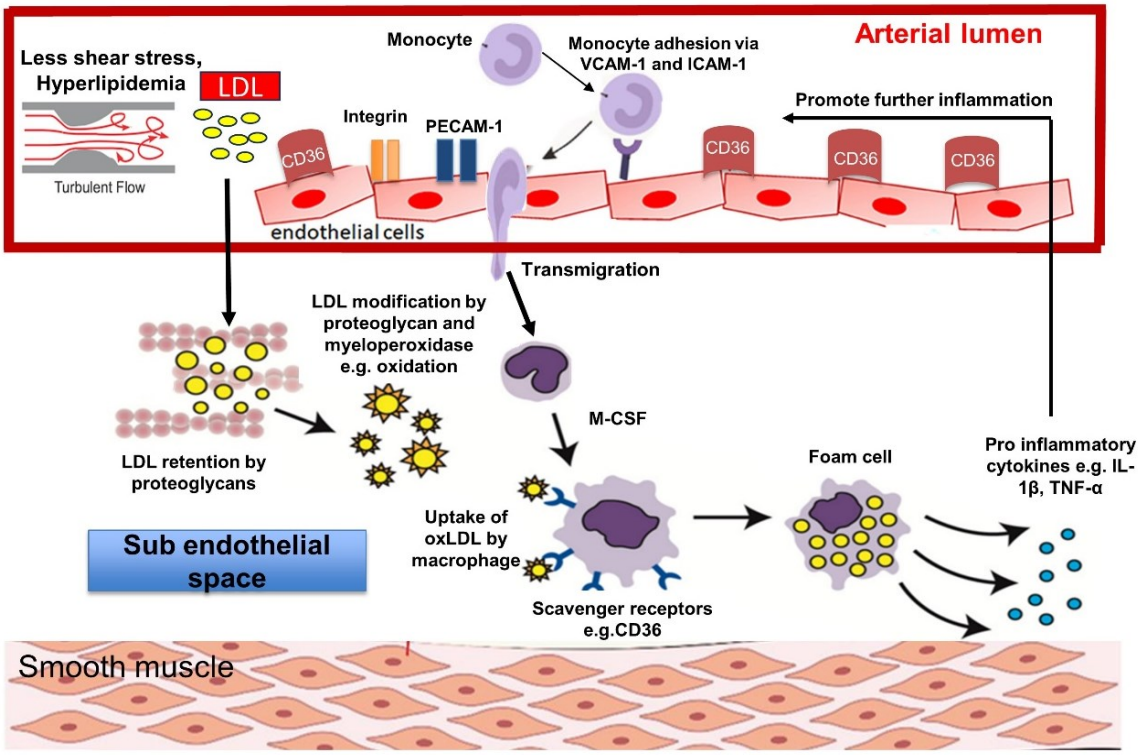

Figure 1: LDL infiltration, retention, and formation of macrophage foam cells via macrophage CD36 uptake of ox-LDL in the arterial wall. In hyperlipidemia, elevated levels of LDL results in activation of mechanosensors due to loss of shear stress which activates the endothelium to, selectins (P and E selectins) and other cell adhesion molecules e.g. I CAM-1 and VCAM-1 resulting in the adhesion and transmigration of monocytes into the subendothelial space by M-CSF, where they differentiate into macrophages. Increased ROS/RNS alters the properties of proteins and proteoglycans in the subendothelial space resulting in LDL retention and oxidation. This ox-LDL binds to macrophage scavenger receptors, CD36, and is then internalized leading to the formation of foam cell and release of more proinflammatory cytokines which enhance monocyte recruitment. This recruitment of monocytes/macrophages to activated EC leading to formation of foam cells is an important step in the initiation of atherogenesis. CD36, cluster of differentiation-36; ICAM, intercellular cell adhesion molecule 1; IL-1β, interleukin-1-beta; LDL, low-density lipoprotein cholesterol; M-CSF, macrophage colony stimulating factor; ox LDL, oxidised low density lipoproteins; TNF-α, tumor necrosis factor alpha; SR-A1, scavenger receptor type 1; VCAM-1, vascular cell adhesion molecule 1.

These lipid laden macrophages are then trapped inside the arterial intima through a mechanism relying on ox LDL-mediated CD36 signaling. Specific Src kinases (such as Lyn) are activated through this signaling pathway, leading to phosphorylation and activation of focal adhesion kinase (FAK), ultimately resulting in actin polymerization (220). Within this intracellular pathway ROS productions occurs through NADPH-oxidase causing oxidative inhibition of Src homology 2–containing phosphotyrosine phosphatase (SHP-2) and persistent FAK activation, which disrupts the dynamics of cytoskeleton. As a result, of this cytoskeletal rearrangement macrophages experience an increased spreading but reduced migration, ultimately leading to their entrapment within the arterial intima (Figure 2) (220).

Another mechanism involved in oxLDL macrophage trapping is through loss of macrophage cell polarity loss. OxLDL, via CD36, triggers the retraction of front-end lamellipodia and the loss of cell polarity. This effect is attributed to oxLDL's activation of the Vav/Rac (a guanine nucleotide exchange factors that activate the Rho GTPases (Racs), pathway and the subsequent deactivation of non-muscle myosin II (Figure 2) (221). The interaction between ox LDL and CD36 continuously triggers the release of cytokines and ROS/RNS which then attract immune cell infiltrates and enlarge the ox LDL pool and foam cell formation into the arterial intima (10, 222, 223). The arterial inflammation resulting from foam cells additionally contributes to the buildup of lipids and inflammatory cells, thus facilitating the development of fatty streaks and the narrowing of the arterial lumen. Over time, the ongoing recruitment of immune cells and smooth muscle cells proliferation play a role in creating a fibrous cap that covers the fatty streak, the hallmark of established atherosclerosis (224).

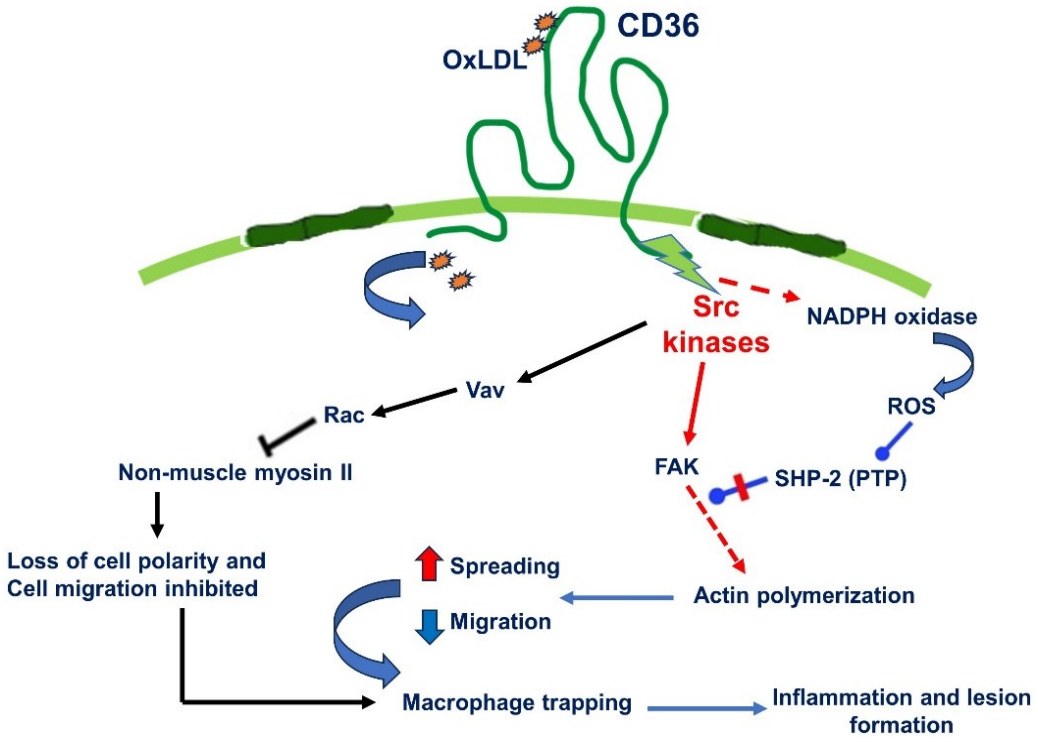

Figure 2: Illustration outlining the CD36-dependent process of macrophage entrapment in the intima. Ox LDL interacts with CD36 to activate Src kinases like Lyn, which phosphorylate and activate FAK and polymerize actin. OxLDL interactions with CD36 generate intracellular ROS via NADPH oxidase, which inactivates SHP-2 and activates FAK, interrupting cytoskeletal dynamics. This increases cell spreading and decreases migration, trapping cells in the neointima and promoting atherosclerosis development. Loss of cell polarity represents an additional mechanism for macrophage trapping. Ox LDL, mediated by CD36, triggers the retraction of front-end lamellipodia and the loss of cell polarity. This mechanism results from the activation of the Vav/Rac pathway by oxLDL, followed by the inactivation of non-muscle myosin II and macrophage trapping in the neointima. PTP, protein tyrosine phosphatase, Src homology 2–containing phosphotyrosine phosphatase (SHP-2), focal adhesion kinase (FAK), nicotinamide adenine dinucleotide phosphate (NADPH) oxidase, Vav/Rac (a guanine nucleotide exchange factors that activate the Rho GTPases (Racs).

To summarize, the prevailing body of evidence indicates that CD36 plays a pivotal role as a receptor involved in recognizing, accumulating, and metabolism of FA and lipids in various cells and tissues. Consequently, CD36 may serve as a molecular link connecting the development of

dyslipidemia, atherosclerosis and IR. If this is indeed the case, it could potentially serve as a compelling target for therapeutic interventions aimed at addressing atherosclerosis, type II diabetes, obesity, and the CVDs associated with them.

Diets rich in high-fat content contribute to the development of hyperlipidemia which leads to ED and the disruption of metabolic regulation. These factors are foundational to conditions associated with IR and CVD (225). We, as well as others, have demonstrated that CD36 is involved in obesity, atherosclerosis, and insulin IR. It plays a dual role by facilitating the uptake of ligands and promoting inflammatory signaling pathways, leading to the release of ROS and cytokines (82, 133, 226-229). The focus of this earlier research was primarily on macrophages, adipocytes, the heart, and skeletal muscle. Although a complete deletion of CD36 had a protective effect against HFD-induced obesity and IR, the specific deficiency of CD36 in macrophages, achieved through a bone marrow transplant method, did not provide protection, despite a reduction in macrophage inflammatory pathways (228). Protection against atherosclerosis was observed in cases of complete CD36 deficiency as well as specifically in macrophages (82, 226, 229).

Alterations in EC have been shown to initiate atherosclerosis enabling the prediction of atheroprone locations in the vascular system based on EC inflammation and dysfunction (230-232). Hyperlipidemia induces a pro-atherogenic environment with reduced shear stress, elevated FA levels, and the alteration of lipoprotein molecules. These modifications stimulate EC pro-inflammatory pathways, resulting in the expression of chemotactic factors for immune cells and surface receptors as illustrated in Figure 3 of our ED model. This figure elucidates the potential impact of EC CD36 on ED.

To study the role of EC transport of FAs and to assess how the absence of CD36 affects the initiation of atherosclerosis, FA uptake, and tissue metabolism, our laboratory (Dr. Febbraio) generated EC CD36-specific KO mice. This was achieved by breeding floxed (fl) CD36 mice with Tie2e cre+ mice and then generated an atherosclerosis model by crossing these mice with LDLR KO mice, leading to the creation of EC CD36 KO/LDLR KO or control fl/fl CD36 /LDLR KO mice.

Using EC CD36 KO mouse model we provided evidence that support the significant role of EC CD36 in FA uptake, regulation of systemic metabolism and the initiation of atherosclerosis. In the absence of EC CD36, we observed a decrease in atherosclerosis and noted metabolic

differences that aligned with a reduced ability to hydrolyze and uptake FA, leading to decreased FA oxidation and subsequently, a reduction in energy production.

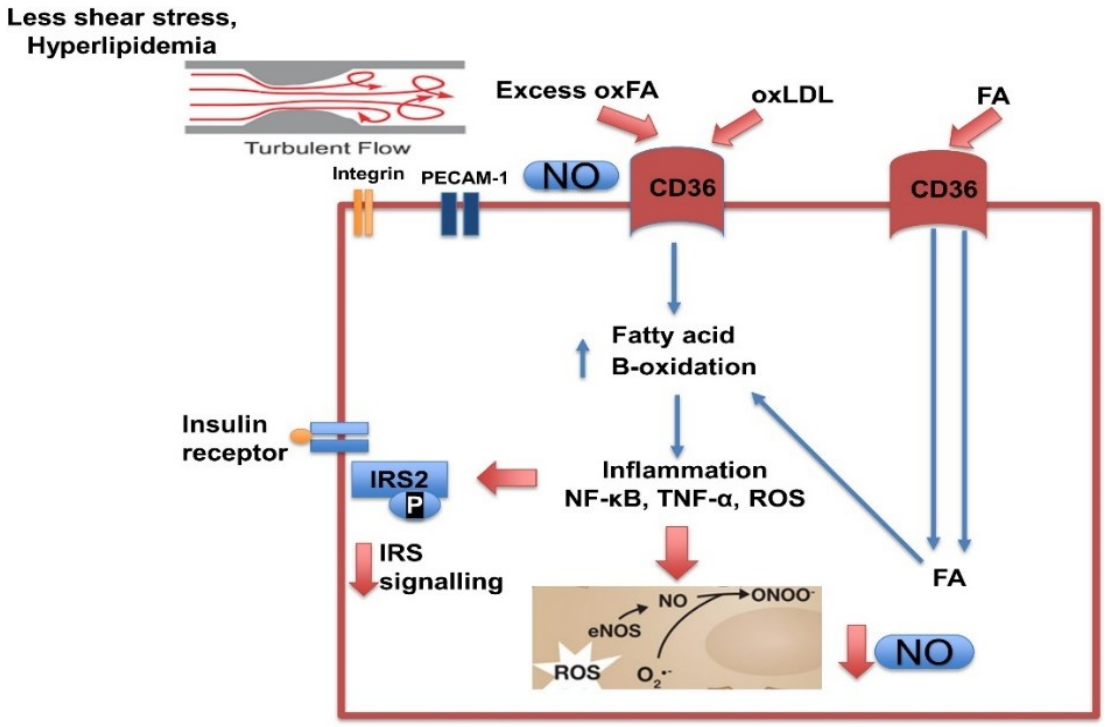

Figure 3: EC Dysfunction Model. Reduced shear stress due to turbulent blood flow caused by hyperlipidemia. is detected by endothelial mechanosensors e.g., integrins and PECAM which then signal and activate the endothelium. Hyperlipidemia combined with EC activation and increase in ROS due to reduced shear stress leads to the generation of oxidized FA and ox LDL which are ligands for CD36. It has been shown that when CD36 interacts with ox LDL or excess FA this promotes inflammation and release of cytokines and ROS. Excess FA and oxFA are associated with incomplete β-oxidation leading to inflammation which can result in IR. Increased ROS production leads to is uncoupling of eNOS, (an enzyme responsible for NO production) and reduction in NO, an important player in the maintenance of normal EC function. Platelet endothelial cell adhesion molecule-1 (PECAM-1), Nitric oxide (NO), oxidized FA (oxFA), IRS2 (Insulin receptor substrate 2, endothelial nitric oxide synthase (eNOS), Peroxynitrite ($ONOO^-$), NF-κB, (TNF-α), reactive oxy species (ROS).

1.18 Hypothesis and Objective

We studied the role of EC transport of circulating FAs and examined how the deletion of CD36 impacts the onset of atherosclerosis, EC FAs uptake and tissue metabolism. The FA uptake and metabolism play a central role in the functioning of organs like the heart, skeletal muscle, and adipose tissue (127). EC CD36 functions as a regulator for the FA uptake by parenchymal cells, leading to significant downstream implications regarding glucose utilization and insulin response ((116). The objective of this study was to determine the role of EC CD36 in FA uptake and to investigate differences in development of atherosclerosis and changes in metabolic phenotype.

We hypothesize that CD36 is a major EC receptor of FAs and proinflammatory atherogenic ligands, and that its metabolic phenotype seems to exhibit differences in atherosclerosis that appear to correlate with changes in EC inflammation and FA uptake.

Chapter 2 - Materials and Methods

2.1 Ethics

All animal procedures were prior approved by the University of Alberta Animal Care and Use Committee AUP # 0001953,0570 (Febbraio). Procedures were performed in accordance with Canadian Council on Animal Care guidelines concerning care, use and euthanasia.

2.2 Generation of EC CD36 KO/LDLR KO Mouse Model to Study the Role of EC CD36 in Atherosclerosis and FA Metabolism

To investigate the role of loss of EC CD36 on atherosclerosis and FA metabolism, our laboratory (Dr. Febbraio) generated floxed (fl) CD36 mice in the C57Bl/6j genetic background. This was achieved by specifically targeting exon 2, which contains the translation start site and the first transmembrane domain. The inclusion of exon 3 was needed due to its proximity, as previously described (156) and shown in Figure 4.

The targeting vector was engineered to generate fl/fl CD36 mice for the creation EC specific CD36 KO mice. The vector was constructed using the lox-p sites, a 34 base pair sequence upstream and downstream of the target gene. These sites were inserted because they are specialized binding sites for the cre recombinase (enzyme system used to knock out a gene), which binds to these sites and recombines them. To positively select the embryonic stem cells (ES) with lox p sites, a neomycin resistant cassette was also inserted into the vector. The targeting vector was then electroporated into the ES cells, where the plasma membrane allows the vector to enter and bind to the DNA by homologous recombination upstream and downstream of the targeted gene.

Subsequently, the ES cells were subjected to neomycin antibiotic treatment, wherein the cells that successfully incorporated the neomycin cassette were selectively retained while the remaining cells were eliminated. The confirmation of homologous recombination was achieved through polymerase chain reaction (PCR) analysis. Following that, the ES cells were introduced into the blastocyst, which was then transplanted into the embryo of wild type (WT) mice. In order to determine the germline transmission, the chimera mice were subjected to mating with WT mice, followed by breeding with Flp recombinase mice to eliminate the neo cassette and obtain the fl mice These fl mice were then bred to EC specific Tie2e cre + mice **(233, 234)** and this breeding strategy resulted in the generation of EC CD36 KO mice. Subsequently, the EC CD36 KO mice were bred with LDLR KO mice (a well-established model in the field of atherosclerosis) to get EC

CD36 KO/LDLR KO and the littermate controls fl/fl CD36/LDLR KO. The genotypes of these mice were verified by PCR.

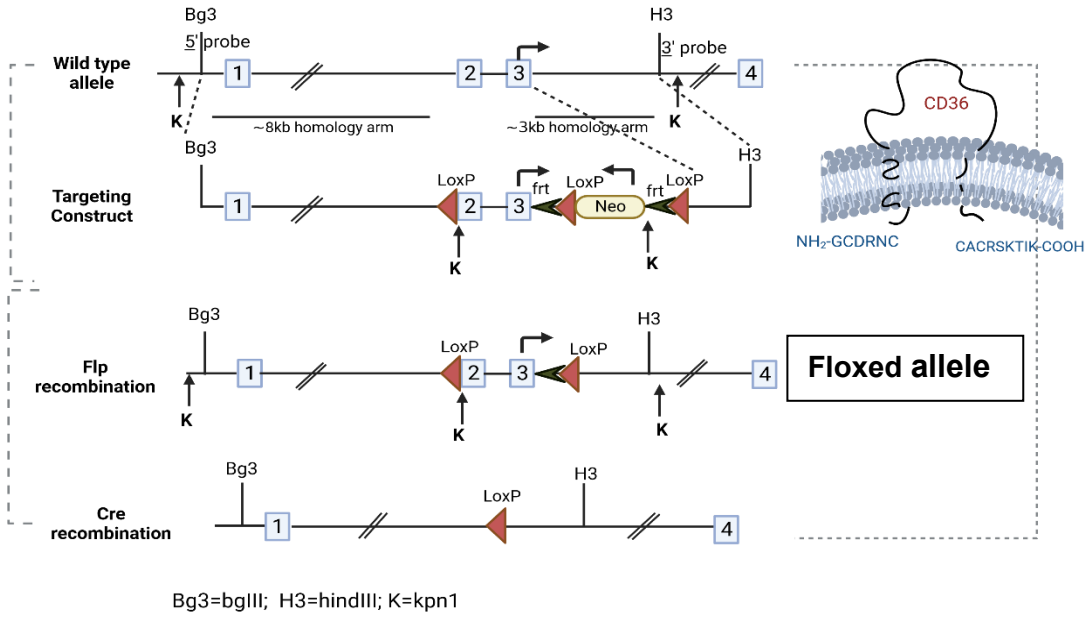

Figure 4: Generation of CD36 KO mice. Fl/fl CD36 mice generated by homologous recombination in ES cells by using a targeting construct (WT=endogenous allele). The genome was altered to include both lox P sites (shown by black arrows) and FRT sites (indicated by grey arrows). Flanking the Neo gene are the FRT sites, inserted to enable the selection of embryonic stem (ES) cells. Neo gene was then removed using FLP recombinase. Fl CD36mice were created by injecting fl CD36 ES cells into blastocysts. Exons 2 and 3, which resulted in a null allele, were then deleted using cre recombinase excision. Bg3 and H3 are restriction enzyme sites for BglIII and HindIII, respectively. The direction of transcription/translation is represented by black arrows.

2.3 Genotyping and Gel Electrophoresis

Identification and genotyping were accomplished by performing tail DNA analysis of the animals. The digestion process involved immersing each sample in a solution consisting of 200µl of 0.1M EDTA, 1% sodium dodecyl sulphate (SDS), 0.1M NaCl, 0.05M Tris, pH 7.5, supplemented with 100 ng/ml of proteinase K (#39450-01-6, Sigma Aldrich). The digestion process was carried out overnight in a water bath maintained at a temperature of 55 °C. Serial

extraction with equal volume Tris-saturated phenol (#108-95-2, Thermo Fisher Scientific,) and chloroform (#67-66-3, Thermo Fisher Scientific,) separated nucleic acids from protein and other tissue constituents. The DNA was then precipitated with two volumes of 100% ethanol. The pellet underwent air drying and was subsequently resuspended in a solution consisting of 100 µl of Tris-EDTA (0.01M Tris, pH 8, 0.001M EDTA) supplemented with 20 ng per ml of RNAse. A. PCR was performed using DNA dilutions at a ratio of 1:100.

To perform PCR the primers used were, WT primers (~600 base pairs), 5' CAGCTCATACATTGCTGTTTATGCATG; 3' GGTACAATCACAGTGTTTTCTACGTGG and CD36 KO primers (~800 base pairs), 5' CAGCTCATACATTGCTGTTTATGCATG ;3' CCGCTTCCTCGTGCTTTACGGTATC and for LDLR, WT primers (~351 base pairs), 5' TATGCATCCCCAGTCTTTGG, 3' CTACCCAACCAGCCCCTTAC and LDLR KO (~179 base pairs), 5' TATGCATCC CCA GTCTTT GG, 3' ATAGATTCGCCCTTGTGTCC.

The final master mix was prepared using the Ready-to-use PCR master mix (2X) (DreamTaq Green, K1082, Thermo Fisher Scientific). The PCR master mix comprised of DreamTaq DNA polymerase, 2X DreamTaq green buffer, deoxyribose nucleotide triphosphate (dNTPs), and a solution of magnesium chloride with a concentration of 0.004M. The final master mix was prepared using sterile PCR grade water and comprised of 1X PCR master mix and 1µm of each primer. Reactions were conducted using a volume of 10 µl. The samples were then processed using the PCR thermocycling protocol outlined in Table 1, using a model T100 Thermal Cycler (Bio-Rad).

Table 1. PCR thermocycler protocol

Temperature (°C)	**Time**
94 (denature)	2 minutes
94 (denature)	30 seconds
54 (anneal)	30 seconds
72 (extension)	60 seconds
Repeat	34x
72 (extension)	10 minutes
4	hold

For visualization, we resolved the PCR products on a 1.5% agarose (#9012-36-6, Thermo Fisher Scientific,) gel with 0.85 M ethidium bromide (BP1302-10, Thermo Fisher Scientific) gel. Tris-borate-EDTA (TBE) was employed as the running buffer, consisting of a solution containing 0.089M Tris, 0.089M Boric acid, and 0.002M EDTA. For molecular weight determination, a Gene Ruler 1 kilobase (kb) DNA ladder (# SM1331, Thermo Fisher Scientific) was loaded. and for 25 minutes, samples were electrophoresed at a constant amperage of 15 mA. The gel pictures were captured using the ChemiDoc Imaging system (ChemiDoc MP Imaging System, version 4.1, Bio-Rad) with UV light.

2.4 Experimental Design

In our study, six to eight-week-old EC CD36 KO/LDLR KO and fl/fl CD36/LDLR KO control mice were fed a high fat, high cholesterol diet for 3 6- and 16-weeks weeks for atherosclerosis studies with separate cohorts of male and female mice being studied at each time. The 3 and 6-weeks time points were chosen to address the hypothesis that EC CD36 has a role in lesion initiation. Fasting glucose and weights were measured before euthanasia at 3 and 6 weeks. Following that, blood was taken as previously described to isolate plasma, which was then refrigerated at -20 ºC. Plasma was then used to assess 3-nitrotyrosine (3-NT), triglycerides (TG), total and free cholesterol levels, glucose tolerance test (GTT) and fast protein liquid chromatography (FPLC). Later, at 16 weeks, the aortas of the mice were isolated to perform aorta morphometry as described above. Study design is depicted in Figure 5.

To determine the impact of loss of EC CD36 on metabolism. Four-week-old fl/fl CD36 and EC CD36 KO mice were housed and kept in metabolic cages. The mice were fed a normal chow (NC) diet, and the Comprehensive Laboratory Animal Monitoring System (CLAMS) (Columbus Instruments) was used for indirect calorimetry. After 4 weeks fasting glucose and weights were measured before euthanasia. Following that, plasma was isolated and later used to perform untargeted metabolomics by chemical isotope labeling (CIL) liquid chromatography mass spectrometry (LC-MS) and blood was used for flow cytometry (Figure 5).

We also investigated the effect of loss of EC CD36 in a diabetogenic scenario, feeding the mice ingredient-matched diets containing 10% and 45% fat for 12 weeks. GTT was performed at

8 weeks' time point and after 12 weeks, the mice were sacrificed and blood was drawn to extract plasma as discussed above to perform TG, cholesterol assay and FPLC (Figure 5).

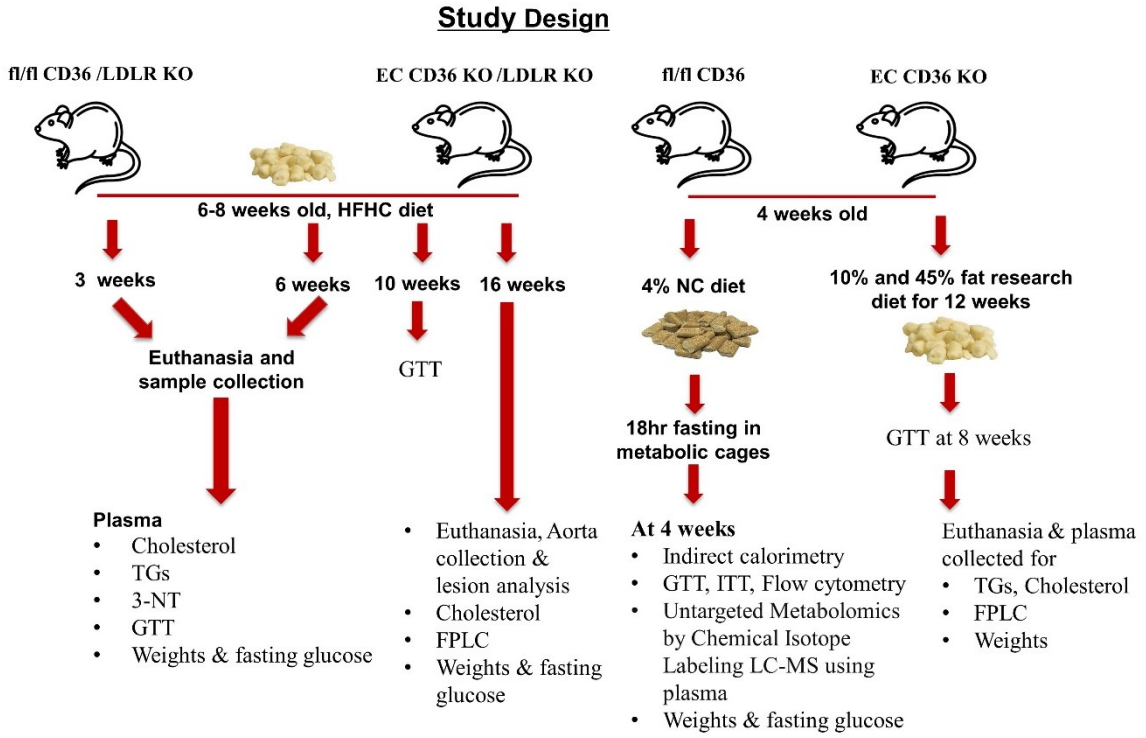

Figure 5: Experimental design to study the role of loss of EC CD36 on atherosclerosis and FA metabolism. Six to eight weeks old, EC CD36 KO/LDLR KO and fl/fl CD36/LDLR KO mice were fed high fat high cholesterol (HFHC) diet for 3, 6, and 16 weeks for atherosclerosis studies (different cohorts) followed by euthanasia and sample collection (plasma and aorta). For metabolic analyses, 4 weeks old EC CD36 KO mice were fed with NC for 4 weeks and ingredient-matched diets for 12 weeks followed by euthanasia and plasma collection.

2.5 Diets

EC CD36 KO/LDLR KO and fl/fl CD36/LDLR KO mice were fed a diet containing 42.7 kilocalorie (kcal) % carbohydrate, 42 kcal% fat, and 1.25% added cholesterol (TD 96121, Envigo) for 3, 6, and 16 weeks for atherosclerosis studies. This diet was used previously in CD36 KO/LDLR KO studies to induce CD36-dependent atherosclerosis **(216, 226, 235)**. For metabolic

analyses, mice were fed a low fat (4%) NC and ingredient-matched diets containing 35 kcal% carbohydrate and 45 kcal% fat (D12451, Research Diets, Inc.) or 70 kcal% carbohydrate and 10 kcal% fat (D12450H, Research Diets, Inc.); the amount of sucrose is the same in both the diets (691 kcal%).

2.6 Total and Free Cholesterol Measurement in EC CD36 KO/LDLR KO Mice

To measure total and free cholesterol in the plasma of these mice two separate colorimetric assay kits (#99-02601, #993 – 02501, Wako chemicals, Fujifilm, Japan) were used. In the total cholesterol assay, cholesterol ester hydrolase hydrolyzes serum cholesterol esters to free cholesterol and FA. Together with the already free cholesterol, newly released cholesterol was oxidized by cholesterol oxidase to generate hydrogen peroxide. Hydrogen peroxide formed then participates in a reaction that produces a blue pigment in the presence of peroxidase, 3,5-dimethoxy-N-ethyl-N-(2-hydroxy-3-sulfopropyl)-aniline sodium salt, and 4-aminoantipyrine. The amount of cholesterol in the sample is determined by measuring the absorbance of the blue colour.

To perform the assay, a colour reagent solution was prepared by dissolving its contents in the buffer solution provided in the assay kit. A standard solution was prepared by 1:1 dilution of the provided standard in deionized water. Cholesterol standards were then prepared by serial dilution in the concentration range of 100 mg/dL – 1200 mg/dL. Blank wells only received the colour reagent solution, 2 µl of the plasma samples were loaded in duplicates as per the planned 96 well plate layout. Next, 300 µl of the prepared colour reagent solution were added in each well using a multichannel pipette and this was followed by incubation of the plate at 37 ºC for 5 min. Following incubation readings were taken at an interval of every 5min for 45 min at a wavelength of 600 nm, using a Synergy™ H1 Multimode Microplate Reader (Agilent BioTek SH1MSN). Data were analyzed using Gen 5 2.07 software. The results were averaged between duplicate wells and the mean OD of the blank was subtracted from the standard, control and sample wells.

To determine the proportion of free cholesterol in plasma, the cholesterol oxidase reaction was utilized to produce hydrogen peroxide in the same way as total cholesterol is produced. A 96 well plate was used to perform this assay. Colour reagent solution was prepared by dilution in the buffer solution provided in the kit. Cholesterol standards were prepared in the concentration range of 50 mg/dL – 400mg/dL by serial dilution using the standard stock solution diluted 1:1 in

deionized water. Blank wells only received the colour reagent solution. 5 µl of the plasma samples were loaded in duplicate as per the planned 96 well plate layout. Afterwards, 300 µl of the prepared colour reagent were added to each well using a multichannel pipette and this was followed by incubation of the plate at 37 ºC for 5 minutes. After incubation absorbance was measured immediately and continued for 45 minutes at 5 minutes intervals using a Synergy™ H1 Multimode Microplate Reader (Agilent BioTek SH1MSN) at a wavelength of 600 nm and analyzed using Gen 5 2.07 software. The results were averaged between duplicate wells and the mean OD of the blank was subtracted from the standard, control and sample wells.

2.7 TG Measurement in EC CD36 KO/LDLR KO Mice

Triglyceride levels were also measured using a colorimetric assay kit (#290-63701, Wako chemicals, Fujifilm, Japan). Lipoprotein lipase catalyzes the hydrolysis of TG into glycerol and FA. Triglycerides are broken down into their primary components, glycerol and fatty acids, by this enzyme. Glycerol kinase then transforms glycerol to glycerol-3-phosphate, which is oxidized by glycerol-3-phosphate oxidase to generate hydrogen peroxide and produce, blue pigment as previously described.

To perform the triglyceride, assay a colour reagent solution was prepared by dissolving the chromogen substrate in the buffer provided in the assay kit. A standard solution was prepared by 1:2 dilution of the provided standard in deionized water. This was followed by preparation of the triglyceride standards in the concentration range of 100 mg/dL – 888 mg/dL by serial dilution. Blank wells only received the colour reagent solution. 2 µl of the plasma samples were loaded in duplicate as per the planned 96 well plate layout. Next, 300 µl of the prepared colour reagent solution were added to each well using a multichannel pipette. The plate was incubated at 37 ºC for 5 min. Absorbance and data were obtained in the same way as for cholesterol assay described above.

2.8 3-NT ELISA in EC CD36 KO/LDLR KO mice

An ELISA 3-NT kit (# NBP2-66363, Novus Biologicals) was used for quantitative determination of 3-NT concentrations in plasma samples of EC CD36 KO/LDLR KO and fl/fl CD36/LDLR KO mice. For this competitive ELISA method as depicted in Figure 6, a 96 well

micro-plate provided in the kit has been pre-coated with 3-NT (a marker of peroxynitrite), an important indicator of inflammation, and NO production.

In this assay 3-NT in the sample or standard competes with a fixed amount of 3-NT antigen labelled on the plate for sites on the Biotinylated Detection Ab specific to 3-NT. Unbound antibody is washed. (The more antigen in the sample, the less antibody will be able to bind to the antigen in the well). Then, Avidin conjugated to HRP is added to each well followed by addition of the Substrate Reagent. Further, the enzyme-substrate reaction is terminated by adding Stop Solution and the color change can be measured spectrophotometrically.

To perform this assay first a stock solution of 100 ng/ml by adding 1 ml of reference standard and sample diluent was prepared This was followed by making of serial dilutions in the concentration range of 0 ng/ml-100 ng/ml. Biotinylated detection antibody 1X working solution was prepared and 50 µl of plasma and standards were loaded in duplicates as per the 96 well plate layout. Immediately, 50 µl of the detection antibody was added. into each well except the blank one and the plate was covered with sealer and incubated for 45 min at 37°C. Afterwards, 100 µl of HRP Conjugate followed 90 µl of Substrate reagent was added into each well and in between these two steps washing and incubation was performed as specified in the protocol. Finally, 50 µl of Stop solution was added into each well and to determine the OD of the samples the plate was immediately read and continued for 45 minutes at 5 minutes intervals using a Synergy™ H1 Multimode Microplate Reader (Agilent BioTek SH1MSN) at a wavelength of 450 nm and reactions were monitored and analyzed using Gen 5 2.07 software. Duplicate readings from each standard and samples were averaged and the mean OD of the blank was subtracted from the standard, control and sample wells.

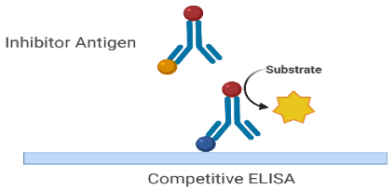

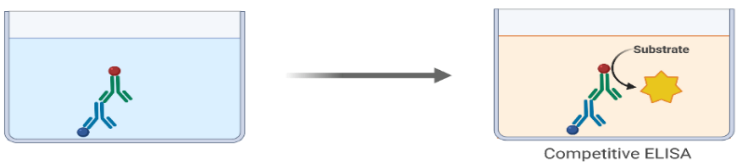

Figure 6: 3-NT competitive ELISA assay mechanism. Sample and reference antigens compete for labelled antibody binding. A multi-well plate is pre-coated with reference antigen and sample is pre-incubated with labelled antibody. More or less free antibodies will bind the reference antigen depending on the sample's antigen content. As the sample contains more antigen, less reference antigen will be recognized, and the signal will be weaker.

2.9 Lipoprotein Analysis in EC CD36 KO/LDLR KO Mice

For lipoprotein analyses prior to sacrifice mice were fasted overnight. The analyses were performed by the Lipidomics Core Facility, part of the Faculty of Medicine and Dentistry at the University of Alberta, Edmonton, Canada which receives financial support from the Faculty of Medicine & Dentistry, the Women and Children's Health Research Institute, and Canada Foundation for Innovation awards to contributing investigators. The plasma cholesterol and triglycerides distribution among the VLDL, LDL, and HDL fractions were measured using FPLC (236, 237).

Plasma aliquots (15 µl for cholesterol analysis; 27 µl for triglyceride analysis) was injected by auto sampler into an Agilent 1200 HPLC instrument that was outfitted with a Superose 6 HR 10/300 gel-filtration FPLC column. The FPLC system isolate the lipoproteins based on their size. An in-line assay for total cholesterol (Cholesterol-SL reagent from Sekisui Diagnostics, 234-60) or triglycerides (Triglyceride-SL reagent from Sekisui Diagnostics, 236-60) was performed using post-elution reactions at 37°C. These reactions were monitored in real-time at 505 nm, with data analysis performed using Agilent ChemStation software. The first, second, and third peak were attributed to VLDL, LDL and HDL respectively, and the area under each peak was calculated.

2.10 Glucose Tolerance Testing (GTT)

To perform GTT mice were fasted overnight for approximately 12-16 hours and were transferred to clean cages with no food or faeces present in the cage. After weight recording the mice received an intraperitoneal injection of 2 mg glucose/g of body weight. Blood was drawn from a tail vein at 10, 20, 30, 60, 90 and 120 min after the administration of glucose. Glucose was measured using an ACCU-CHEK Advantage Glucometer.

2.11 Insulin Tolerance Testing

To perform insulin tolerance test (ITT), mice were fasted for 4 hours and then given an intraperitoneal bolus of 0.75 U insulin (Novolin; Novo Nordisk, Canada) per kilogram of body weight. Blood glucose levels were measured at 0, 15, 30, 60, and 120 min from tail vein blood with an ACCU-CHEK Advantage glucometer. Between each of these time points, mice were returned to their cages and monitored continuously.

2.12 Indirect Calorimetry

Four-week-old fl/fl CD36 and EC CD36 KO mice were housed and kept in metabolic cages. The mice were observed over a 12-hour light: 12-hour dark cycle (0600-1800 light) with ad libitum access to food (NC) and water after a 24-hour acclimatization period. The CLAMS was used for indirect calorimetry. Respiratory exchange ratio (RER), defined as the ratio of carbon dioxide to oxygen generation, was used to determine the percentage contribution of fat (RER = 0.7) and carbohydrates (RER = 1) to total body energy metabolism. The cumulative activity of the mice was determined by summing the Z counts for rearing or jumping with the total counts for stereotyped behaviours such as grooming and scratching, as well as ambulatory mobility. The freely available web-based software tool CalR was used to evaluate the data (238).

2.13 Flow Cytometry

Flow cytometry analysis was conducted on mouse blood samples. In order to acquire single-cell suspensions, spleen samples were ground between sterile frosted glass slides in 7ml of red blood cell lysis buffer. The red blood cell lysis buffer consisted of 0.15mM NH_4Cl, 10mM $KHCO_3$, and 0.1mM disodium ethylenediaminetetraacetic acid, with a pH of 7.2. Subsequently, the resulting mixture was filtered through sterile nylon mesh. Red blood cell lysis buffer was applied twice to whole blood collected by cardiac puncture. After washing, cell pellets were resuspended in PBS containing 2mM EDTA and 0.5% bovine serum albumin. Fluorophore-conjugated antibodies with specificity to mouse cell antigens were as follows: anti-CD11b (M1/70) (# 550993, BD Biosciences), anti-CD11c (HL3) (#561022, BD Biosciences), anti-SiglecF (E50-2440) (#552125, BD Biosciences), anti-Ly6G (1A8) (#561236, BD Biosciences), anti-CD36

(JC63.1) (#10009870, Cayman Chemical). Live/dead fixable dead cell stains (Thermo Fisher Scientific) were used to exclude dead cells. CD11b+/c+ cells were analyzed for CD36 expression. Paraformaldehyde-fixed cells were acquired using a BD LSR Fortessa flow cytometer (BD Biosciences, University of Alberta Flow Cytometry core) and analyzed with FlowJo (version 10) software.

2.14 Untargeted LC-MS Metabolomics Analysis

For metabolomic analysis, 4 weeks old mice fed with low fat,4% NC diet. were fasted overnight prior to sacrifice and plasma was collected as discussed above. The mice plasma samples were sent for untargeted metabolomics by CIL LC-MS using 4 channels analysis, to The Metabolomics Innovation Centre, University of Alberta, Edmonton, Canada.

For plasma samples, metabolites were first extracted via methanol protein precipitation with three volumes of cold methanol. Four chemistries were used to derivatize metabolites from different submetabolomes: dansylation for amines/phenols, p-dimethylaminophenacyl (DmPA) bromide labeling for carboxylic acids, base-activated dansylation for hydroxyls and dansylhydrazine (DnsHz) labeling for carbonyl metabolites.

After chemical isotope labeling, a control or pooled sample was prepared by mixing aliquots of individual samples and was labeled by ^{13}C-reagent. This ^{13}C-labeled control served as the internal standard and was spiked into all ^{12}C-labeled individual samples as reference, generating the ^{12}C -/^{13}C -labeled mixtures. This mixing of ^{12}C-labeled samples and ^{13}C-labeled pooled was based on liquid chromatography ultraviolet (LC-UV) quantification of dansylated metabolites for sample amount normalization (239). These light and heavy labeled derivatives were shown as a peak pair in the mass spectra, and the relative quantification is done using the peak ratio of the individual peak pairs.

Labelled plasma extracts were analyzed using an Agilent 1290 LC linked to Bruker Impact II QTOF Mass Spectrometer (Agilent, Palo Alto, CA). The samples were injected onto an An Agilent eclipse plus reversed phase C18 column (100 × 2.1 mm, 1.8 µm particle size,). For LC-MS, LC solvent A was 0.1% (v/v) formic acid in water, and solvent B was 0.1% (v/v) formic acid in ACN. The gradient was: 0 min 25% B, 10 min 99% B, 15 min 99% B, 15.1 min 25% B, 18 min 25% B. The flow rate was 400 µl/min. The column temperature was kept at 40 ºC. All MS spectra

were collected in positive ion mode with a scan range of m/z 220 to 1000 at a spectral acquisition rate of 1 Hz. All the samples were injected in random order. Quality control samples and amino acid standards were injected every 9 sample runs to monitor the performance of the LC-MS. The sample injection volume was fixed at 25 µL except in the injection amount optimization experiment where the injection volume varied. Data analysis was performed using IsoMS Pro 1.2.16 (NovaMT Inc.) and NovaMT Metabolite Database v3.0.

A control or a pooled sample was prepared by mixing aliquots of individual samples and was labeled by ^{13}C-reagent. This ^{13}C-labeled control served as the internal standard and was spiked into all ^{12}C-labeled individual samples according to the liquid chromatography ultraviolet (LC-UV) quantification result using the normalization method. Further, the ^{12}C -/^{13}C -labeled mixtures were generated and analyzed using LC-MS. These light and heavy labeled derivatives were shown as a peak pair in the mass spectra, and the relative quantification is done using the peak ratio of the individual peak pairs. To analyse the data a web based free software MetaboAnalyst was used.

2.15 Time to Thrombosis and Hemoglobin (Hb) Assay

Mice were anesthetized through the administration of an IP injection mixture containing ketamine/xylazine (100 mg/kg ketamine and 10 mg/kg xylazine in a volume of 100 µl). The tail of the mouse, marked at 1 mm from the tip, was immersed in a 15 mL conical tube containing PBS for 2 minutes at 37˚C. Subsequently, the tail was cut at the marked point, and blood was collected in a 15 mL conical tube with PBS at 37˚C, with the bleeding time noted until cessation. Furthermore, 200 µl of blood was transferred to a 96-well plate, and absorbance was measured at an OD of 550 nm using the Synergy™ H1 Multimode Microplate Reader (Agilent BioTek SH1MSN) (This assay was performed and analysed by Dr. Mohamed Omar)

2.16 Dual-Energy X-Ray Absorptiometry (DEXA)

The assessment of fat body mass was conducted utilizing DEXA (Faxitron, model DXA UltraFocus, Hologic) following the manufacturer's guidelines. The acquisition, image processing, and analysis procedures were carried out using the accompanying Faxitron Vision software (Faxitron Bioptics LLC.) (This experiment was performed and analysed by Dr. Linnet Immaraj).

2.17 Impact of a CD36 Inhibitor on *P. gingivalis* Mediated Atherosclerosis Study

2.18 Animals

To study the impact of a CD36 inhibitor on *P. gingivalis* mediated atherosclerosis, six to eight-week-old LDLR KO mice (10x backcrossed to C57Bl/6J; B6.129S7-Ldlr^{tm1Her}/J, strain # 002207, The Jackson laboratory) were maintained and bred in a specific pathogen-free facility. The University of Alberta Health Sciences Laboratory Animal Services (HSLAS) housed and cared for all mice. An important characteristic of the LDLR KO strain is that mice do not develop atherosclerosis unless they are fed a high fat diet. (226, 240).

2.19 Experimental Design and *P. gingivalis* Infection

The number of mice was determined by performing a power calculation analysis using this website http://www.statisticalsolutions.net/pss_calc.php. Based on a prior study conducted in our laboratory where male LDLR KO mice infected with *P.gingivalis* developed a mean atherosclerotic lesion area of 7% and *P.gingivalis*-infected CD36 KO/LDLR KO mice showed a 14% mean lesion area (216), our power calculation indicated the group size per treatment to be 13 (80% power, alpha = 0.05).An extra 3 mice per group were included because these were long studies and there was the potential for malocclusion, dermatitis, and complications due to multiple intraperitoneal (IP) injections/anesthesia.

In this study, only male mice, were used because in the previous study (216) no difference was found based on sex. These mice were fed a high fat, western diet (Harlan Teklad 88137, Envigo) *ad libitum* (21 % fat, 0.15 % cholesterol, no cholate) for 16 weeks to induce atherosclerosis. This diet has been extensively utilized to promote atherosclerosis lesion development in LDLR KO mice (216, 241, 242). To induce *P.gingivalis* infection, *P.gingivalis* (American Type Culture Collection (ATCC ®) strain #33277^{TM}) bacteria were grown under anaerobic conditions (Mitsubishi AnaeroPack™ 2.5L anaerobe jar, Thermo-Scientific R685025; AnaeroPack™/Anaero Anaerobic Gas Generator, Thermo-Scientific R681001) in Schaedler broth (BBL Schaedler Broth with Vitamin K1, L007496, Becton Dickinson) containing 1 % vitamin K1

and hemin for 24-48 hours until the optical density (OD) of the culture reached 1.3 at 660 nm (approximately 10^9 CFU/ml). The Schaedler's broth components are listed below in Table 2.

Table 2. Schaedler's Broth with Vitamin K1 and Hemin*

Reagents	Amount
Casein	8.1g
Peptic digest of animal tissue	2.5g
Papaic digest of soybean meal	1.0g
Dextrose	5.82g
Yeast extract	5.0g
Sodium chloride	1.7g
Dipotassium phosphate	0.82g
Hemin	0.01g
Vitamin K1	0.01g
L-cystine	0.4g
TRIS aminomethane	3.0g
Milli-Q water	Up to 1000ml

*Autoclaved for 15 minutes at 121°C, pH 7.6 ± 0.2 at 25 °C

Bacterial cultures grown to saturation were centrifuged at 20,000 x g for 5minutes. Cultured *P. gingivalis* were then resuspended at a concentration of ~2×10^9/ml in sterile phosphate-buffered saline (PBS) containing 2 % carboxymethyl cellulose which is a thickener to promote bacterial adherence before oral inoculation of mice. Mice were then orally lavaged with 200 µl carboxymethyl cellulose containing *P. gingivalis* by using a micro applicator brush, at the gingival margin throughout the mouth, on alternate days for two weeks (7 inoculations). After oral lavage, mice were allowed to recover on a heat pad prior to return to their cages. This procedure was performed in a level 2 biocontainment facility at HSLAS. Prior to lavage the mice were anesthetized to surgical plane by administering an IP injection mixture of ketamine/xylazine (100

mg/kg ketamine and 10 mg/kg xylazine in a volume of 100 µl). The oral lavage protocol was adapted from the method by Lalla *et al.* (243).

Simultaneously, both groups of the mice were administered the drug, AP5055 which was synthesized by The Centre for Drug Research and Development (Vancouver, BC), at >95% purity, as determined by liquid chromatography-mass spectrometry. The chemical structure of the AP5055, a CD36 inhibitor is represented in the Figure below (Figure 7) (244). One-half of the mice received an IP injection of AP5055 (1 mg/kg) in 1 % dimethyl sulfoxide (DMSO), and the other half received an IP injection of the vehicle alone (1 % DMSO), every other day starting from day one and continuing for 16 weeks. Mice were weighed every week and checked for any adverse effects of the drug. After 16 weeks mice were fasted overnight and euthanized by pentobarbital overdose (200 mg/kg IP, Euthanyl, BiMeda-MTC Animal Health Inc, 00141704) followed by bilateral thoracotomy, according to Canadian Council on Animal Care guidelines.

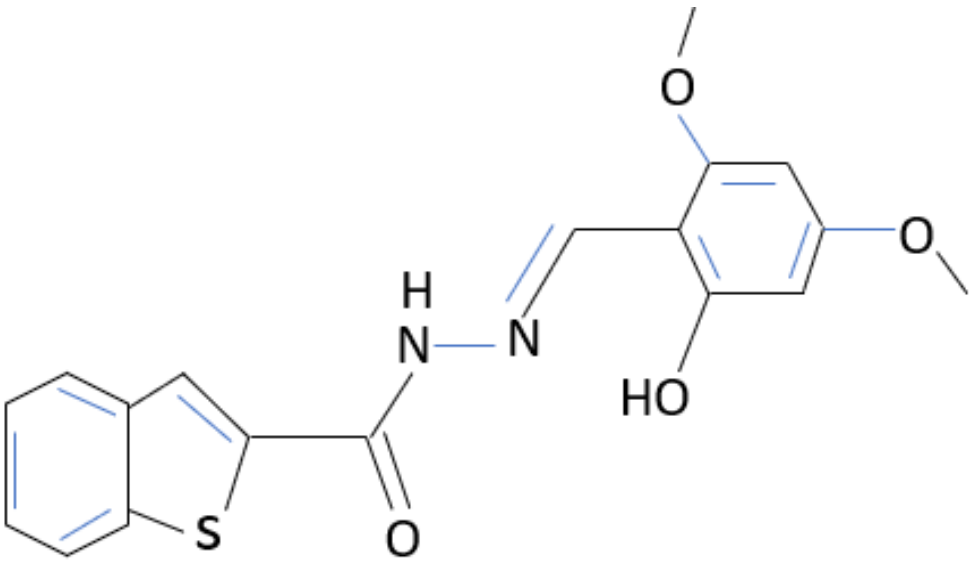

Figure 7: Chemical structure of the drug, AP5055.

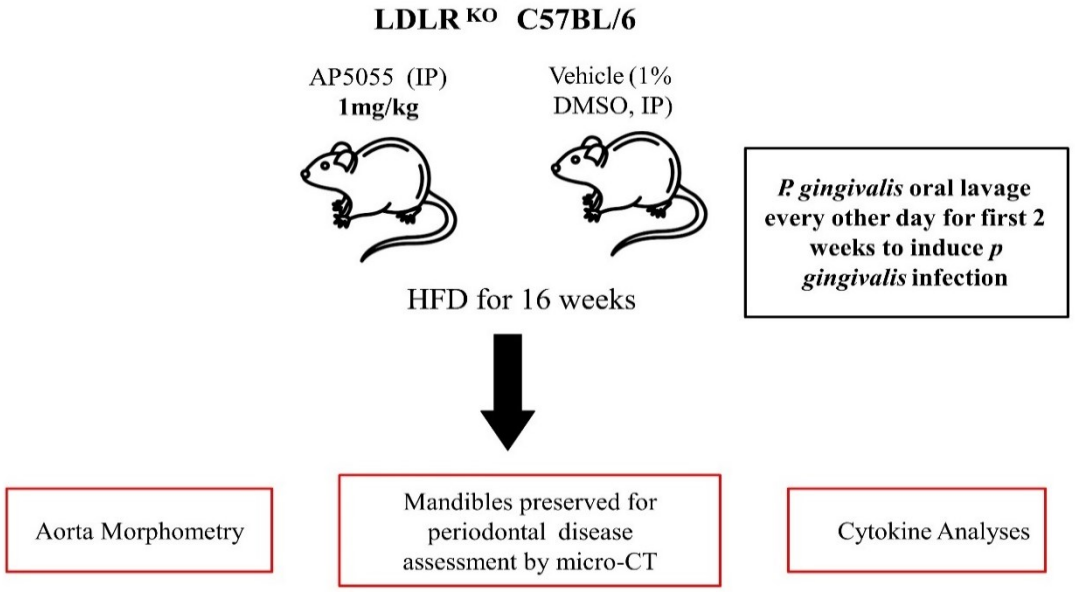

Figure 8: Experimental design to study the impact of a CD36 inhibitor on *Porphyromonas gingivalis* mediated atherosclerosis. LDLR KO mice were fed with high fat diet (HFD) for 16 weeks to induce atherosclerosis and *P. gingivalis* oral lavage was given every other day for the first 2 weeks to induce *P. gingivalis* infection. Half of the mice received the drug AP5055 IP on alternate days, and the other half or the sham mice, received the vehicle, 1% DMSO IP. At 16 weeks mice were sacrificed and aortas were dissected to perform aorta morphometry and lesion burden was determined. Blood was collected to perform cytokine array and mandibles were used to perform micro-CT and immunofluorescence.

2.20 Sample Collection

After euthanization approximately 1ml of blood for plasma analyses (cytokine array) was drawn from the heart using cardiac puncture technique. The blood was collected using a 1 cc syringe containing 80 µl ethylenediaminetetraacetic acid (EDTA), to a final concentration of 4 mM. Blood was centrifuged at 3,800 x g for 5 min to separate plasma which was collected, aliquoted and frozen at -20 ºC. Aorta was carefully isolated to perform aorta morphometry followed by collection of mice heads for micro-CT and later mandibles were used to assess bone loss and to perform immunofluorescence.

2.21 *En face* Aortic Morphometric Analysis in LDLR KO Mice

Following euthanasia of mice, the vasculature was perfused through the heart with 10 ml PBS followed by 5 ml buffered formalin (Formaldefresh, Thermo Fisher Scientific). The entire aorta from the heart, including the subclavian, right and left carotid arteries, and extending 2-5 mm after bifurcation of the iliacs, was dissected free of fat and post-fixed in buffered formalin for 24 hours at 4°C and then stored in PBS at 4°C.

Aortae were stained in a microcentrifuge tube containing oil red-O, (#00625, Millipore 442 Sigma) for 30min and then de-stained in another microcentrifuge tube filled with methanol for 1–2 minutes with agitation. Oil red-O was used to identify neutral lipids in plaque, to quantify lesion burden. After staining, the aorta was placed on a glass slide, hydrated with PBS under a microscope (model DM2000, Leica Microsystems) and was gently cut through its lumen using tweezers and Noyes spring scissors (Fine Science Tools, #15012-12) starting from the trifurcated aortic branches down to the iliac arteries. This was followed by opening and flattening the aorta on the glass slide using tweezers and avoiding disturbance of the plaque present in the aorta. Afterwards, a cover slip was placed on the aorta in PBS. This was followed by digital scanning of the aorta.

En face morphometry was performed in a blinded fashion. Using the Adobe Photoshop software firstly, the auto levels of the image were adjusted, and the black colour was selected. Afterwards the invert selection tool was used to select the inverse of the current selection. Total image pixels (red + white) were determined by the histogram followed by deselection of the invert option. Further, only red lesions on the aorta were selected and the values were recorded. Three independent measurements of lesion area (red pixels) were selected and averaged for each aorta. The lesion area was expressed as mean percent ± SE of total aortic area (Figure 9).

Figure 9: Representative image of *en face* oil red O-stained aorta.

2.22 Cell Culture and Secreted Alkaline Phosphatase (SEAP) Promoter Activity Assay

All cell culture procedures were performed using sterile materials in a level 2 biosafety cabinet. RAW-Blue cells (InvivoGen) which are derived from murine RAW 264.7 cells, a mouse macrophage-like line and express Toll like receptor-2 (TLR-2), CD36 and a nuclear factor kappa-light-chain-enhancer of activated B cells (NF-κB) SEAP reporter construct, were cultured in Dulbecco's Modified Eagle's Medium (DMEM) (#SH 30081.01, Hyclone) supplemented with 10% heat-inactivated fetal bovine serum (FBS) and 100 U/mL penicillin and 100 µg/mL streptomycin at 37° C with 5% CO_2 in a humidified incubator.

2.23 Cell Growth and Maintenance

These cells were grown on non-treated cell culture plates which does not facilitate cell attachment. To maintain and prevent the overgrowth, cells were divided when they reached 80–90% confluency. After changing the media, the cells were disaggregated by repeated pipetting and resuspended in a fresh medium and transferred to a conical tube (15 ml). The suspended cells were centrifuged at 300 x g for 3 minutes. After spinning the supernatant was discarded, and the pellet was resuspended in 5 ml of fresh DMEM medium and transferred to the petri dish with an addition of another 5ml of the fresh medium. In some cases, the remaining cells were frozen with the addition of 10 % DMSO in a cryogenic tube and stored at -80°C.

2.24 SEAP Assay

To perform the SEAP assay, cells were centrifuged, resuspended in a fresh medium and 10^5 cells/well were seeded in a 12-well plate and incubated overnight. Next day, when the cells reached 70-80% confluence, they were pre-treated with 125µg/ml or 150 µg/ml of AP5055, or vehicle, for 30 min, followed by exposure to heat killed *P. gingivalis* (a source of *P. gingivalis* lipopolysaccharide (LPS); 1:1000 dilution of 10^{10} CFU/ml, InvivoGen). To heat kill the bacteria, they were heated to 85 ° C for 10 min. After overnight incubation, cell culture supernatants were collected to measure SEAP activity with QUANTI-Blue (InvivoGen, Figure 10) detection medium, 25 µl of supernatant from each cell culture well were transferred to 200 µl of prepared QUANTI-Blue in triplicates using a separate 96 well plate. The plate was then incubated at 37° C

for 1 hour and afterwards the OD readings were taken at an interval of every 5min for 45 min at a wavelength of 635 nm, using a Synergy™ H1 Multimode Microplate Reader (Agilent BioTek SH1MSN). The average of the control wells was subtracted from the test wells.

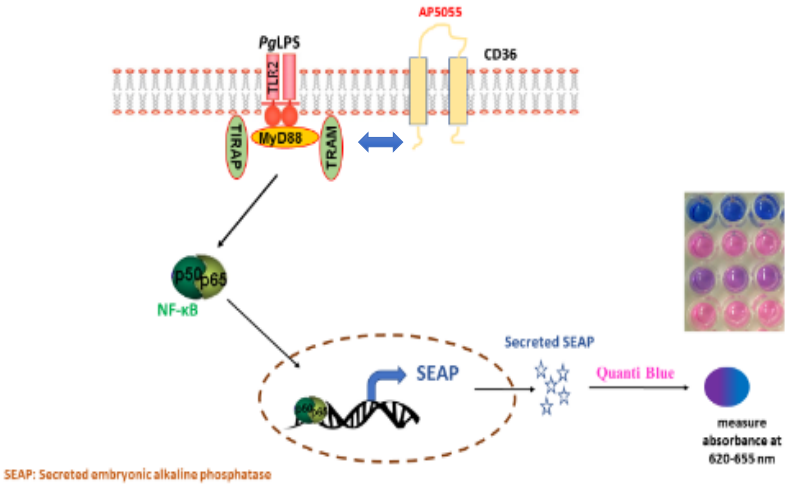

Figure 10: NF- κB-dependent SEAP assay mechanism. After TLR-stimulation by *P. gingivalis LPS*. NF- κB pathway is activated which results in nuclear translocation of NF-κB, resulting in SEAP expression. Cell culture supernatants are collected which are incubated with a colorimetric enzyme assay called QUANTI Blue and a microplate reader is used for the measurement of the absorbance ranging from 620-655 nm.

2.25 Total Cholesterol Measurement in LDLR KO Mice

Total plasma cholesterol was measured using a colorimetric cholesterol assay kit (#STA-384, Cell Biolabs Inc.). To perform this assay, a 96 well plate was used. Assay diluent was prepared by 1:25 dilution in deionized water. Cholesterol standards were prepared by serial dilutions in the concentration range of 0 µM – 12 µM using an assay diluent. This was followed by preparation of cholesterol reaction reagents, comprised of cholesterol oxidase, horseradish peroxidase (HRP), fluorescence probe, and cholesterol esterase at specific concentrations by diluting in the assay diluent provided in the kit.

In this assay the enzyme cholesterol esterase hydrolyzes cholesterol esters into cholesterol, which is subsequently oxidized by cholesterol oxidase to produce the ketone cholest-4-en-3-one and hydrogen peroxide. A specific colorimetric probe is then used to detect the hydrogen peroxide. The reaction between the probe and hydrogen peroxide is catalyzed by horseradish peroxidase enzyme.

To measure the cholesterol in plasma samples each plate well received 50 µl of plasma and the cholesterol reaction reagent solution The cholesterol standards and plasma samples were loaded using a multichannel pipette in duplicates. The 96 well plate contents were mixed thoroughly, and the plate wells were covered with tin foil to protect the reaction from the light. Subsequently, the plate was incubated for 45 min at 37 ºC. Immediately after incubation the OD readings were obtained using a Synergy™ H1 Multimode Microplate Reader (Agilent BioTek SH1MSN) at every 5min for a period of 45 min at a wavelength of 570 nm. The results were averaged between duplicate wells and the mean OD of the blank was subtracted from the standard, control and sample wells.

2.26 Cytokine Array in LDLR KO Mice

The relative expression levels of 40 cytokines in plasma were compared between five pooled samples each from vehicle and AP5055 treated LDLR KO mice, using the Proteome Profiler Mouse Cytokine Array Panel A (#ARY006, R&D Systems) The assay mechanism is represented in Figure 11. In this assay nitrocellulose membranes, which were coated with 40 different anti-cytokine antibodies in duplicates were used. The five AP5055 group plasma samples (each 100 µl) and five from the vehicle treated group (each100 µl) was pooled in separate wells. These samples were selected based on atherosclerotic plaque percentages which were closer to the average values in the two groups. Two membranes were submerged in the blocking buffer in a 4 well plate and incubated for 1 hour on a rocking shaker. While the membranes were being blocked, dilutions of the plasma samples from the two groups were completed using the buffer solution provided in the array kit. This was followed by adding the detection antibody cocktail to the prepared samples, mixing and incubating at room temperature for 1 hour.

Next, the sample/antibody combination was incubated with the blocked membrane overnight at 2-8 ºC on a rocking platform shaker. By incubating overnight, any combination of

cytokine/antibody present on the nitrocellulose membrane would lead to its binding to the corresponding captured antibody. The next day, membranes were removed from the 4 well plate and washed three times separately in a plastic container to remove unbound protein. Subsequently, membranes were removed from the washing buffer container and Streptavidin-HRP and chemiluminescent detection reagents were applied sequentially and then incubated as specified. As per the proportion of cytokine bound, each spot on the membranes emits light, as shown in the Figure 12.

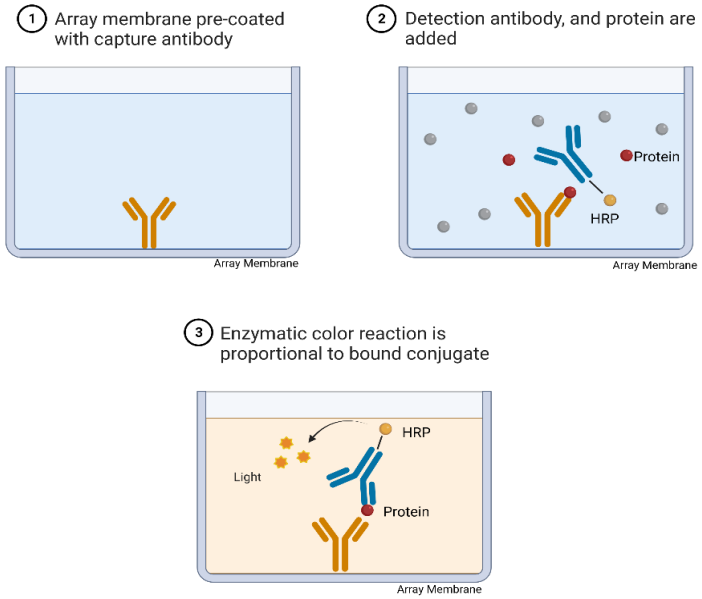

Figure 11: The Proteome Profiler Mouse Cytokine Array Kit, Panel A Mechanism. An immunoassay that utilizes a membrane-based sandwich technique. The samples are combined with a mixture of biotinylated detection antibodies (Step 1) and afterwards subjected to incubation with the array membrane, which contains duplicate spots of capture antibodies specific to target proteins (Step 2). The visualization of captured proteins is achieved through the utilization of chemiluminescent detecting reagents in Step 3. The magnitude of the signal generated is directly proportional to the quantity of analyte that has formed a binding interaction.

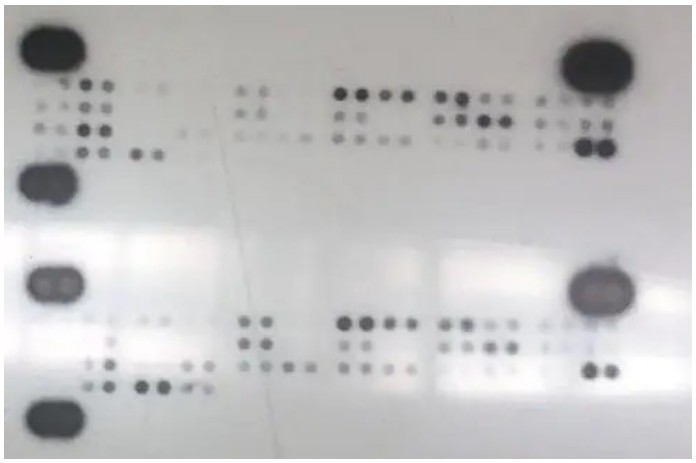

Figure 12: Proteome Profiler Mouse Cytokine Array Kit, Panel A.

Further, to capture and analyze this image, both the membranes were transferred onto chromatography paper and any extra wash buffer was wiped away by blotting the edges of the membranes with the chromatography paper. After that, the membranes were placed on a plastic sheet and saturated in 500 µl of chemiluminescence detection buffer. A second plastic sheet was placed directly on top of the membranes before being moved to the ChemiDoc Gel Imaging System, (Bio-Rad Laboratories, Figure 13). for imaging. A capture mode was used that took images at 1 to 10-second intervals over a total time of 3 minutes. Pixel densities were measured with a fixed selection of circular area and was placed over the grid-identified spot for each cytokine and chemokine. Each cytokine was measured in duplicate and the average density of the duplicate cytokine spots was determined, and the negative control spot density was subtracted from that value. Corresponding values on different membranes were compared to determine the difference between samples.

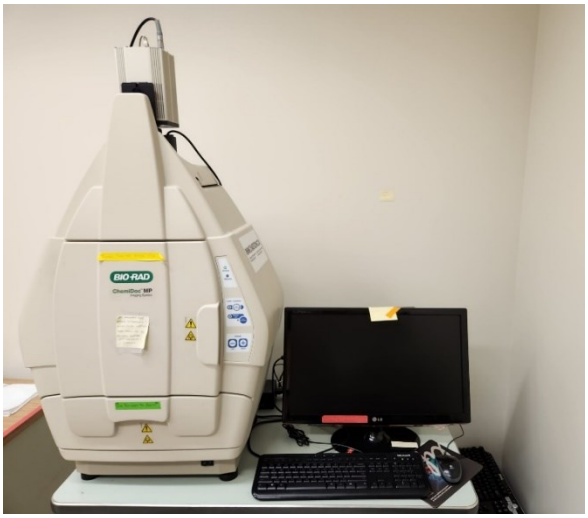

Figure 13: ChemiDoc Gel Imaging System, Bio-Rad Laboratories, Hercules, CA.

2.27 Micro-Computed Tomography (micro-CT) Analysis in LDLR KO Mice

Mandibles of five LDLR KO mice per group were subjected to fixation in a 10% buffered formalin solution for a duration of 24 hours at a temperature of 4° C. Subsequently, they were stored in PBS at 4° C until they were ready for micro-CT analysis (Milabs U-SPECT-II/CT, The Netherlands, Figure 14). The mandibles were imaged using a voxel size of 25 μm and the scanning parameters included a voltage of 70 kVp, a current of 114 μA, an aluminium filter with a thickness of 0.5 mm, and an integration time of 500 ms. As the mandibles were not separated from the craniofacial complex, the nasal septum and occlusal plane of the first molars were used as reference points to position the mandibles within the machine. Reconstruction of the images was completed by using the MILabs software (version 2.38). During the reconstruction phase coronal, sagittal and axial planes were aligned. A 3D construction was created using Avizo software (version 9.1, Thermo Fisher Scientific). For alveolar bone measurements, we used a protocol developed and published by our laboratory previously (245).

Figure 14. Milabs U-SPECT-II/CT, The Netherlands.

According to this protocol, to evaluate the alveolar bone levels of mice mandibles, 3 landmarks were defined: the cemento-enamel junction (CEJ), alveolar bone crest (ABC), and root apex. The distance from the CEJ to ABC was measured as a ratio of total root length (TRL) in the first and second mandibular molars using the identified landmarks as shown in Figure 15. The images were initially orientated on the coronal plane of the first molar to make the sagittal plane measurement (mesial and distal). The sagittal plane measurements were then taken through the long axis of the first molar of the root apex and the middle of the pulp chamber. In healthy mice/humans, the distance should be quite small, and increase with increasing bone resorption, brought on as a consequence of inflammation. Eight measurements were established: two (mesial and distal) in the sagittal plane and six in the coronal plane (mesiobuccal, middle-buccal, distobuccal, mesiolingual, middle-lingual, and distolingual) totaling 32 measurements per animal (first and second mandibular molars). The measurements were recorded in millimeters and compared to the control mice using this formula: CEJ−ABC to TRL % = (CEJ to ABC) / TRL×100 Bone loss= (CEJ−ABC to TRL% AP5055 group) − (CEJ−ABC to TRL% control group).

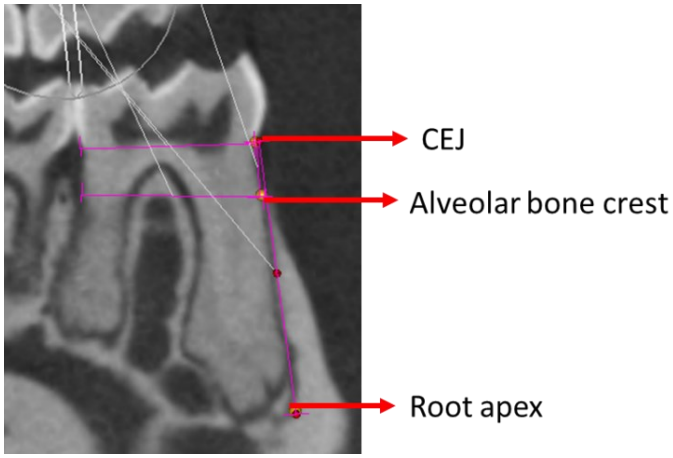

Figure 15. Sagittal view of landmarks used for measurements in the sagittal view CEJ, ABC and root apex.

2.28 Statistical Analyses

Results are presented as the standard error of the mean (SEM). Data were assessed for normal distribution by Shapiro–Wilk test. If normally distributed, and had equal variances, the significance was evaluated using a non-paired, two-tailed t-test or one-way Anova. For non-normally distributed data, the significance was evaluated using the non -parametric Mann-Whitney test. The statistical significance was set at $p < 0.05$. Analyses and graphs were performed using GraphPad Prism software.

Chapter 3 - Results

3.1 Unraveling the Role of EC CD36 in Metabolic Dysregulation in EC CD36 KO Mice Under NC and HFD Conditions

The rationale to conduct this study lies in unraveling the involvement of EC CD36 in the interplay of HFDs, FA uptake, and systemic metabolism. In addressing our hypothesis, the study has generated insightful findings, affirming that EC CD36 significantly influences systemic metabolism, affecting processes such as glucose clearance, energy substrate utilization, and the development of atherosclerosis. The outcomes underscore the substantial role of dyslipidemia, particularly arising from HFDs, on the development of dysfunctional endothelium. CD36 is identified as a receptor for pathological ligands induced by HFDs and plays a crucial role in FA uptake. Additionally, the study reveals sex-specific effects, as male EC CD36 KO mice exhibit heightened carbohydrate utilization and diminished energy expenditure, while female EC CD36 KO/LDLR KO mice manifest reduced atherosclerosis.

3.2 Validation of Cre Expression Specificity

To confirm the specificity of Tie2e cre expression and ensure that the genetic construct accurately targets the intended cell population, we employed flow cytometry on blood samples and gated on the CD11b+/c+ population. CD11b and CD11c are distinct cell surface markers often used to identify specific populations of immune cells. As shown in Figure 16, there was no loss of CD36 expression in the EC CD36 KO samples (Figure 16 B) compared with the fl/fl CD36 control group (Figure 16 A). These findings agree with those of prior studies employing this cre driver (233-235).

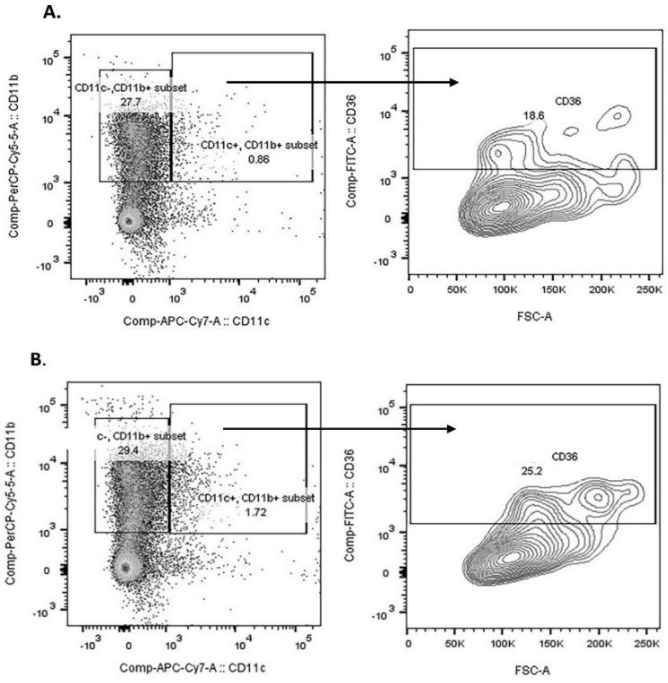

Figure 16: Flow cytometry analysis of the mouse blood. Blood was prepared for flow cytometry and cells were gated on the CD11b+/c+ population. CD36 expression was similar in EC CD36 KO (Figure 16 A) and fl/fl CD36 samples (Figure 16 B), demonstrating no loss of expression of CD36 on the monocyte population.

3.3 GTT 4-Week-Old Mice Fed a NC Diet

To determine the impact of the loss of EC CD36 on systemic metabolism, we began with young mice that were similar in weight. We performed GTT on both male and female 4-week-old EC CD36 KO mice. The results showed that their glucose clearance was comparable to that of the corresponding control mice of the same sex, as shown in Figure 17 A & B and the area under the curve (AUC) did not exhibit statistical significance. The results suggest that, at the early age of 4 weeks, the loss of EC CD36 did not have a discernible impact on systemic metabolism, specifically in terms of glucose clearance. This information contributes to the broader understanding of the role of EC CD36 in metabolic processes and provides a baseline for potential age-dependent or gender-specific effects that may be explored in subsequent stages of this study.

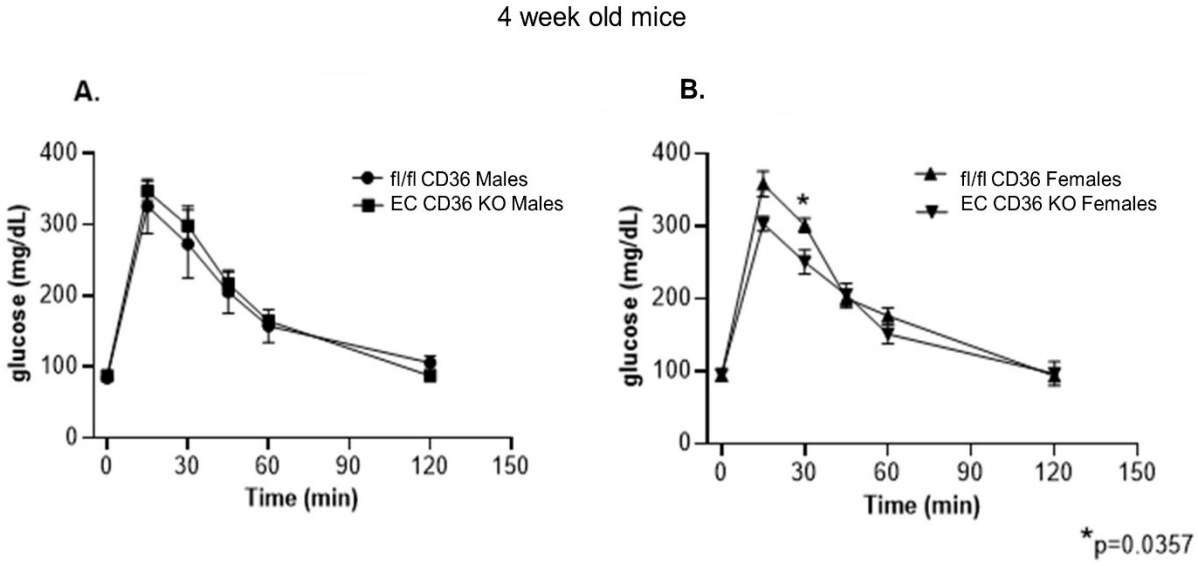

Figure 17: GTT of NC fed EC CD36 KO and fl/fl CD36 mice.**A.** Four-week-old male mice showed no differences (fl/fl CD36, n=3; EC CD36 KO, n=6). **B.** Four-week-old female mice showed a significant (*p =0.0357 Mann-Whitney) difference at 30 minutes; AUC was not significant (fl/fl CD36, n=5; EC CD36 KO, n=3).

3.4 ITT 4-Week-Old Mice Fed a NC Diet

ITT was also performed on both male and female 4-week-old EC CD36 KO mice. The results of the ITT (Figure 18) showed a resemblance to the pattern observed in GTT. Specifically, both male and female mice exhibited comparable insulin sensitivity when compared to control groups of the same sex. This suggests that the absence of the CD36 in ECs did not significantly alter insulin sensitivity in either male or female mice during the ITT.

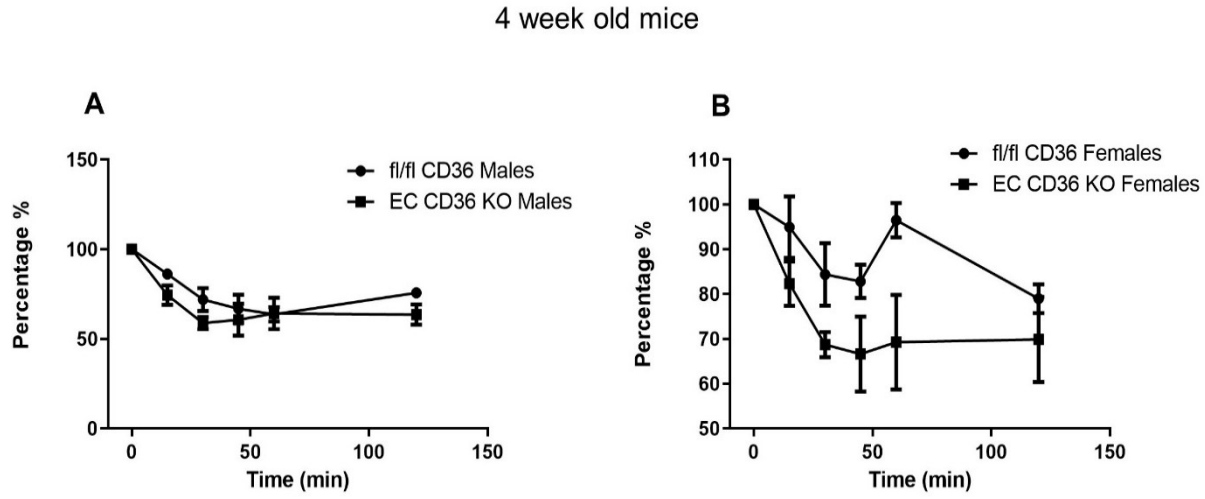

Figure 18: ITT of NC fed EC CD36 KO and fl/fl CD36 mice.**A.** Four-week-old male mice showed no differences in insulin sensitivity (fl/fl CD36, n=3; EC CD36 KO, n=6). **B.** Four-week-old female mice showed no significant difference in insulin sensitivity (fl/fl CD36, n=3; EC CD36 KO, n=6). AUC not significant.

3.5 Weight and Fasting Glucose Levels of Mice on NC Diet

We found no change in the weights of the mice between the two groups (Figure 19 A). However, at 4 weeks, male EC CD36 KO mice had significantly (*p< 0.05) lower glucose levels than control mice. Females, on the other hand, showed no difference between the EC CD36 KO and control group (Figure 19 B). Despite the initial GTT results not indicating a significant impact on glucose clearance at 4 weeks, the subsequent finding of significantly lower glucose levels in male EC CD36 KO mice underscores the importance of investigating specific metabolic parameters. This suggests a subtle yet meaningful difference in glucose metabolism and implies sex-specific variations in how the absence of EC CD36 influences glucose metabolism in young mice.

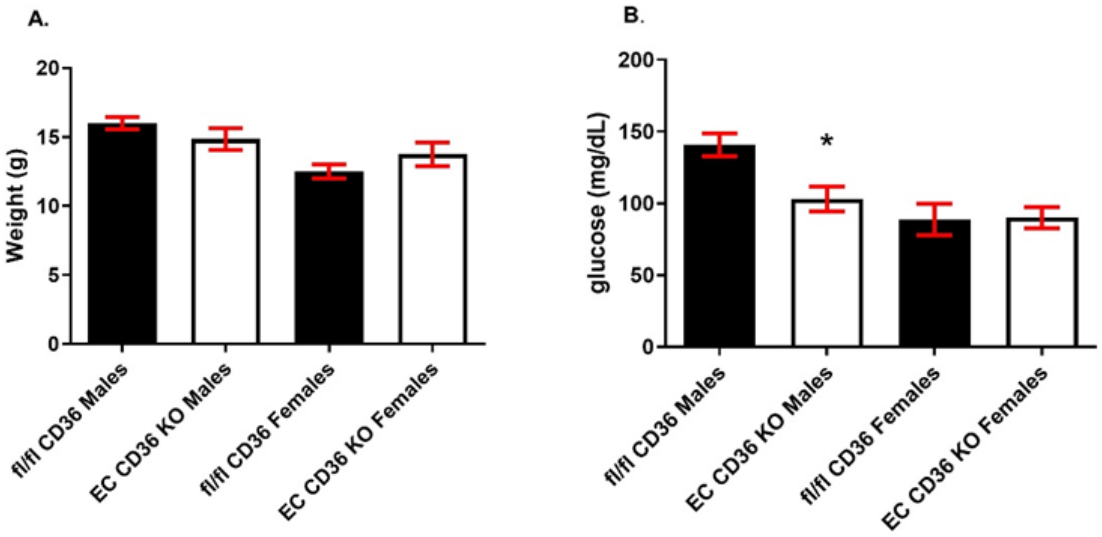

Figure 19: Weight and fasting glucose levels of 4-week-old mice on NC diet. **A.** No difference in weights of mice between the two groups. **B.** Male EC CD36 KO mice had significantly (*p< 0.05) lower fasting glucose levels than control mice. (fl/fl CD36 males, n=7; EC CD36 KO males, n=6, fl/fl CD36 females, n=4; EC CD36 KO females, n=4).

3.6 Indirect Calorimetry

To assess the metabolic characteristics of these mice indirect calorimetry was performed using CLAMS monitoring system which comprises a controlled environment where mice were housed and kept in metabolic cages. This method indirectly calculates the heat generated by living organisms by measuring their carbon dioxide production and oxygen consumption. Indirect calorimetry analysis of 4-week-old NC-fed EC CD36 KO and controls revealed that both strains of male mice used a mix of carbohydrates and fats early in the light period (Figure 20 A, RER). EC CD36 KO males had reduced levels of oxygen consumption (Figure 20 B) and carbon dioxide production (Figure 20 C), indicative of decreased energy expenditure, when compared with controls.

Although cumulative food consumption remained consistent (Figures 20 D and E), there was a difference in the timing of feeding. Male EC CD36 KO mice exhibited increased food intake during the light period, which was associated with an elevated level of carbohydrate metabolism after the midpoint of the light period as shown in Figure 20 A. The increase in carbohydrate consumption by EC CD36 KO males persisted until late in the dark phase. EC CD36 KO males showed considerably less locomotor activity (Figure 20 F). Female mice did not vary in any parameter measured.

The results suggest that EC CD36 KO in male mice led to alterations in energy metabolism, characterized by reduced energy expenditure, changes in feeding patterns with increased carbohydrate consumption, and decreased locomotor activity. These effects were not observed in female mice, indicating a sex-specific impact of EC CD36 KO on metabolic differences

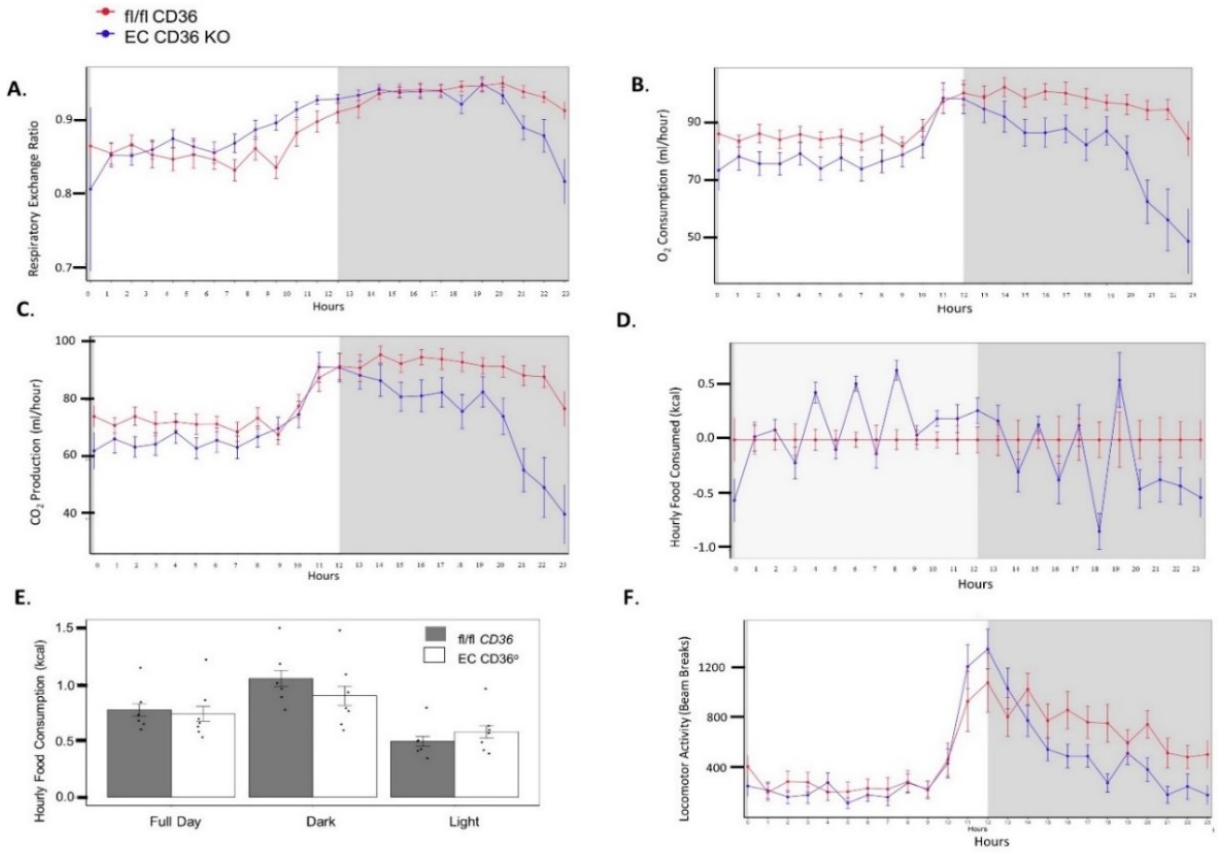

Figure 20: Indirect calorimetry of four-week-old NC fed male fl/fl CD36 and EC CD36 KO mice. Plots show data from a 12-hour light: 12-hour dark cycle after a 24-hour acclimation period. White panel=light phase; grey panel=dark phase. **A.** Respiratory exchange ratio. **B.** O_2 consumption. **C**.CO_2 production. **D**. Cumulative hourly food consumption. **E**. Light and dark cycle food consumption, EC CD36 KO male mice ate more during the light period. **F**. Locomotor activity.

3.7 Fat Mass Distribution in Global and EC CD36 KO Mice

To investigate how the absence of EC CD36 influences basal systemic metabolism, we employed DEXA to evaluate the distribution of fat mass in global and EC CD36 KO mice. This imaging technique allows us to quantify and analyze the composition of body tissues, providing insights into the impact of EC CD36 loss on the distribution of fat. We observed a significant decrease in the percentage of fat mass in both male and female mice with either global or EC CD36

KO when compared to their sex matched controls (Figure 21 A&B). This finding suggests that the absence of EC CD36 is associated with alterations in fat mass distribution in these mice.

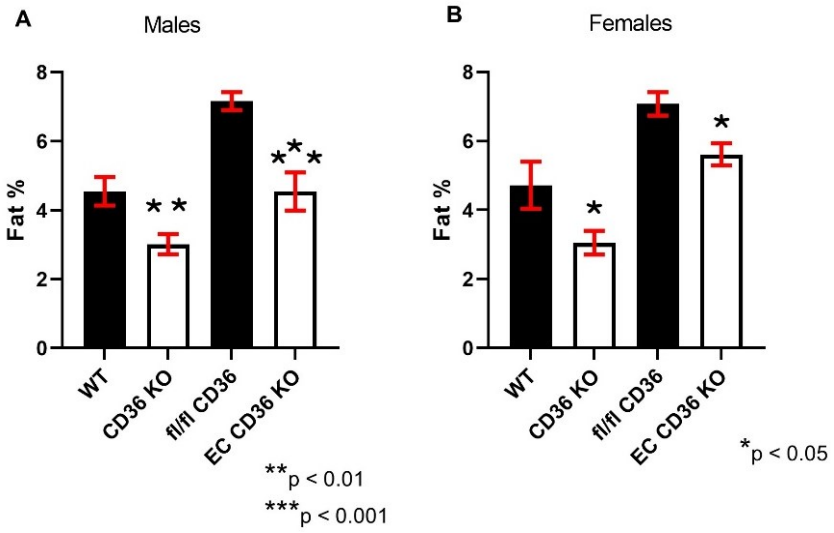

Figure 21: Fat mass percentage in males and females global and EC CD36 KO mice. **A.** Males in both global and EC CD36 KO groups showed a significant reduction in body fat percentage (**p < 0.01, ***p < 0.001). **B.** Females in both global and EC CD36 KO groups exhibited a significant decrease in body fat percentage (*p < 0.05).

3.8 Time to Thrombosis and Hb Assay

To determine the impact of CD36 absence in ECs on the coagulation process and blood Hb levels, we monitored the time to thrombosis and assessed hemoglobin concentrations. Our observations revealed a significantly shorter time to thrombosis in both global and EC CD36 KO mice (Figure 22 A). Although a similar trend was noted in global and EC CD36 double KO mice, the data for double KO is preliminary due to a limited sample size. The Hb assay results mirrored the pattern observed in the time to thrombosis, both male and female EC CD36 KO mice exhibited a significant decrease in OD, correlating with reduced Hb levels in the blood compared to their respective sex-matched controls (Figure 22 B).

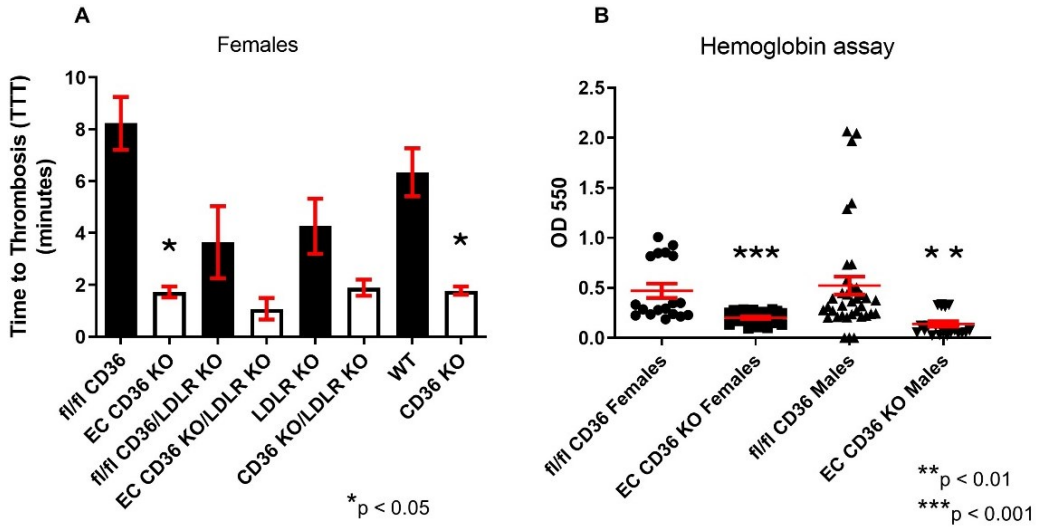

Figure 22: Time to thrombosis and Hb assay in global and EC CD36 KO mice. **A.** Females in both the global and EC CD36 KO groups exhibited a significant reduction in time to thrombosis (*$p < 0.05$). **B.** Both male and female mice in the global and EC CD36 KO groups showed a substantial decrease in Hb levels (**$p < 0.01$, ***$p < 0.001$).

3.9 Plasma Metabolomic Analysis of Mice Fed NC Diet Using CIL LC-MS and Univariate Analysis

To carry out metabolomic analyses, 4-week-old mice, administered a low-fat 4% NC diet, underwent overnight fasting before their sacrifice. Plasma, collected as described earlier, was obtained from a total of 18 samples distributed among the groups as follows: 5 in the Males (fl/fl CD36) group, 5 in the Males (EC CD36 KO) group, 4 in the Females (fl/fl CD36) group, and 4 in the Females (EC CD36 KO) group. Subsequently, the plasma samples underwent untargeted metabolomics analysis using chemical isotope labeling LC-MS with a 4-channel approach. The analyses were conducted at The Metabolomics Innovation Centre, University of Alberta, Edmonton, Canada, and the data were extracted from the report provided by the metabolomics core. The objective of the analyses was to gain specific insights into the role of CD36 in regulating EC metabolism. This was achieved by examining changes in plasma metabolite levels, potentially serving as indicators for the metabolic alterations associated with EC CD36 KO mice. Metabolomics provides a comprehensive perspective on the small molecules involved in cellular

processes. Analyzing the plasma metabolome enabled the identification of shifts in various metabolic pathways, contributing to a holistic understanding of how CD36 deficiency in ECs influences systemic metabolism.

A total of 21 LC-MS data were processed for each channel. After data processing, four-channel LC-MS results from one sample were combined. Less commonly detected peak pairs (metabolites) were filtered out to ensure data quality. After filtering, 6440 ± 102 peak pairs per sample were retained. The table below (Table 3) shows the peak pair numbers detected in each sample. The number of peak pairs among all groups was in close proximity. Peak pairs without data present in at least 80.0% of samples in any group were filtered out. Applying this 80%-rule ensures that only the commonly detectable peak pairs are retained for further analysis, without the use of excessive missing-value imputation. A three-tier ID approach was used to perform metabolite identification. 6175 peak pairs were positively identified or putatively matched. Among them, 338 peak pairs were positively identified in tier 1 (CIL Library); 1195 peak pairs were putatively identified with high-confidence in tier 2 (LI Library); 1213, 2555 and 874 peak pairs were matched in the zero-, one-, and two-reaction libraries, respectively. The tables (table 4 and 5) present the significantly changes top 40 metabolites in tiers 1 and 2 for Male fl/fl CD36 and EC CD36 KO mice. Similarly, for female fl/fl CD36 and EC CD36 KO mice, the significantly altered top 25 and top 40 metabolites in tiers 1 and 2 are displayed in Table 6 and Table 7, respectively.

Table 3. Number of peak pairs (metabolites) detected in each sample.

Group	Number of Peak Pairs
Males (fl/fl CD36)	6490
Males (fl/fl CD36)	6506
Males (EC CD36 KO)	6479
Males (EC CD36 KO)	6362
Males (fl/fl CD36)	6423
Males (EC CD36 KO)	6271
Males (EC CD36 KO)	6466
Males (EC CD36 KO)	6139
Males (fl/fl CD36)	6495
Males (fl/fl CD36)	6475
Females (EC CD36 KO)	6459
Females (EC CD36 KO)	6461
Females (fl/fl CD36)	6426
Females (fl/fl CD36)	6314
Females (fl/fl CD36)	6405
Females (fl/fl CD36)	6475
Females (EC CD36 KO)	6408
Females (EC CD36 KO)	6484
QC	6575
QC	6564
QC	6560

QC= quality control.

3.10 Comparison Between Males (fl/fl CD36) Group and Males (EC CD36 KO) Group

A volcano plot (Figure 23) was constructed by plotting the fold change (FC) of each metabolite against the p-value. The FC was calculated as mean (Males (fl/fl CD36)) / Mean (Males (EC CD36 KO)). When using FC > 1.2 or < 0.83, $p < 0.05$, and q-value (or false discovery rate (FDR)-adjusted p-value) < 0.25 as criteria, the analysis showed that 406 peak pairs with FC > 1.2, q-value < 0.25 and 293 peak pairs with FC < 0.83, q-value < 0.25 (corresponding p-value threshold is 0.043). Without considering FDR adjustment and using FC > 1.2 or < 0.83 and $p < 0.05$ as criteria, the analysis showed that 460 peak pairs with FC > 1.2, $p < 0.05$ (in red) and 336 peak pairs with FC < 0.83, $p < 0.05$ (in blue). Among them, 42 peak pairs can be positively identified in tier 1 using the labeled metabolite library (CIL) Library, 142 peak pairs can be high-confidence putative identified in tier 2 using linked identity library (LI) Library and 576 peak pairs can be putatively identified in tier 3 using MyCompoundID (MCID library).

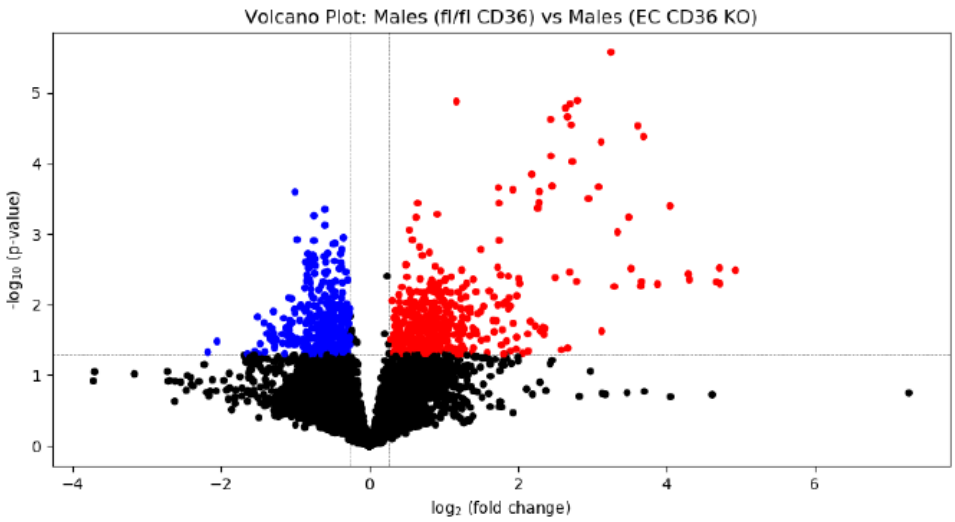

Figure 23: Male (fl/fl CD36) and Male (EC CD36 KO) volcano plot showing differentially expressed metabolites. The x-axis represents FC, and the y-axis represents p-values. Up-regulated metabolites with statistical significance are represented by each of the red plot points. Down-regulated metabolites with statistical significance are represented by blue plot points. (fl/fl CD36 n=5, EC CD36 KO n=5).

Plasma acetylcarnitine levels in male EC CD36 KO mice were elevated in comparison to the control group (Figure 24 A). Conversely, the male EC CD36 KO group exhibited a decrease in phenylalanyl-glutamine levels when compared with the fl/fl CD36 mice (Figure 24 B). Acetylcarnitine is involved in fatty acid metabolism and energy production, so changes in its levels may reflect alterations in the mitochondrial metabolic processes and elevated acetylcarnitine levels in EC CD36 KO mice might be indicative of a compensatory response in FA transport. The decreased phenylalanyl-glutamine levels may suggest changes in amino acid utilization or transport in the absence of EC CD36. This could be due to altered signaling pathways or metabolic flux affecting amino acid metabolism.

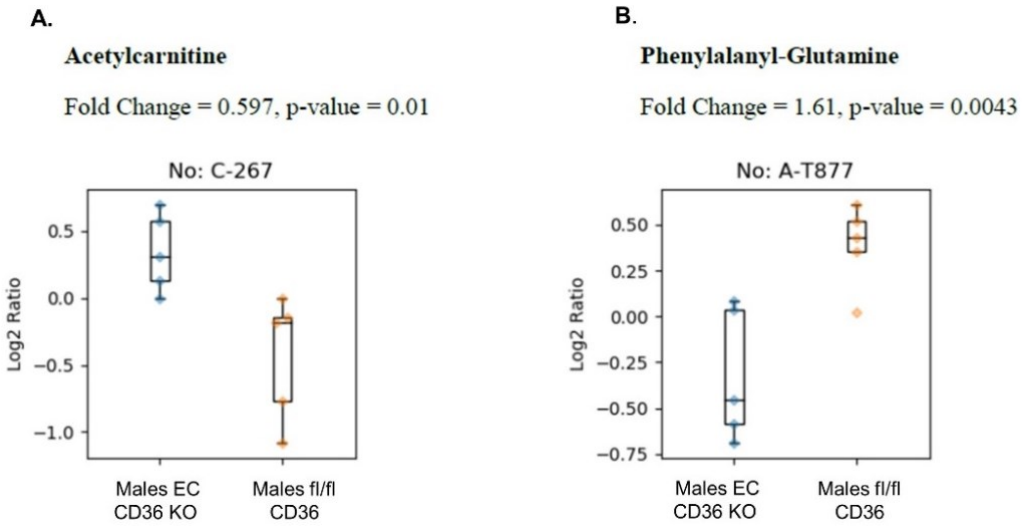

Figure 24: Box plots illustrating two significantly altered metabolites in Males (fl/fl CD36) vs Males (EC CD36 KO). Acetylcarnitine **(A)** and phenylalanyl-Glutamine **(B)** in tier 1, serving as examples of changes in metabolite concentrations in the two male groups.

3.11 Comparison Between Females (fl/fl CD36) Group and Females (EC CD36 KO) Group

A volcano plot (Figure 25) was constructed by plotting the FC of each metabolite against the p-value. FC was calculated as Mean (Females (fl/fl CD36)) / Mean (Females (EC CD36 KO)). When using FC > 1.2 or < 0.83, $p < 0.05$, and q-value (or FDR-adjusted p-value) < 0.25 as criteria, the analysis showed that 312 peak pairs with FC > 1.2, q-value < 0.25 and 451 peak pairs with FC < 0.83, q-value < 0.25 (corresponding q-value threshold is 0.24). Without considering FDR adjustment and using FC > 1.2 or < 0.83 and $p < 0.05$ as criteria, the analysis showed that 312 peak pairs with FC > 1.2, $p < 0.05$ (in red) and 451 peak pairs with FC < 0.83, $p < 0.05$ (in blue). Among them, 26 peak pairs can be positively identified in tier 1 using CIL Library, 98 peak pairs can be high-confidence putative identified in tier 2 using LI Library and 584 peak pairs can be putatively identified in tier 3 using MCID library.

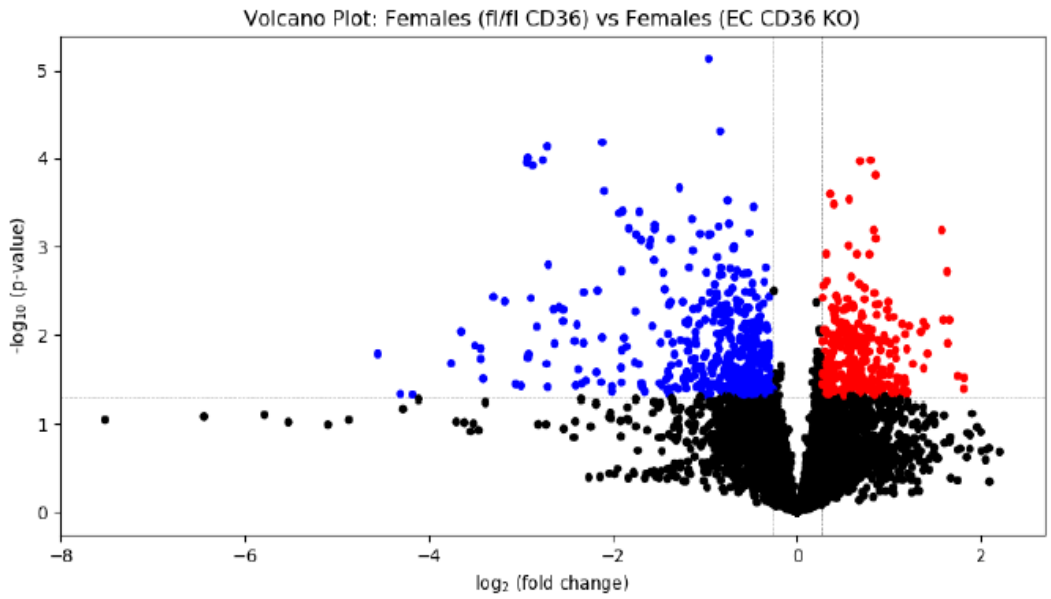

Figure 25: Females (fl/fl CD36) and Females (EC CD36 KO) volcano plot showing differentially expressed metabolites. The x-axis represents FC, and the y-axis represents p-values. Up-regulated metabolites with statistical significance are represented by each of the red plot points. Down-regulated metabolites with statistical significance are represented by blue plot points. (fl/fl CD36) n=4, EC CD36 n=4).

Plasma threonine levels in female EC CD36 KO mice were increased in comparison to the control group (Figure 26 A). Conversely, the female EC CD36 KO group showed a decrease in xanthurenic acid levels when compared with the fl/fl CD36 mice (Figure 26 B). The increased threonine levels could be a result of compensatory mechanisms initiated in response to the absence of EC CD36. Xanthurenic acid is a metabolite of tryptophan. The decreased levels of xanthurenic acid in female EC CD36 KO mice may suggest alterations in tryptophan metabolism.

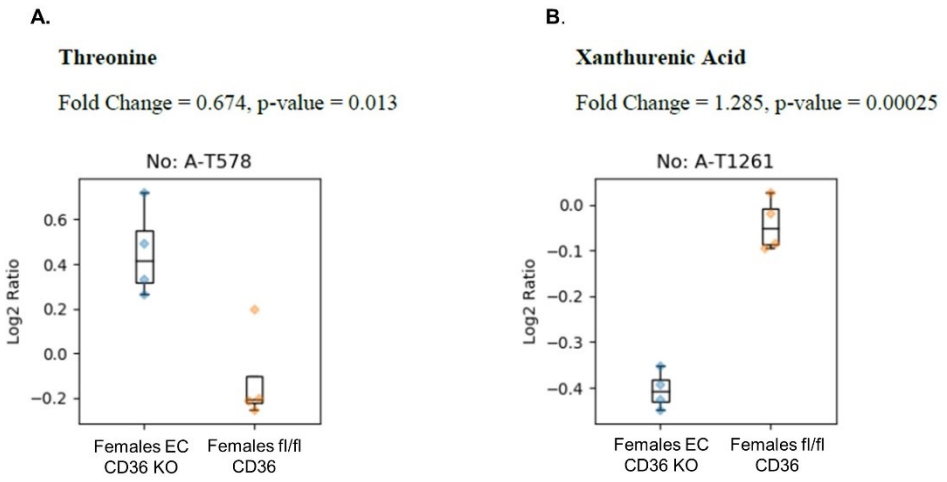

Figure 26: Box plots illustrating two significantly altered metabolites in Females (fl/fl CD36) vs Females (EC CD36 KO). Threonine **(A)** and xanthurenic acid **(B)** in tier 1, serving as examples of changes in metabolite concentrations in the two female groups.

3.12 Comparison Between All Groups Multivariate Analysis

3.12.1 Principal Component Analysis (PCA) Plot

To comprehend the intricate and multivariate characteristics inherent in metabolomics datasets, principal component analysis (PCA) was conducted. This analysis served several purposes, including dimensionality reduction, exploration of data structure, visualization of sample clustering based on similarity, highlighting differences in metabolite groups, classification, identification of discriminative metabolites for group discrimination, and acting as a quality control tool. In Figure 27, PCA plot for four groups (males fl/fl CD36, males EC CD36 KO, females fl/fl CD36, and females EC CD36 KO) and quality control are presented. The absence of abnormal samples is evident, suggesting a stable distribution of data in close proximity to quality control standards. Notably, the cluster of samples from male EC CD36 KO mice is distinctly separated from the other three groups (males fl/fl CD36, females fl/fl CD36, females EC CD36 KO), indicating greater overlap among the latter. This implies substantial differences in the metabolite profiles of male EC CD36 KO mice compared to the other experimental groups.

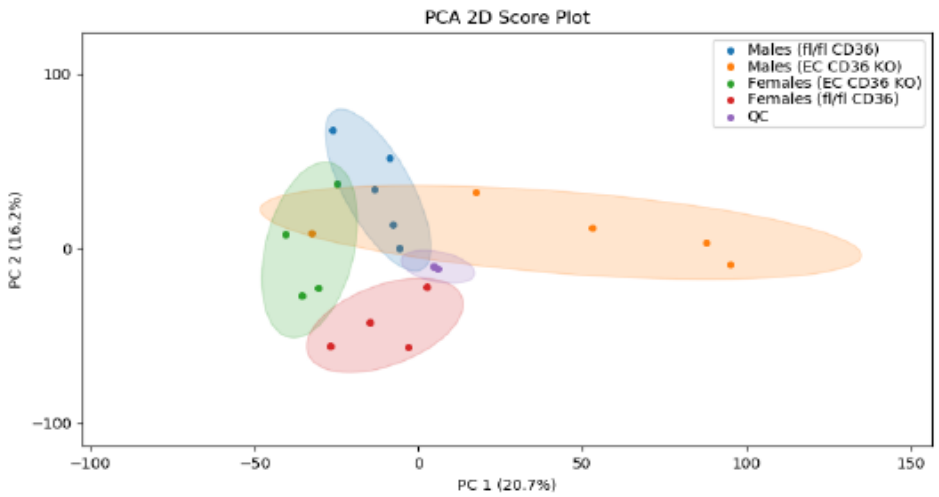

Figure 27: PCA 2D Score plot. PCA multivariate analysis was used to find abnormal samples and evaluate the repeatability of experimental data. The plot illustrates a distinct separation of samples within the EC CD36 KO cluster from the other group clusters.

3.12.2 Heat Map Analysis

The cluster heat map analysis (Figure 28) illustrates the relative concentrations of the top one hundred significantly altered metabolites. The heat map indicates a notable decrease in metabolite concentrations in the plasma of male EC CD36 KO mice compared to fl/fl CD36 controls. Conversely, female EC CD36 KO mice exhibit a significant increase in metabolite concentrations compared to their sex-matched controls. These results highlight the potential differences in metabolic responses based on sex and absence of CD36 in ECs.

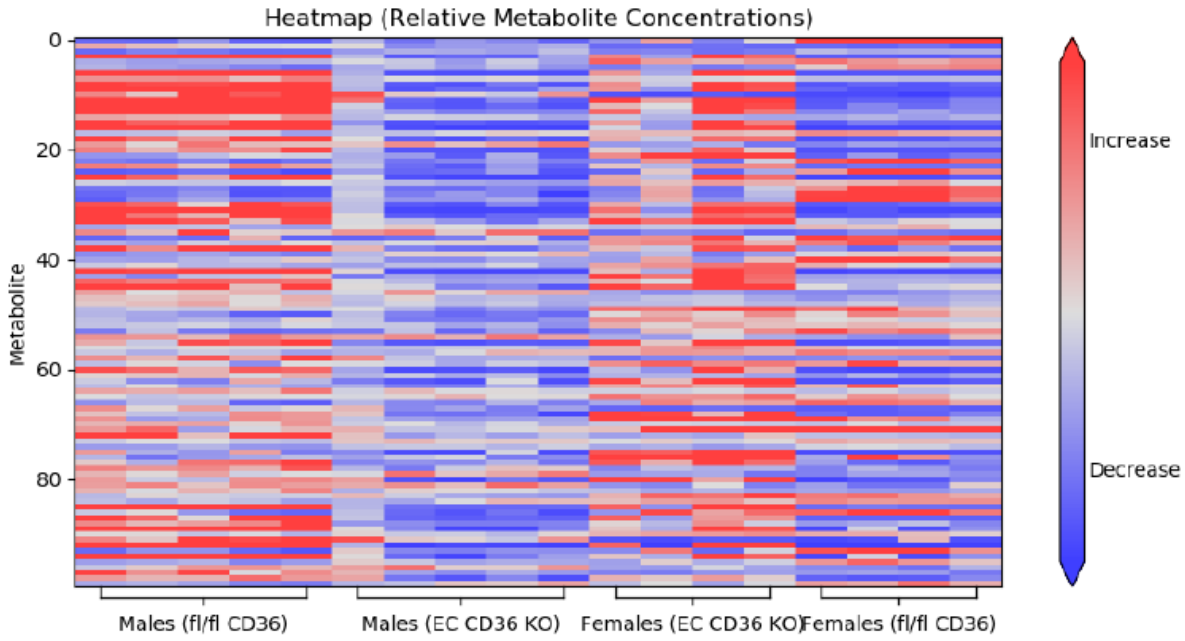

Figure 28: Heatmap Analysis showing top 100 of significantly altered metabolites ranked by p-value. Significant reduction in metabolite concentrations in the plasma of male EC CD36 KO mice when compared to the fl/fl CD36 controls. In contrast, female EC CD36 KO mice demonstrate a marked elevation in metabolite concentrations compared to their sex-matched controls.

Table 4. List of top 40 significantly altered metabolites in Males fl/fl CD36 vs EC CD36 KO (tier 1)

	Metabolite	NovaMT Library No.	Fold Change	p-value	Significance
1	Phenylalanyl-Glutamine	AN02592001	1.60970258	0.004321	Significant Increase
2	p-Octopamine	AN00662000	1.65294894	0.008503	Significant Increase
3	3,4-Dihydroxymandelic Acid	AN01076000	2.03336394	0.01022	Significant Increase
4	gamma-Gulonic acid gamma-lactone	AN00993006	2.22676282	0.010284	Significant Increase
5	Acetylcarnitine	AN01351000	0.59658606	0.010316	Significant Decrease
6	Decanal/2-Decanone	AN00704003	0.80574785	0.011756	Significant Decrease
7	Mesaconic Acid	AN00392001	0.62817596	0.012127	Significant Decrease

8	Tetrahydrocortisone	AN03559004	0.78127398	0.013134	Significant Decrease
9	Acetaldehyde	AN00014000	0.8143191	0.013854	Significant Decrease
10	Glycyl-Tyrosine	AN01801000	1.42109095	0.014046	Significant Increase
11	3-Methoxytyramine	AN00847006	1.48552048	0.014614	Significant Increase
12	4-Hydroxyproline	AN00406000	1.69282137	0.014687	Significant Increase
13	4-Acetylresorcinol	AN00647014	0.78121059	0.014727	Significant Decrease
14	Indole-3-carboxaldehyde	BM00559000	0.67084871	0.015694	Significant Decrease
15	A-Ketoisovaleric Acid	AN00266001	0.58724148	0.017041	Significant Decrease
16	Homoserine	AN00291001	1.33422852	0.01805	Significant Increase
17	Butanal/Butanone	AN00061006	0.82469703	0.018518	Significant Decrease
18	Normetanephrine	AN01069002	1.71305893	0.019114	Significant Increase
19	Hexanone/2-hexanone/Isopropyl ethyl ketone	AN00167001	0.81695487	0.019256	Significant Decrease
20	Pyridoxal	AN00842000	0.66275229	0.019676	Significant Decrease
21	3-Hydroxyphenylacetic Acid	AN00647003	0.73731735	0.021619	Significant Decrease
22	Octaldehyde	AN00376001	0.81621171	0.02203	Significant Decrease
23	3-Hydroxyanthranilic Acid	AN00657006	1.83004398	0.022123	Significant Increase
24	Propanal	AN00026003	0.82598559	0.02229	Significant Decrease
25	Glutamine	AN00574000	1.33958621	0.024976	Significant Increase
26	Methylguanidine	AN00066000	1.59190958	0.025985	Significant Increase
27	L-Isoglutamine	BM00574006	2.72366727	0.026033	Significant Increase
28	Urocanic acid	AN00478002	0.48650787	0.028404	Significant Decrease
29	3,4-Dihydroxybenzeneacetic Acid	AN00856002	0.71715354	0.028937	Significant Decrease
30	Cystine	AN01818000	1.8543095	0.031055	Significant Increase
31	1,5-Anhydrosorbitol	AN00796004	2.07001738	0.032823	Significant Increase
32	Succinic acid semialdehyde	AN00177003	0.81349911	0.036	Significant Decrease

33	Salicin	BP02490000	1.89246055	0.036865	Significant Increase
34	Glycolic Acid	AN00080000	1.50825786	0.039136	Significant Increase
35	4-Methoxybenzoic Acid	BM00647009	0.65156794	0.039437	Significant Decrease
36	Picolinic Acid	AN00318000	0.56006553	0.041868	Significant Decrease
37	Glutaminyl-Proline/Prolyl-Glutamine	AN01860000	1.45559947	0.043496	Significant Increase
38	Methyl alpha-D-glucopyranoside	AN01218003	1.38296445	0.044749	Significant Increase
39	Glutaminyl-Glutamate	AN02336002	1.622247	0.044802	Significant Increase
40	Aspartyl-Glycine	AN01163001	1.30888954	0.046943	Significant Increase

Table 5. List of top 40 significantly altered metabolites in Males fl/fl CD36 vs EC CD36 KO (tier 2)

	Metabolite	**NovaMT Library No.**	**Fold Change**	**p-value**	**Significance**
1	Isopentenyladenine-9-N-Glucoside	AN03572000	1.548795	0.000577	Significant Increase
2	Isomer 2 of Valproylglycine	AN01306001	0.563677	0.001892	Significant Decrease
3	Hydroquinone	AN00227003	0.599952	0.002238	Significant Decrease
4	(3S)-3-Isopropenyl-6-oxoheptanoic acid	BM01083000	0.664502	0.002505	Significant Decrease
5	Isomer 1 of Valproylglycine	AN01306001	0.602226	0.002793	Significant Decrease
6	2-Hydroxy-5-carboxymethylmuconate semialdehyde	AN01288001	2.01516	0.004499	Significant Increase
7	2-Dehydro-3-deoxy-galactonic acid/2-Dehydro-3-deoxy-D-gluconic acid	AN00993001	1.813244	0.006536	Significant Increase
8	Tetrahydropentoxyline	AN03582000	1.678107	0.006685	Significant Increase
9	4-(3-Pyridyl)-3-butenoic acid	AN00785003	0.634177	0.008833	Significant Decrease
10	2-Hydroxy-2,4-pentadienoic acid	AN00252002	1.955403	0.008986	Significant Increase
11	1-Pyrroline-5-carboxylic acid	AN00247000	1.75334	0.013314	Significant Increase
12	gamma-Carboxyglutamic acid	AN01178000	1.395734	0.014175	Significant Increase
13	N-Acetylmuramic acid	AN02590000	2.393262	0.014787	Significant Increase

14	5'-Carboxy-gamma-chromanol	AN02801000	0.448676	0.015514	Significant Decrease
15	2-Amino-3,7-dideoxy-D-threo-hept-6-ulosonic acid	AN01184000	1.380081	0.017138	Significant Increase
16	N2-Acetyl-L-Hydroxylysine	PR01349003	0.694456	0.017258	Significant Decrease
17	3-O-Methylgallic Acid	BM01076001	2.125535	0.017858	Significant Increase
18	(S)-4-Hydroxymandelic Acid	BM00856001	0.374271	0.018077	Significant Decrease
19	3-Hydroxy-cis-5-tetradecenoylcarnitine	AN03787000	0.469632	0.020056	Significant Decrease
20	Isovanillic acid	AN00856010	0.395241	0.020468	Significant Decrease
21	N-Acetyl-L-Formylkynurenine	PR02375000	2.08917	0.021005	Significant Increase
22	m-Methylbenzoic acid	BM00460000	0.582403	0.021758	Significant Decrease
23	4-O-Methylgallic acid	AN01076002	2.081658	0.022141	Significant Increase
24	Tyrosyl-Phenylalanine	AN03081001	1.482402	0.022649	Significant Increase
25	gamma-Glutamylserine	AN01757008	0.471322	0.023069	Significant Decrease
26	5-epi-Valiolone	BM01198000	4.958841	0.0236	Significant Increase
27	Isomer 1 of 2,3-Diaminosalicylic acid	AN00858000	1.759278	0.025284	Significant Increase
28	Isomer 2 of L-beta-Ethynylserine	BM00380002	1.743454	0.029737	Significant Increase
29	Isomer 1 of Nordeoxycholic Acid	AN03717000	0.563302	0.029809	Significant Decrease
30	Xylulose	AN00622000	1.380108	0.03114	Significant Increase
31	Isomer 1 of Gly-leu-tyr	AN03406000	0.64895	0.031922	Significant Decrease
32	gamma-Amino-gamma-Cyanobutanoic Acid	BM00373003	1.312191	0.032201	Significant Increase
33	Isomer 1 of 4-Methylene-L-glutamine	BM00716001	0.5192	0.032403	Significant Decrease
34	3-keto-7alpha,12alpha-Dihydroxy-5alpha-cholanic acid	AN03968005	3.59407	0.032899	Significant Increase
35	Isomer 2 of N (6)-Methyllysine	AN00744000	1.394982	0.03403	Significant Increase
36	4-Amino-4-Deoxychorismic Acid	AN01643000	1.921375	0.036771	Significant Increase
37	5-Hydroxyectoine	AN00716000	0.55986	0.036835	Significant Decrease
38	Isomer 1 of 5-Hydroxyindoleacetic acid	AN01180000	0.631492	0.039574	Significant Decrease

39	Geranic Acid	BM00866012	2.641748	0.040805	Significant Increase
40	N-Acetyl-5-Hydroxy-L-tryptophan	PR02102001	1.674762	0.041189	Significant Increase

Table 6. List of top 26 significantly altered metabolites in Females fl/fl CD36 vs EC CD36 KO (tier 1)

	Metabolite	NovaMT Library No.	Fold Change	p-value	Significance
1	Xanthurenic Acid	AN01356001	1.284765	0.000251	Significant Increase
2	Indole-3-carboxaldehyde	BM00559000	1.330581	0.00508	Significant Increase
3	Cortisol	AN03543000	1.387838	0.007603	Significant Increase
4	Gly-Norleucine	AN01133007	1.384226	0.011856	Significant Increase
5	Threonine	AN00291000	0.67409	0.012595	Significant Decrease
6	Cystathionine	AN01608000	0.807029	0.012707	Significant Decrease
7	Glutamyl-Isoleucine	AN02110000	1.322574	0.012801	Significant Increase
8	Homoserine	AN00291001	0.808219	0.013582	Significant Decrease
9	Alanyl-Glutamine	AN01530001	0.539878	0.020499	Significant Decrease
10	Seryl-Phenylalanine	AN01996002	0.724041	0.021745	Significant Decrease
11	Carnosine	AN01660003	0.612984	0.022975	Significant Decrease
12	4-Acetylresorcinol	AN00647014	1.271674	0.023184	Significant Increase
13	Prolyl-Threonine	AN01516001	0.716614	0.0254	Significant Decrease
14	5-Hydroxylysine	AN00774001	0.754179	0.027003	Significant Decrease
15	Threoninyl-Glutamate	AN01936001	0.750435	0.030921	Significant Decrease
16	Acetic Acid	AN00031000	0.373241	0.032222	Significant Decrease
17	4-Hydroxyproline	AN00406000	0.665946	0.033775	Significant Decrease
18	Galacturonic acid	AN01214008	2.236499	0.035433	Significant Increase
19	Lysyl-Proline	AN01861000	0.687067	0.035898	Significant Decrease
20	Glycerone/Methylglyoxal	AN00130008	1.880869	0.036576	Significant Increase

21	N, N-Dimethylglycine	AN00189004	0.723257	0.037514	Significant Decrease
22	3,4-Dihydroxymandelic Acid	AN01076000	0.782123	0.03994	Significant Decrease
23	2-Aminobenzoic Acid	AN00468006	0.48519	0.041282	Significant Decrease
24	3-Methoxytyramine	AN00847006	0.651396	0.042669	Significant Decrease
25	Acetoacetic acid	AN00177002	1.238316	0.04695	Significant Increase
26	Serine	AN00202000	0.804576	0.047967	Significant Decrease

Table 7. List of top 40 significantly altered metabolites in Females fl/fl CD36 vs EC CD36 KO (tier 2)

	Metabolite	**NovaMT Library No.**	**Fold Change**	**p-value**	**Significance**
1	Threoninyl-Alanine	AN01168002	3.357741	0.02945	Significant Increase
2	L-Allothreonine	AN00291005	0.701169	0.007492	Significant Decrease
3	Isomer 1 of 3-Amino-2-piperidone	AN00255000	0.749626	0.017901	Significant Decrease
4	Isomer 1 of (S)-5-Amino-3-oxohexanoic acid	AN00561008	1.230939	0.022561	Significant Increase
5	N-Carboxyethyl-g-aminobutyric acid	AN00957000	0.661456	0.008368	Significant Decrease
6	3-Hydroxy-L-proline	AN00406014	0.694286	0.001991	Significant Decrease
7	5-Aminopentanal	AN00174001	0.811182	0.023852	Significant Decrease
8	Isovanillic acid	AN00856010	1.619668	0.040048	Significant Increase
9	Diethylamine	AN00067000	0.826638	0.044089	Significant Decrease
10	(3S,5S)-3,5-Diaminohexanoic acid	AN00578005	0.797397	0.019615	Significant Decrease
11	Pyridoxamine	AN00863000	0.793946	0.018922	Significant Decrease
12	gamma-Glutamyltryptophan	AN03154002	1.663261	0.00398	Significant Increase
13	3-Aminopropanal	AN00065001	0.548075	0.009825	Significant Decrease
14	Prolyl-Valine	AN01489000	0.782487	0.015335	Significant Decrease
15	N-Acetyl-3-Hydroxyanthranilic acid	PR01229010	1.664992	0.019114	Significant Increase
16	3-Methoxy-4-Hydroxyphenylethyleneglycol	AN01079002	1.342785	0.003621	Significant Increase

17	Monodehydroascorbic Acid	AN00951000	1.838478	0.011491	Significant Increase
18	Tabtoxin Biosynthesis Intermediate 4	BM01168004	3.519912	0.031143	Significant Increase
19	L-beta-Aspartyl-L-Glycine	AN01163000	0.78275	0.013152	Significant Decrease
20	N-Methylethanolamine Phosphate	AN00681000	0.723305	0.043021	Significant Decrease
21	3-Hydroxy-L-proline	AN00406013	0.671581	0.025987	Significant Decrease
22	4-Methyl-L-Glutamic Acid	BM00754000	0.75107	0.004871	Significant Decrease
23	Aminomalonic acid	AN00287000	0.469459	0.039226	Significant Decrease
24	4-(3-Pyridyl)-3-butenoic acid	AN00785003	1.441818	0.03257	Significant Increase
25	L-2,3-Dihydrodipicolinic acid	AN00873000	0.721343	0.02679	Significant Decrease
26	Histidinyl-Proline	AN01998000	0.705217	0.029937	Significant Decrease
27	1-Pyrroline-5-carboxylic acid	AN00247000	0.592957	0.041513	Significant Decrease
28	Isomer 1 of L-2,3-Dihydrodipicolinic acid	AN00873000	0.739243	0.013113	Significant Decrease
29	Isomer 1 of Propionylglycine	AN00406010	0.620957	0.013541	Significant Decrease
30	3-Hydroxy-2-methylpyridine-4,5-dicarboxylic acid	AN01252000	0.56753	0.002095	Significant Decrease
31	Quinolinic acid	AN00832002	0.661348	0.042923	Significant Decrease
32	Isomer 1 of 13(S)-HPOT	AN02857002	1.405553	0.012282	Significant Increase
33	8-Methyl-6-nonenoic acid	AN00898021	1.470757	0.046495	Significant Increase
34	(S)-2,3,4,5-Tetrahydropyridine-2-Carboxylic Acid	AN00360000	0.541611	0.021288	Significant Decrease
35	Dehydroalanine	AN00113001	0.619519	0.027647	Significant Decrease
36	Carbapenem Biosynthesis Intermediate 6	BM00842003	1.583691	0.035309	Significant Increase
37	N-Acetyl-Dehydroalanine	PR00381000	0.72519	0.01262	Significant Decrease
38	2-Hydroxy-2-Hydropyrone-4,6-Dicarboxylic Acid	BM01100003	1.389419	0.049755	Significant Increase
39	Lipoxin A4	AN03427001	1.580531	0.031842	Significant Increase
40	Prostaglandin E2	AN03427004	1.878689	0.01499	Significant Increase

3.13 Weight Changes Over a 12-Week Period of 10 and 45 kcal% Fat Diets

To determine the effect of loss of EC CD36 in a diabetogenic setting. We fed the mice diets that matched in terms of ingredients. These diets comprised either 35 kcal% carbohydrate or 45 kcal% fat (D12451, Research Diets, Inc.) or 70 kcal% carbohydrate and 10 kcal% fat (D12450H, Research Diets, Inc.). The additional carbohydrates in the latter diet were in the form of starch, and the sucrose content remained consistent between both diets. At baseline, mice of the same sex exhibited no differences in weight. Over the course of the 12-week diet, weight gain exhibited comparable patterns in both the male and female groups. Although there were small transient differences between the female groups at 6 and 9 weeks. (Figure 29 A-D).

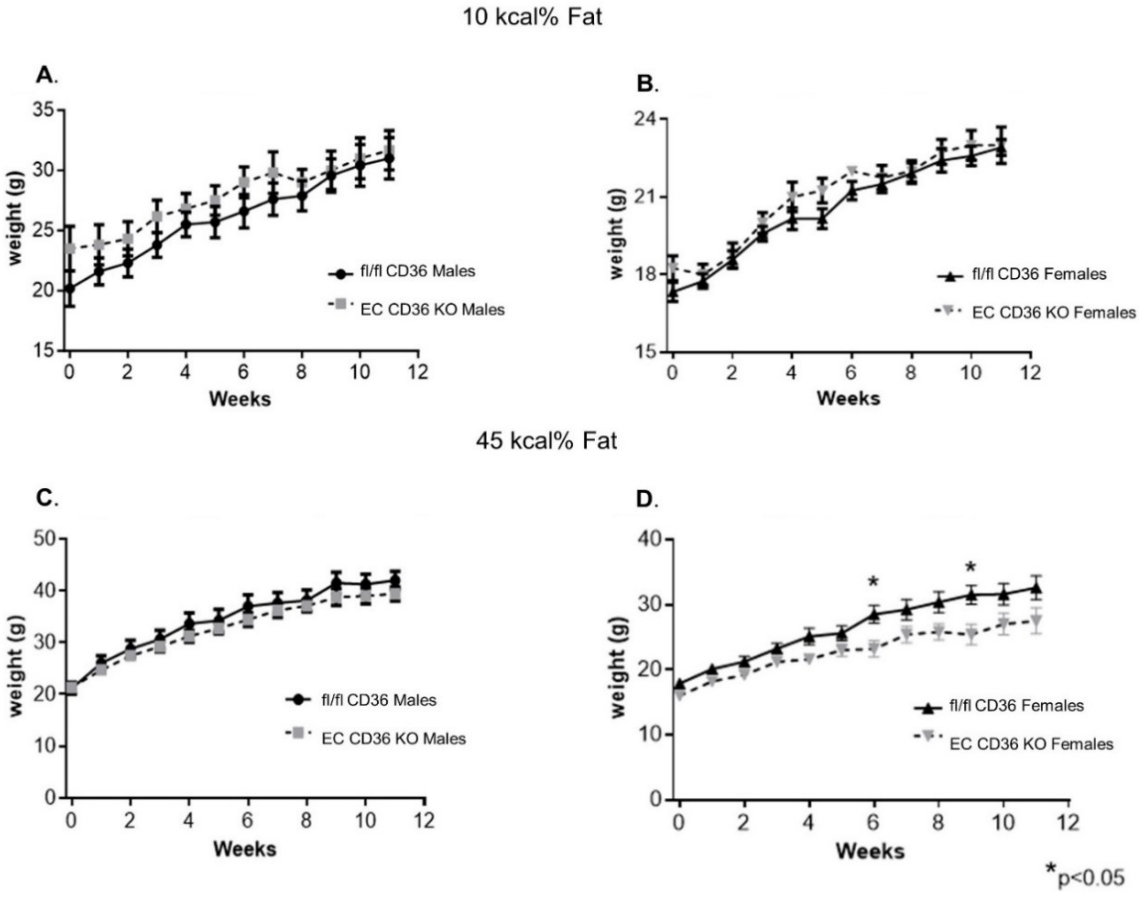

Figure 29: Change in weight over time of EC CD36 KO and fl/fl CD36 mice fed ingredient matched diets. **A.** Male mice fed the 10 kcal% fat diet. (fl/fl CD36, n=10; EC CD36 KO, n=6). **B.** Female mice fed the 10 kcal% fat diet (fl/fl CD36, n=12; EC CD36 KO, n=4). **C.** Male mice fed the 45 kcal% fat diet. (fl/fl CD36, n=8; EC CD36 KO, n=9). **D.** Female mice fed the 45 kcal% fat diet (fl/fl CD36, n=12; EC CD36 KO, n=5). There was a significant (*p ≤0.05) difference in weight at the 6- and 9-week time points.

3.14 GTT After 8 Weeks of 10 and 45 %kcal Fat Diets

Following 8 weeks of diet feeding, we performed GTT to compare glucose clearance between the groups (Figures 30 A-D). In female EC CD36 KO mice, enhanced glucose clearance was observed in comparison to the control groups, regardless of the diet they were fed as shown in Figures 30 B and D. Female mice fed the 10 kcal% fat diet showed significant differences at 30, 45, 60, and 120 minutes. Moreover, there was a significant difference in the AUC between the female groups (fl/fl CD36: 26,939 ± 688; EC CD36 KO: 20,815 ± 625, $p = 0.001$). Similarly, female mice fed with the 45 kcal% fat diet showed significant differences at 30, 45, and 60 minutes. The AUC also showed a significant difference (fl/fl CD36: 32,822 ± 1,813; EC CD36 KO: 23,733 ± 62,135, $p = 0.0238$). Furthermore, male EC CD36 KO mice exhibited improved glucose clearance compared to controls when fed the 45 kcal% diet (Figure 30 C). Male mice fed with the 45 kcal% fat diet showed significant differences at 15, 30, 45, and 60 minutes. The AUC also differed significantly between the male groups (fl/fl CD36: 36,455 ± 1,589; EC CD36 KO: 28,080 ±1,974, $p < 0.02$). The results suggest that the loss of EC CD36 is associated with improved glucose clearance, particularly in the context of different dietary conditions and sex differences.

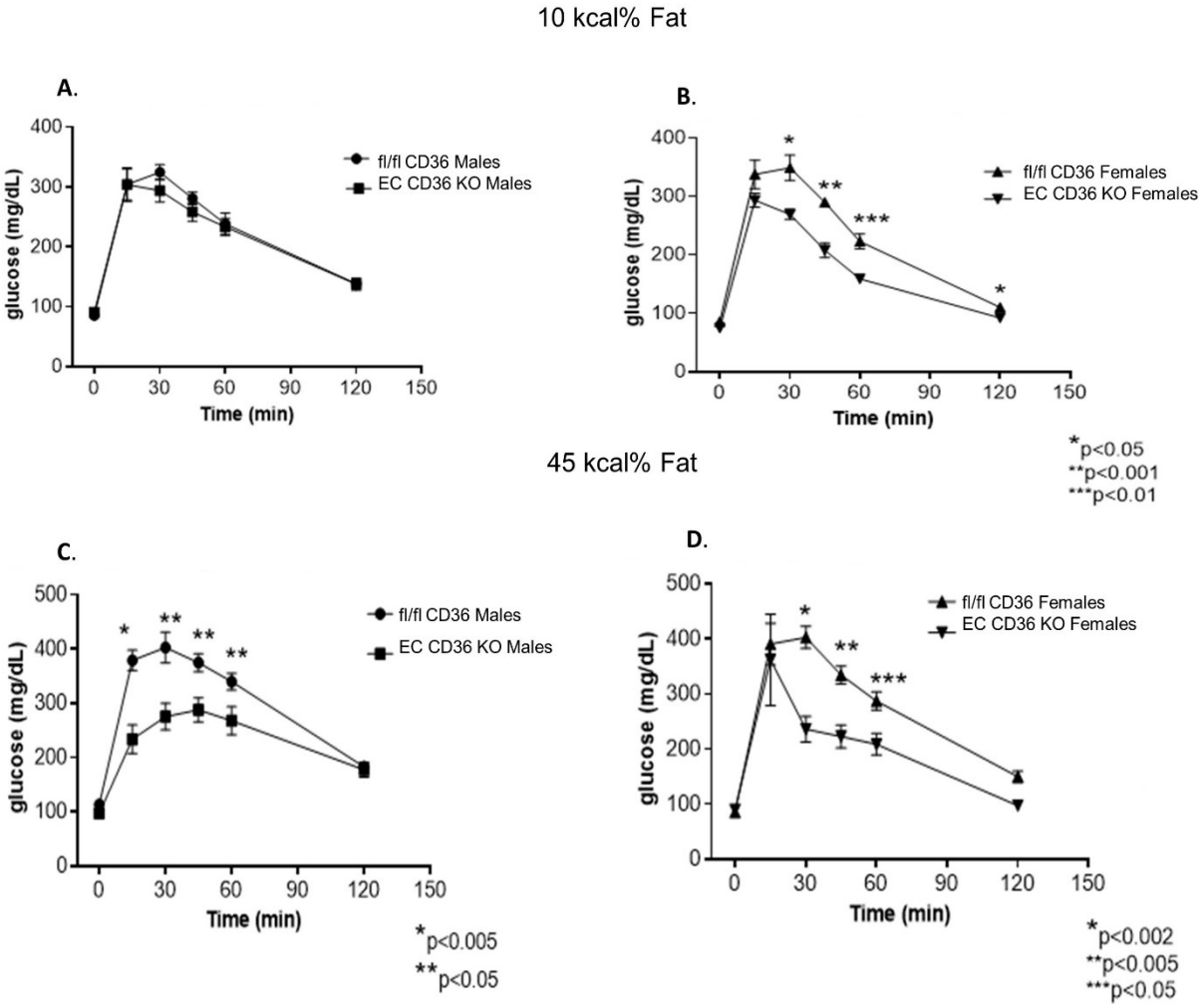

Figure 30: GTT of EC CD36 KO and fl/fl CD36 mice after 8 weeks feeding ingredient matched diets. **A.** Male mice fed the 10 kcal% fat diet showed no significant differences. (fl/fl CD36, n=5; EC CD36 KO, n=6). **B.** Female mice fed the 10 kcal% fat diet showed significant differences at 30, 45, 60 and 120 minutes. AUC was significantly (p=0.001) different (fl/fl CD36, n=5; EC CD36 KO, n=3). **C.** Male mice fed the 45 kcal% fat diet showed significant differences at 15, 30, 45 and 60 minutes. AUC was significantly (p<0.02) different (fl/fl CD36, n=5; EC CD36 KO, n=3). **D.** Female mice fed the 45 kcal% fat diet showed significant differences at 30, 45 and 60 minutes. AUC was significantly (p=0.0238 Mann-Whitney) different (fl/fl CD36, n=5; EC CD36 KO, n=3).

3.15 Lipoprotein Analysis of Mice With 10 and 45 kcal % Fat Diets

Lipoprotein analysis revealed that the cholesterol distribution was similar between the groups of both sexes when they were on either diet as shown in Table 8. However, differences in the distribution of TGs were observed, particularly in female mice (Table 8). Specifically, in female EC CD36 KO mice on the 10 kcal% fat diet, there was a higher percentage of TGs in the LDL/IDL (intermediate density lipoprotein) fraction in comparison to the control group. In the case of male and female EC CD36 KO mice on the 45 kcal% diet, both exhibited a greater percentage of TGs in the LDL/IDL fractions (Table 8) when compared with the control groups. Furthermore, female EC CD36 KO mice showed lower overall levels of TGs. The findings indicate that the lack of EC CD36 is linked to changes in the distribution of TG, particularly in response to different dietary conditions and with sex-specific variations.

Table 8. Lipoprotein analysis of mice fed with the 10% and 45 kcal % fat diets.

Males	fl/fl CD36	EC CD36 KO	fl/fl CD36	EC CD36 KO
10 kcal% fat	Cholesterol	(% of total)	Triglyceride	(% of total)
VLDL	2	1	62	69
LDL/IDL	9	11	30	26
HDL	89	88	9	5
Females	fl/fl CD36	EC CD36 KO	fl/fl CD36	EC CD36 KO
10 kcal% fat	Cholesterol	(% of total)	Triglyceride	(% of total)
VLDL	2	2	51	41
LDL/IDL	7	11	39	48
HDL	91	87	11	11

Males	fl/fl CD36	EC CD36 KO	fl/fl CD36	EC CD36KO
45 kcal% fat	Cholesterol	(% of total)	Triglyceride	(% of total)
VLDL	0.3	0.7	54	37
LDL/IDL	20	14	39	48
HDL	80	86	7	15
Females	fl/fl CD36	EC CD36 KO	fl/fl CD36	EC CD36 KO
45 kcal% fat	Cholesterol	(% of total)	Triglyceride	(% of total)
VLDL	0.8	0.5	27	25
LDL/IDL	11	9	46	64
HDL	88	91	27	12

3.16 Cholesterol and TG after 12 Weeks of 10% and 45% Fat Diets

Following 12 weeks of 10% and 45% diet feeding, we conducted cholesterol and TG assays to evaluate their plasma levels in these mice. Nevertheless, no significant differences were observed between the male and female EC CD36 KO mice and their respective sex-matched controls (Figure 31 A&B). However, it is important to note that this data is preliminary due to the limited sample size, with only one mouse in the EC CD36 KO females 12% diet group.

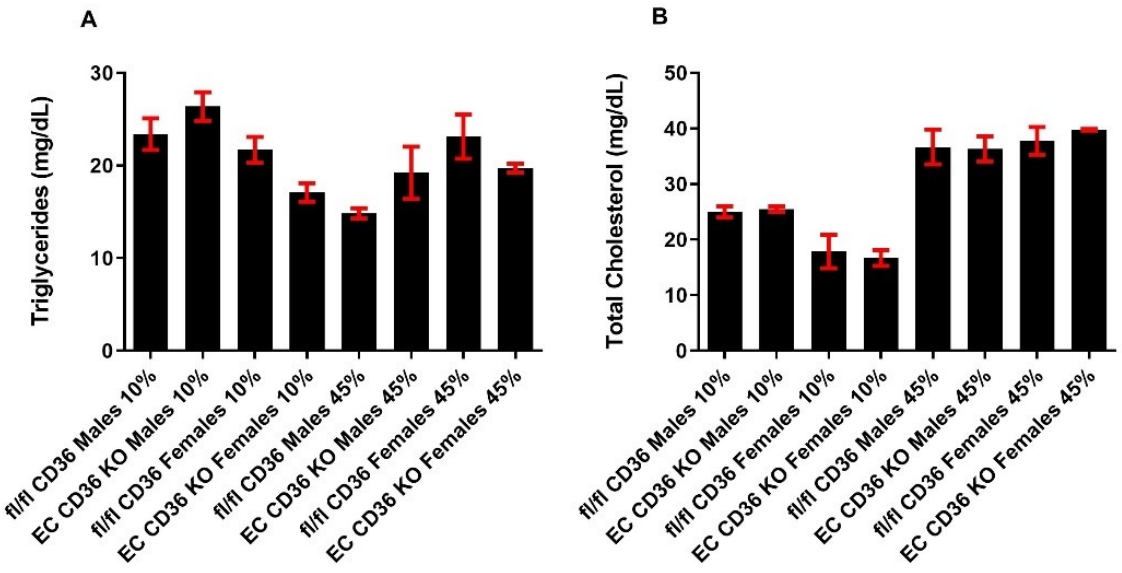

Figure 31: Cholesterol and TG plasma levels in EC CD36 KO and fl/fl CD36 male and female mice after 12 weeks of 10% and 45% diet. **A.** No difference in plasma TG levels were noted between the groups. **B.** No difference in plasma cholesterol levels were noted between the groups. (Males: fl/fl CD36, n =3, EC CD36 KO, n = 3), (Females: fl/fl CD36, n =3, EC CD36 KO, n = 1). Preliminary data due to limited sample size.

3.17 Role of EC CD36 Deficiency on Atherosclerosis Initiation and Development After 16 Weeks of HFHC Diet Study

In this study we sought to explore the specific role of EC CD36 deficiency in the initiation and progression of atherosclerosis following a 16-week period of a HFHC diet. Our investigation aims to unravel the impact of CD36 deficiency within the ECs on the early stages and overall development of atherosclerosis under the conditions induced by an extended consumption of a diet rich in both fats and cholesterol. By exploring the consequences of EC CD36 deficiency over this 16-week duration, we seek to elucidate the intricate interplay between ECs and a HFHC diet in the context of atherosclerosis.

3.18 GTT at Baseline and 3 and 6 Weeks of HFHC Diet

We performed GTT when the mice were 6-7 weeks old, before starting the HFHC diet and at 3 and 6 weeks of the HFHC diet. Before diet initiation we observed that female mice did not show any significant differences in their ability to clear a glucose bolus at the baseline (Figure 32 A). After 3 weeks of diet feeding, female EC CD36 KO/LDLR KO mice showed faster glucose clearance with significant differences at 15, 45, and 60 minutes. Furthermore, the AUC was significantly different (fl/fl CD36/LDLR KO: 23,896 ± 1,920; EC CD36 KO/LDLR KO: 18,409 ± 719, $p < 0.02$) (Figure 32 B). After 6 weeks of diet, female EC CD36 KO/LDLR KO mice exhibited a comparable pattern. However, it is important to note that the data for the 6-week period is preliminary due to the limited sample size, with only two mice in the EC CD36 KO/LDLR KO group (Figure 32 C).

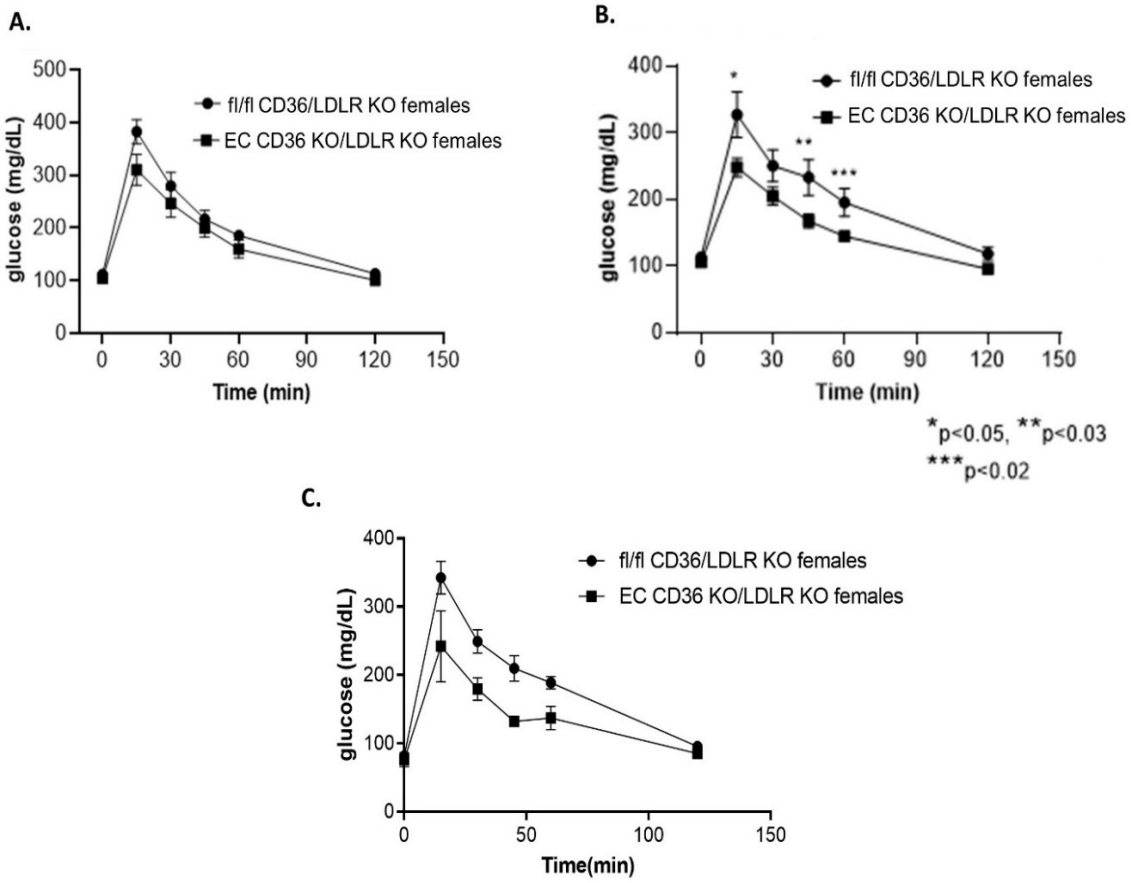

Figure 32: GTT of female EC CD36 KO/LDLR KO and fl/fl CD36/LDLR KO mice at baseline and, after 3 and 6 weeks of HFHC diet feeding. **A.** At 6–7 weeks of age, prior to initiation of the HFHC diet, there were no differences in glucose clearance between the groups. **B.** After 3 weeks diet feeding, female EC CD36 KO/LDLR KO showed significant differences at 15, 45, and 60-minute time points. AUC was significantly ($p < 0.02$) different (fl/fl CD36/LDLR KO, n = 8; EC CD36 KO/LDLR KO, n = 10). **C.** After 6 weeks of diet, female EC CD36 KO/LDLR KO mice demonstrated a consistent trend with enhanced glucose clearance, however this is preliminary data due to limited samples size.

3.19 GTT After 10 Weeks of HFHC Diet

The GTT conducted after 10 weeks of diet revealed that male EC CD36 KO/LDLR KO mice showed a significant difference specifically at the 0-time point (Figure 33 A). However, there were no differences in the AUC. In contrast, female EC CD36 KO/LDLR KO mice exhibited a more rapid glucose clearance than the control group. For female EC CD36 KO/LDLR KO mice, significant differences were observed at all time points, and the AUC was also significantly different (fl/fl CD36/LDLR KO: 30,817 ± 1,142; EC CD36 KO/LDLR KO: 19,331 ± 1,161, $p < 0.0001$). (Figure 33 B). The observed results indicate sex-specific differences in the response to the GTT in EC CD36 KO/LDLR KO mice, with males showing an immediate response and females exhibiting sustained and significant improvements in glucose clearance.

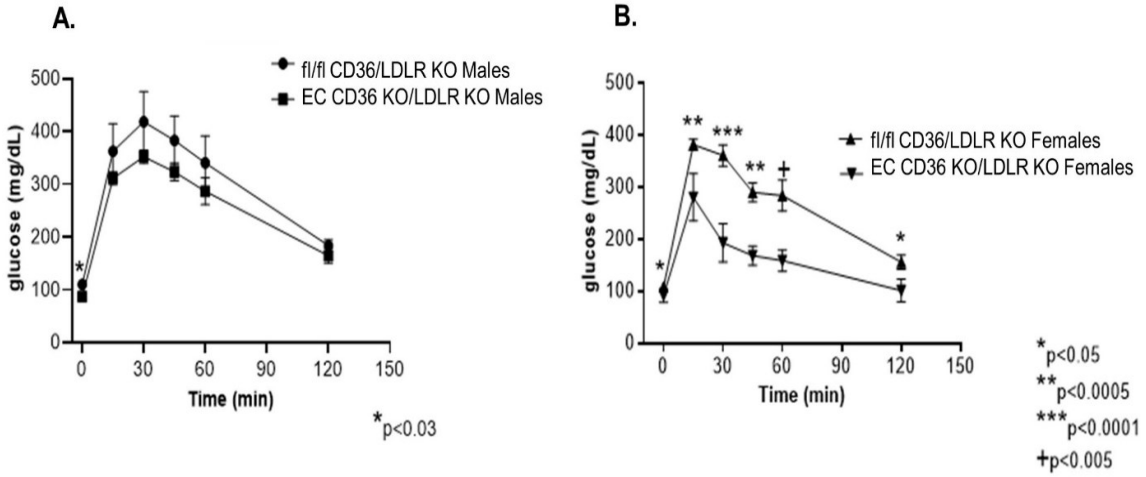

Figure 33: GTT of EC CD36 KO/LDLR KO and fl/fl CD36/LDLR KO mice after 10 weeks of HFHC diet feeding. **A.** Male EC CD36 KO/LDLR KO mice showed a significant difference at the 0-time point. AUC was not different (fl/fl CD36/LDLR KO, n = 4; EC CD36◦/LDLR◦, n = 7). **B.** Female EC CD36 KO/LDLR KO mice showed significant differences at all time points. AUC was significantly different (fl/fl CD36/LDLR KO, n = 9; EC CD36◦/LDLR KO, n = 5).

3.20 Total and Free Cholesterol After 3 and 6 Weeks of HFHC Diet

We measured total and free cholesterol levels in the plasma after 3 and 6-weeks of diet feeding. Regarding free cholesterol levels, we noted a reduction at both the 3 and 6-week time points (Figure 34 A). Nevertheless, at the 3-week time point, the plasma total and free cholesterol levels were significantly ($p < 0.05$) lower in the EC CD36 KO/LDLR KO female mice than in the control group (Figure 34 A & B). The reduction in plasma total and free cholesterol levels in female EC CD36 KO/LDLR KO mice after 3 weeks of diet feeding could be influenced by a combination of factors, including lack of CD36, sex-specific responses, and potential interactions with the dietary composition.

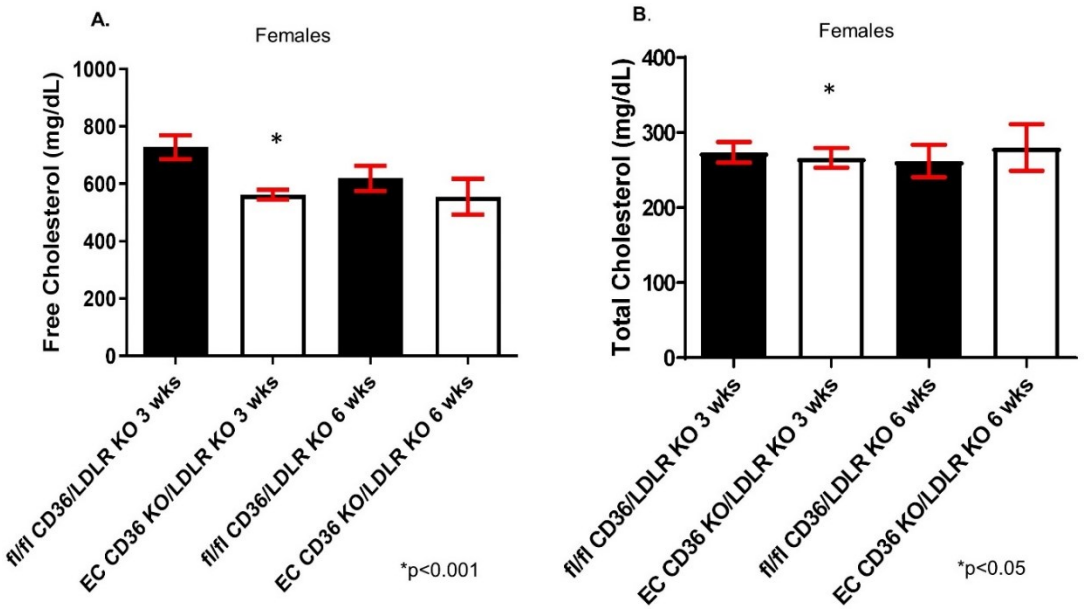

Figure 34: Free and total cholesterol plasma levels in female EC CD36 KO/LDLR KO and fl/fl CD36 LDLR KO mice after 3 and 6 weeks of HFHC diet. **A.** Plasma free cholesterol levels in EC CD36 KO/LDLR KO female mice were significantly lower after 3 weeks of diet. No difference noted after 6 weeks. **B.** Plasma total cholesterol levels in EC CD36 KO/LDLR KO female mice were significantly lower after 3 weeks of diet and no difference observed at 6 weeks. (3 weeks cohort, fl/fl CD36/LDLR KO, n = 10; EC CD36 KO/LDLR KO, n = 13), (6 weeks cohort, fl/fl CD36/LDLR KO, n = 8; EC CD36 KO/LDLR KO, n = 7).

3.21 TG Levels After 3 and 6 Weeks of HFHC Diet

TG levels were also measured after 3 and 6 weeks of the HFHC diet feeding. Plasma TGs were significantly ($p < 0.01$) lower in EC CD36 KO/LDLR KO female mice as compared to the control group after 3 weeks diet. However, at the 6 weeks time point, no difference was observed between the two groups (Figure 35).

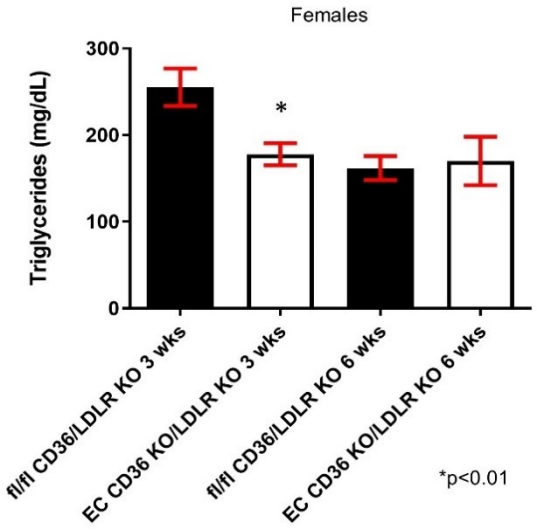

Figure 35: Plasma TGs in female EC CD36 KO/LDLR KO and fl/fl CD36 LDLR KO mice after 3 and 6 weeks of HFHC diet. After 3 weeks of diet TGs were significantly lower in EC CD36 KO/LDLR KO female mice. No difference was observed in TGs levels in mouse plasma after 6 weeks of diet. (3 weeks cohort, fl/fl CD36/LDLR KO, n = 13; EC CD36 KO/LDLR KO, n = 14), (6 weeks cohort, fl/fl CD36/LDLR KO, n = 12; EC CD36 KO/LDLR KO, n = 12).

3.22 3-NT Levels After 3 and 6 Weeks of HFHC Diet

3-NT (a marker for peroxynitrite) serves as an important indicator of inflammation, EC damage, and NO production. We determined 3-NT levels in the plasma of mice, revealing that after 3 weeks, the plasma 3-NT levels were higher in the female EC CD36 KO/LDLR KO mice compared to the control group. However, after 6 weeks of diet, we observed a reduction in 3-NT levels in female EC CD36 KO/LDLR KO mice, though the difference did not reach statistical significance when compared to the control group (Figure 36).

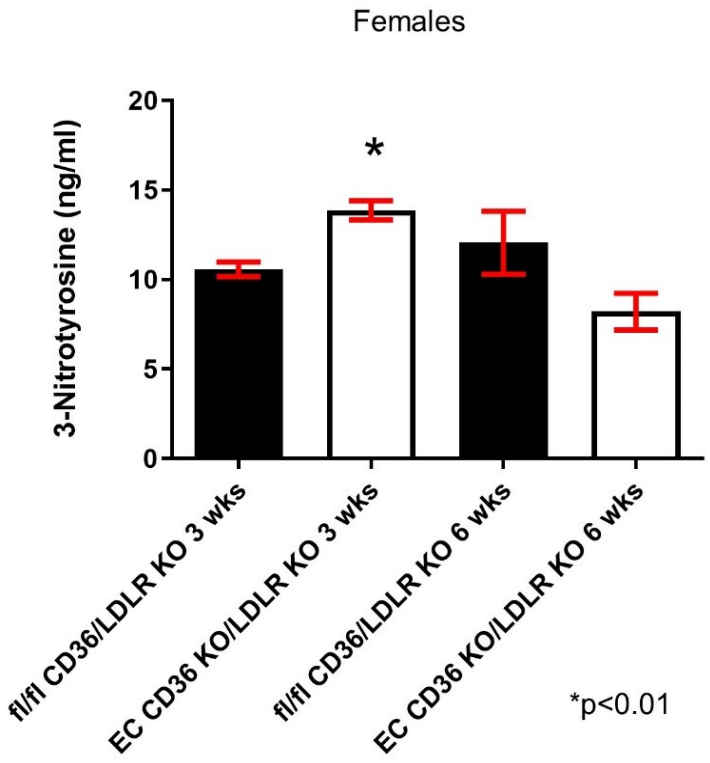

Figure 36: 3-NT levels in plasma of female EC CD36 KO/LDLR KO and fl/fl CD36 LDLR KO mice after 3 and 6 weeks of HFHC diet. 3-NT levels were higher in the female EC CD36 KO/LDLR KO mice after 3 weeks. No difference was observed between the two groups after 6 weeks of diet. (3 weeks cohort, fl/fl CD36/LDLR KO, n = 12; EC CD36 KO/LDLR KO, n = 10), (6 weeks cohort, fl/fl CD36/LDLR KO, n = 7; EC CD36 KO/LDLR KO, n = 10).

3.23 Weight and Fasting Glucose After 3,6 and 16 Weeks of HFHC Diet

After 3 and 6 weeks of HFHC diet no differences in weight and fasting glucose levels were evident between the two groups (Figure 37 A and B). Weights were also measured at the time of sacrifice, and there was no difference noted between the male and female mice groups (Figure 37 C). After 16 weeks of diet, it was determined that there were no significant differences in fasting glucose levels of male mice (fl/fl CD36/LDLR KO: 15.31 ± 2.096% vs. EC CD36 KO/LDLR KO: 11.37 ± 1.884%, p=0.0872). However, EC CD36 KO/LDLR KO female mice exhibited a significant reduction in fasting glucose levels compared with the fl/fl CD36/LDLR KO controls (fl/fl CD36/LDLR KO: 118 ± 8.243 vs. EC CD36 KO/LDLR KO: 87 ± 3.693, *p < 0.0005) (Figure 37 D).

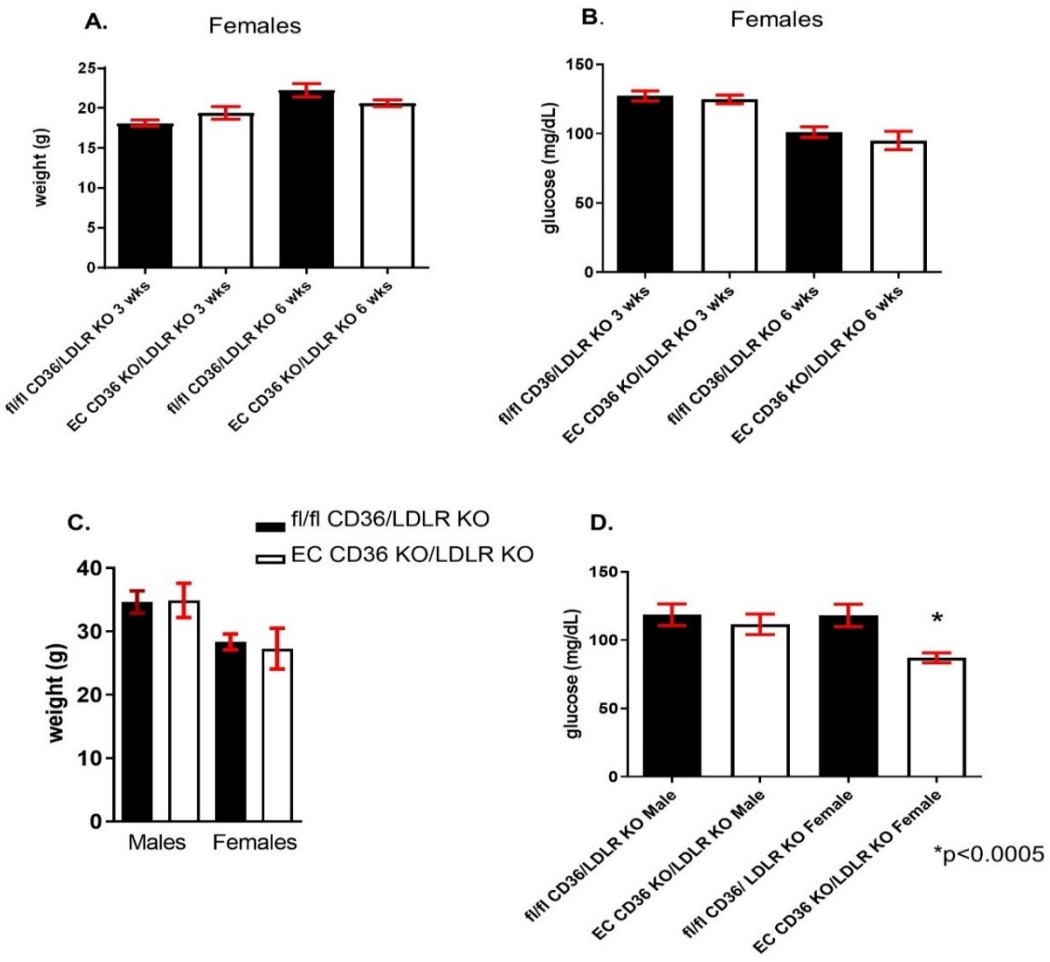

Figure 37: Weight and fasting glucose after 3, 6 and 16 weeks of HFHC diet. **A**. No difference in the weights of fl/fl CD36/LDLR KO and EC CD36 KO/LDLR KO mice observed after 3 and 6 weeks of diet. **B**. No difference in fasting glucose levels was observed between fl/fl CD36/LDLR KO and EC CD36 KO/LDLR KO mice after 3 and 6 weeks of diet **C.** Weights were also not different at endpoint in male or female mice. **D.** Female EC CD36 KO/LDLR KO mice had significantly lower fasting glucose levels than controls after 16 weeks of diet. (3 weeks cohort, fl/fl CD36/LDLR KO, n = 13; EC CD36 KO/LDLR KO, n = 10), (6 weeks cohort, fl/fl CD36/LDLR KO, n = 8; EC CD36 KO/LDLR KO, n = 10).

3.24 Absence of EC CD36 Protects Against Atherosclerosis After 16 Weeks of HFHC Diet

To determine the impact of loss of EC CD36 on atherosclerosis, we bred EC CD36 KO mice with the atherogenic LDLR KO strain. To promote atherosclerosis development, these mice were fed a Western-style diet containing 42.7 kcal% carbohydrate, 42 kcal% fat, and 1.25% added cholesterol (TD 96121, Envigo) for 16 weeks. Whole aortas were stained with oil red O and subjected to *en face* morphometry which revealed no significant difference in male mice (fl/fl CD36/LDLR KO: 15.31 ± 2.096% vs. EC CD36 KO/LDLR KO: 11.37 ± 1.884%, p=0.0872) (Figure 38 A). Conversely, female EC CD36 KO/LDLR KO mice exhibited a noteworthy 41% reduction in aortic lesions (fl/fl CD36/LDLR KO: 12.65 ± 1.896% vs. EC CD36 KO/LDLR KO: 7.447 ± 0.897%, $p < 0.02$), as shown in Figure 38 B. The reduction in aortic lesions in female EC CD36 KO/LDLR KO mice compared to the control group suggests a sex-specific protective effect associated with the loss of EC CD36.

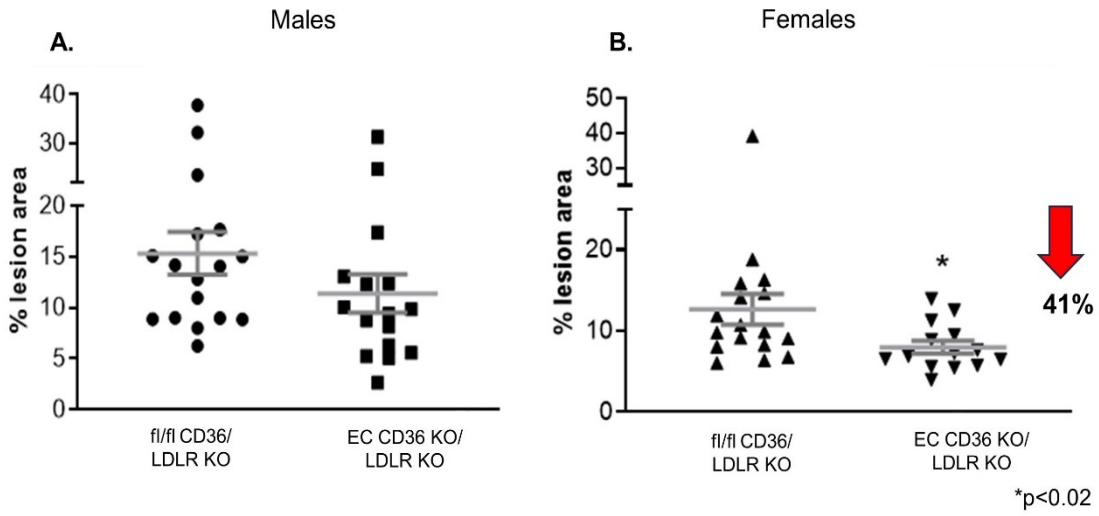

Figure 38: Atherosclerosis lesion analysis. *En face* oil red O aortic lesions were quantified using Adobe Photoshop software after 16 weeks HFHC diet feeding. **A.** Male mice showed no difference in the percentage of atherosclerosis lesion (fl/fl CD36/LDLR KO, n = 17; EC CD36 KO/LDLR KO, n = 16). **B.** Female EC CD36 KO/LDLR KO mice showed a significant (*p <0.02) 41% decrease in the percentage of atherosclerosis lesion compared with controls (fl/fl CD36/LDLR KO, n = 17; EC CD36 KO/LDLR KO, n = 14).

3.25 Total Cholesterol of Mice After 16 Weeks of HFHC Diet

Plasma samples from both male and female mice on the HFHC diet were used to measure total cholesterol levels. Following 16 weeks of diet, no significant differences in the total cholesterol levels of males (fl/fl CD36/LDLR KO: 2,132 ± 103.4 mg/dL vs. EC CD36◦/LDLR◦: 1,967 ± 96.42 mg/dL) or females (fl/fl CD36/LDLR KO: 1,824 ± 68.94 mg/dL vs. EC CD36◦/LDLR KO: 1,680 ± 84.2 mg/dL) were found (Figure 39).

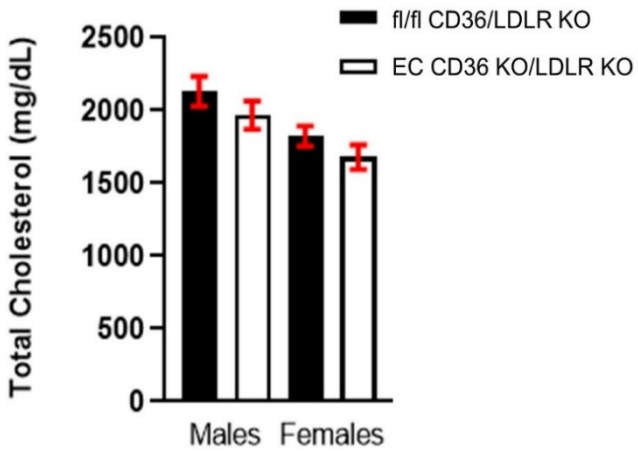

Figure 39: Total cholesterol after 16 weeks of HFHC diet. No differences in male or female mice were observed at the endpoint.

3.26 Lipoprotein Analysis of Mice After 16 Weeks of HFHC Diet

Lipoprotein analysis after 16 weeks showed no differences in male mice (Table 9). Female EC CD36 KO/LDLR KO mice showed a greater percentage of triglycerides in the VLDL fraction compared with controls (Table 9).

Table 9. Lipoprotein analysis of mice fed with the HFHC diet.

Males	fl/fl CD36/ LDLR KO	EC CD36 KO/ LDLRKO	fl/fl CD36/ LDLR KO	EC CD36 KO/ LDLR KO
HFHC Diet	Cholesterol (% of total)		Triglycerides (% of total)	
VLDL	26	26	62	64
LDL/IDL	47	48	27	29
HDL	27	26	12	7
Females	fl/fl CD36/ LDLR KO	EC CD36 KO/ LDLRKO	fl/fl CD36/ LDLRKO	EC CD36 KO/ LDLRKO
HFHC Diet	Cholesterol (% of total)		Triglycerides (% of total)	
VLDL	29	23	72	57
LDL/IDL	54	57	18	24
HDL	18	21	11	20

Chapter 4 - Results

4.1 Impact of a CD36 Inhibitor on *Porphyromonas gingivalis*-Mediated Atherosclerosis Study

This chapter discusses the findings of our research titled "impact of a CD36 Inhibitor on *Porphyromonas gingivalis*-mediated atherosclerosis". Our primary focus in this study was to investigate the potential of a pharmacological intervention targeting CD36, utilizing the drug AP5055, in preventing the increase of atherosclerosis induced by Porphyromonas gingivalis in mice lacking the LDL receptor.

4.2 AP5055 Treatment in LDLR KO Mice Decreases the Atherosclerotic Lesion Burden

En face analysis of LDLR KO mice aortae was performed to examine the efficacy of AP5055 against atherosclerosis. The analysis revealed that LDLR KO mice treated with AP5055 exhibited a reduction in the atherosclerotic lesion area compared to mice treated with the vehicle (7.131 ± 0.732% vs. 10.52 ± 0.661%, $p<0.01$) (Figure. 40 A-B). Statistical analysis showed that the AP5055 treatment group had a 32 % decrease in the atherosclerotic lesion area when compared with the vehicle control group. (Figure 40 C). These findings align with previous research, showing that *P. gingivalis*-infected CD36 KO/LDLR KO mice exhibited a significant reduction in lesion burden compared with *P. gingivalis*-infected LDLR KO mice. Thus, pharmacologically inhibiting CD36 had a comparable effect as genetically deleting it in reducing the increased atherosclerosis induced by *P. gingivalis* infection.

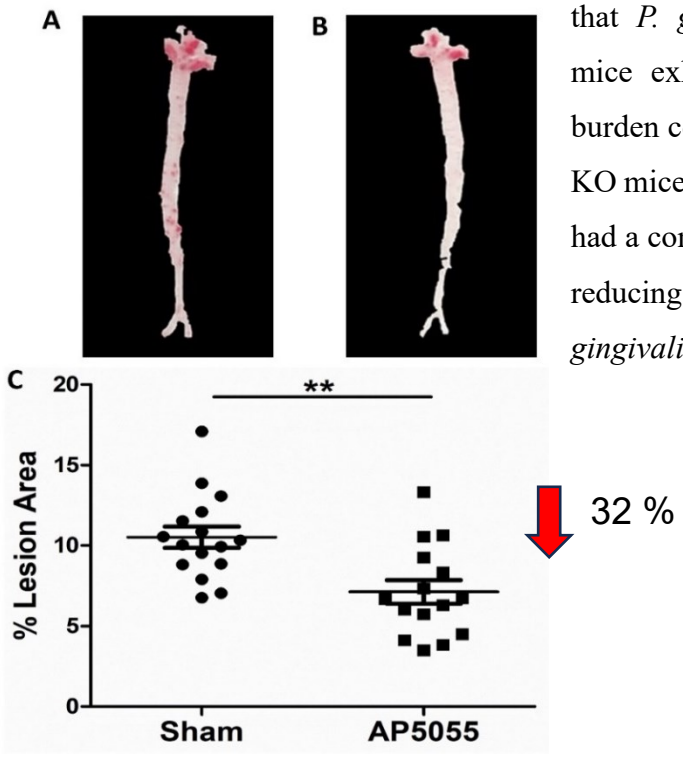

Figure 40: Effect of CD36 inhibitor on lesion burden in the aorta. A, B. Representative aortae from high fat Western diet fed LDLR KO mice orally infected with *P gingivalis* and A, injected with vehicle or B, with AP5055. Oil red-O positive areas indicate atherosclerotic plaque. C. Quantitative analysis of lesion area as a percentage of total aorta. There was a significant difference between the vehicle and AP5055-treated groups. (**p ≤0.01).

4.3 AP5055 Inhibits NF-κB Activation in *P. gingivalis* LPS-Stimulated RAW Blue Cells

We investigated the inhibitory effect of AP5055 on the activation of the NF-κB pathway mediated by *P. gingivalis* LPS. This was performed using murine macrophage RAW-Blue cells that stably express the NF-κB-SEAP reporter gene. NF-κB serves as the critical transcription factor activated downstream of TLR-2 and is responsible for inflammasome activation and cleaving IL-1β into its active, secreted form This cytokine plays a crucial role in both PD and atherosclerosis (216).

In vitro analysis of RAW-Blue cells showed enhanced production of SEAP in cells that were treated with *P. gingivalis* LPS when compared to the control group, in accordance with an increased NF-κB activation (Figure 41). Cells that received a pre-treatment of either 125 μg/ml or 150 μg/ml AP5055, followed by stimulation with *P. gingivalis* LPS, showed a significant reduction of 42% and 55% in SEAP production ($p<0.001$, $p<0.0001$) respectively, when compared with cells that were stimulated with *P. gingivalis LPS* and received vehicle alone. These findings indicate that AP5055 inhibits the *P. gingivalis* LPS-mediated transcriptional activation of *NF-κB.*

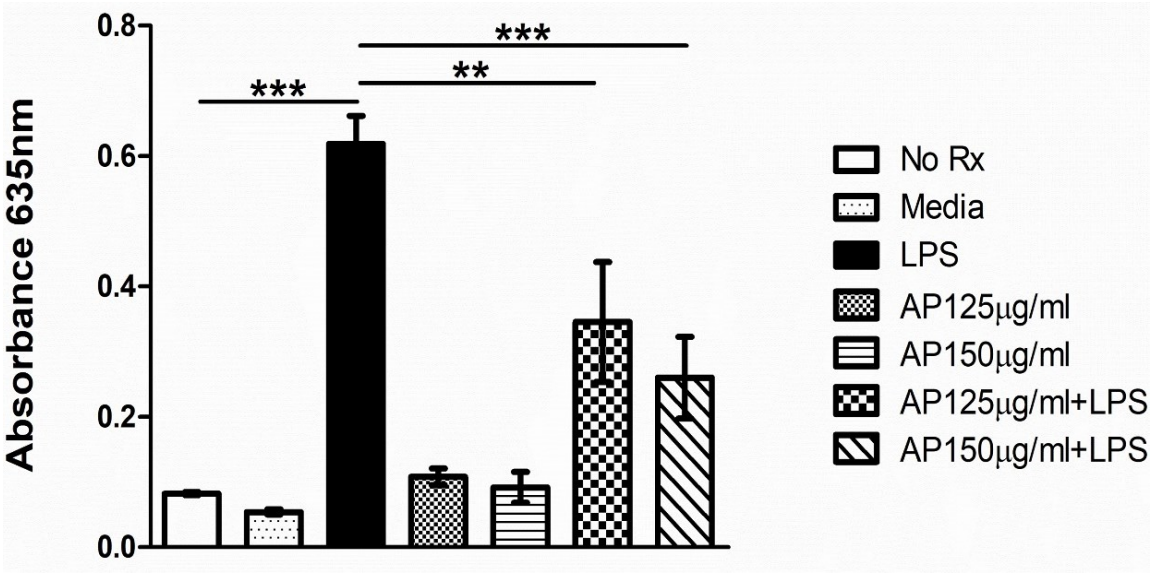

Figure 41: Effect of AP5055 on P. *gingivalis*-mediated activation of NF-κB in murine macrophages. NF-κB activation measured by reporter gene assay (SEAP activity). RAW-Blue cells were incubated with heat-killed *P. gingivalis (*HK-*Pg)* after 30 minutes pre-treatment with different doses of AP5055. SEAP activity as a marker of NF-κB activation was detected using a colorimetric substrate at OD 635nm. (**p ≤ 0.001 *** p ≤ 0.0001). n=4 replicates per group.

4.4 Total Cholesterol and Weight Measurements

At 16 weeks, plasma samples were collected from AP5055 and vehicle-treated LDLR KO mice infected with *P. gingivalis*. The AP5055-treated mice group had significantly (618.5 ± 52.80 mg/dl SEM; $p<0.01$) decreased levels of plasma cholesterol compared with the vehicle-treated group (867.2 ± 58.90 mg/dl SEM) (Figure. 42 A). No significant difference in weight was observed between the two groups (Figure 42 B).

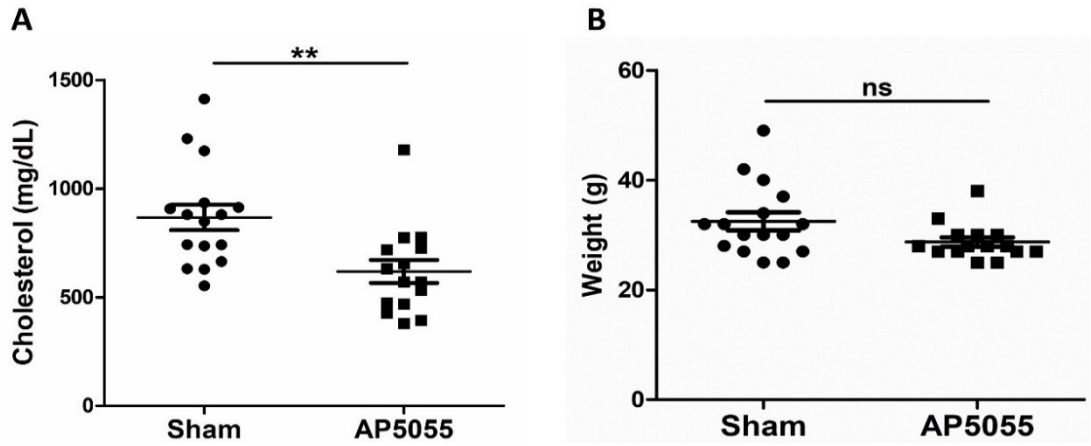

Figure 42: Effect of the CD36 inhibitor on plasma cholesterol levels and weight. Cholesterol and weight were measured at 16 weeks in vehicle and AP5055-treated mice. **A**. Quantitative analysis of cholesterol concentration in plasma samples. There was a significant difference between the vehicle and AP5055-treated groups. (**p ≤0.01). **B.** There was no significant difference in weight between the groups (ns=not significant).

4.5 Effect of AP5055 on Cytokines/Chemokines Expression

Cytokines and chemokines play vital roles as mediators in the onset and progression of atherosclerosis (246). In the AP5055-treated group, circulating levels of pro-inflammatory cytokines such as TNF-α, IL-1α and MCP-1 were significantly reduced ($p < 0.01$) relative to the control group (Figure. 43). In contrast, significantly ($p < 0.001$) increased levels of IL-1ra (2.5-fold) and B lymphocyte chemoattractant (BLC), were also observed ($p < 0.05$). IL-1ra is a naturally occurring IL-1 inhibitor and has been shown to have anti-atherosclerotic roles. Studies have revealed that mice lacking IL-1ra exhibit increased development of atherosclerosis (247).

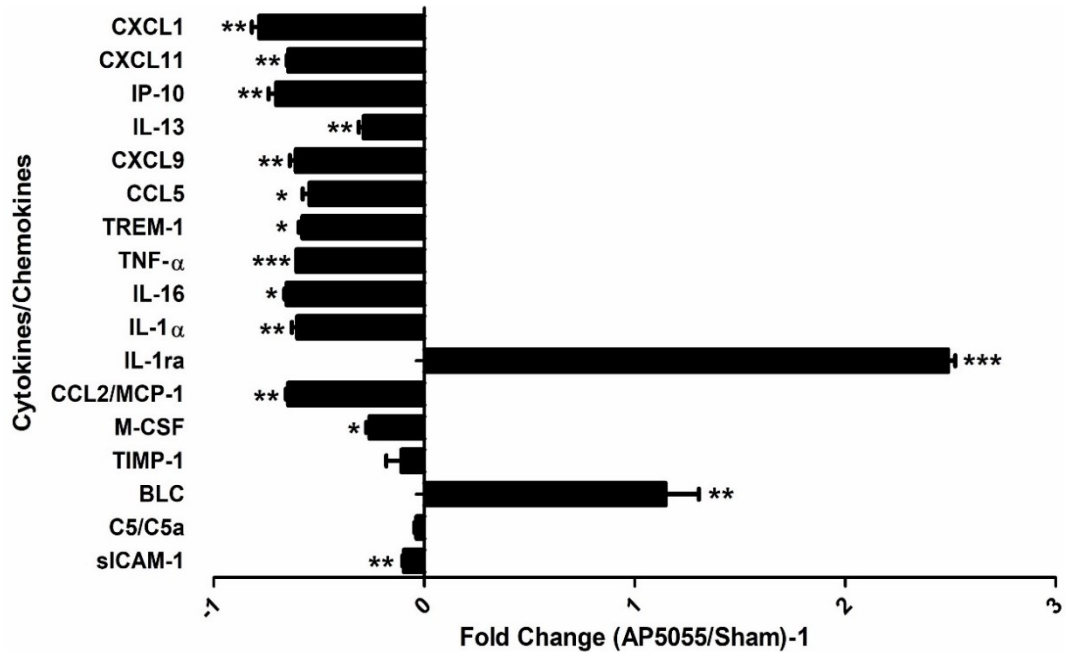

Figure 43: Effect of AP5055 on the production of inflammatory mediators. The relative concentrations of inflammatory cytokines/chemokines in 16-week plasma samples (5 pooled/group) were measured in duplicate using a cytokine array. Densitometric analysis was performed to calculate relative expression levels. The bar-graph represents the fold change in AP5055-treated mice compared with vehicle–treated mice. (*p ≤0.05, **p≤0.01, ***p ≤0.001).

4.6 Alveolar Bone Loss

Micro-CT was used to assess alveolar bone loss in both groups in response to *P. gingivalis* oral lavage. The results of the mandibular measurements showed no statistical difference regarding alveolar bone loss between the AP5055 treated and vehicle-treated groups (Figure. 44). These findings show that both groups experienced equal levels of PD.

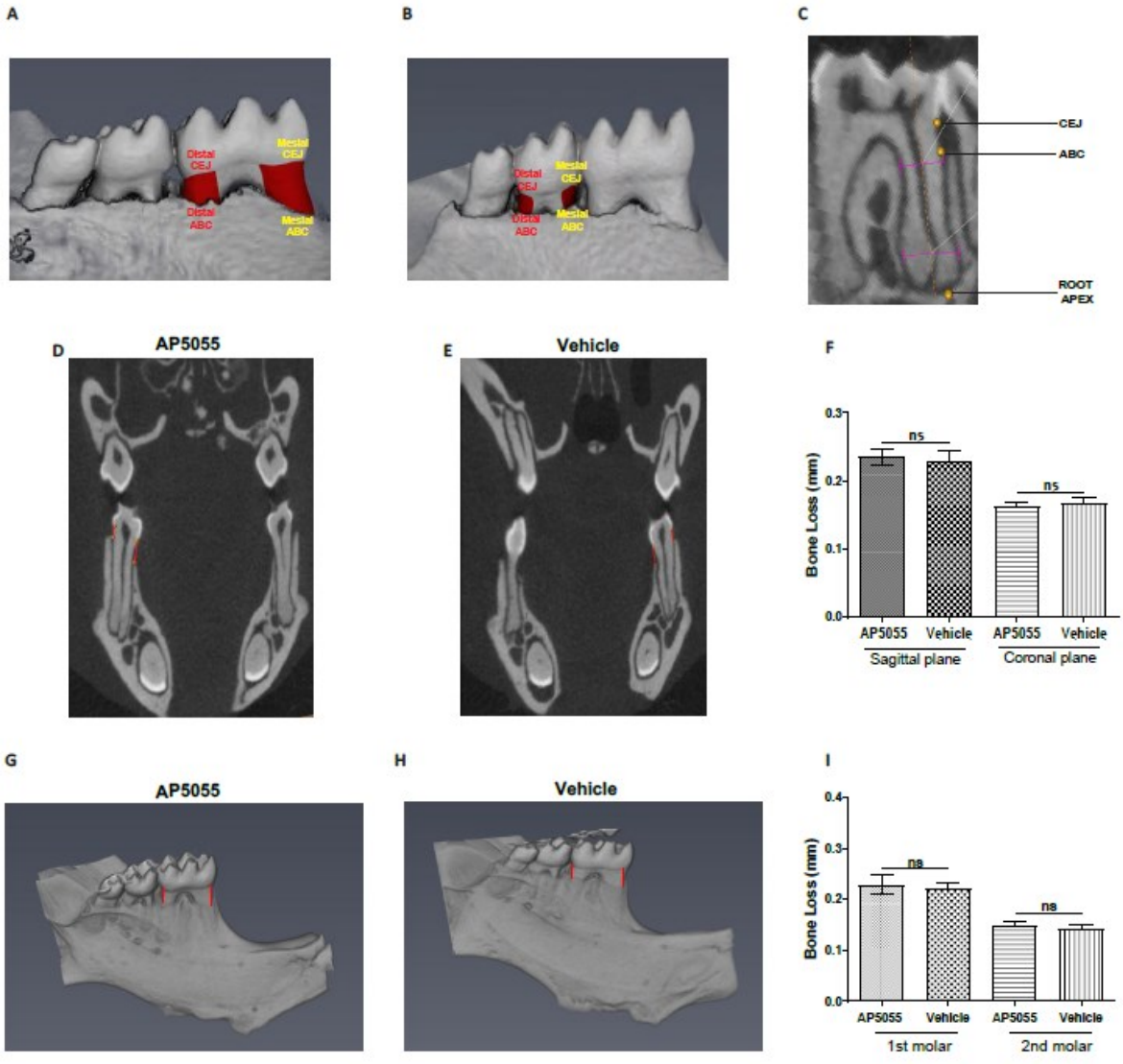

Figure 44: Effect of AP5055 on alveolar bone loss. Micro-CT was used to measure bone loss in the 1st and 2nd molars of the mandible. Representative micro-CT images of coronal plane: **A.** AP5055-treated mice; **B.** Vehicle-treated mice. **C.** quantitative analysis of bone loss of coronal and sagittal plane. Sagittal plane: D. AP5055-treated mice and **E.** Vehicle-treated mice. The red line indicates the distance from the CEJ to ABC. **F.** Dot-plot represents quantitative analysis of bone loss of 1st and 2nd molars respectively. There was no significant difference in bone loss between the groups (ns=not significant).

Chapter 5 - Discussion

CVD stands as the most severe global health issue and the foremost contributor to mortality (1). Within the spectrum of CVD, atherosclerosis, also referred to as coronary artery disease (CAD), emerges as the predominant manifestation (2). Hyperlipidemia induces atherosclerosis-promoting shear stress effects, and elevated plasma FAs and altered lipoprotein ligands activate EC pro-inflammatory pathways (232, 248, 249). FAs play a critical role in supporting cellular functions as essential nutrients, however, the mechanisms through which they are transported into cells remain uncertain (250, 251). Since its recognition as a transporter of FAs, a multitude of research studies have extensively explored the involvement of CD36 in the uptake and utilization of FAs in both mice and humans (35, 130, 159, 252).

5.1 Exploring the Role of EC CD36 in FA Uptake, Atherosclerosis Development, and Metabolic Pathways: Insights from Mouse Models and Molecular Mechanisms

The primary goal of the research outlined in this dissertation was to determine the role of EC CD36 in FA uptake and to investigate differences in the development of atherosclerosis and changes in metabolic characteristics. To achieve this goal, our laboratory (Dr. Febbraio) created an important tool: the EC CD36 KO mouse model. The development of this mouse model is highly significant in moving this field of study forward. Although endothelial CD36 is well-known for its significance in angiogenesis (65, 253), its involvement in the uptake of FAs at this interface has received less attention in research. There is growing recognition that ECs represent a secondary impediment to FAs uptake into tissues (127, 254, 255). While EC were previously perceived as passive barrier to FA diffusion, studies have revealed that CD36 and several of the same proteins involved in tissue FA uptake play a role in regulating this interface (127, 254-257). A recent study by Daquinag *et al.* (150) demonstrated that when lipolysis was induced, there was a decrease in CD36 S-acylation and glycosylation, indicating modifications in its post-translational state. As a result of lipolysis induction, CD36 dissociated from the cell membrane and separated from the proteins, prohibitin and annexin A2. Additionally, there was a shift in the subcellular localization of CD36, as it became associated with caveolae and was trafficked to lipid droplets. While the specific mechanism may lack consensus, it is evident that the absence of CD36 in both mice and humans has systemic repercussions (65).

One of the initial findings that underscored the significance of the endothelium in controlling FA uptake and metabolism revolved around the deletion of the key transcriptional regulator and FA sensor, PPARγ, specifically in ECs. The EC KO mice displayed elevated levels of FAs but demonstrated protection against HFD-induced adiposity and IR, in contrast to the outcomes observed in the control mice. This mouse model also exhibited a significant reduction in EC CD36 expression and closely mirrored the metabolic characteristics of the CD 36 KO model in several aspects (155). This suggests that ECs have substantial regulated control over metabolism. It also indicates that the protection against atherosclerosis in global CD36 KO mice may be partially attributed to alterations in systemic metabolism, particularly due to the significant roles of obesity and IR in promoting atherosclerosis lesion development.

Recognizing the possible interference caused by the absence of CD36 in macrophages and other hematopoietic cells in atherosclerosis progression and systemic inflammation, we generated an EC-specific CD36 KO by crossing to a Tie2e cre mouse, thereby preserving these cell types (233-235). Mice with floxed CD36 alleles were previously developed using C57Bl/6j embryonic stem cells to circumvent potential concerns related to genetic background (156). Consequently, these mice exhibit distinctions from previously documented EC CD36 KO mice, which were generated using the endothelial-specific receptor tyrosine kinase (Tek or Tie 2) cre system on a mixed genetic background. A drawback of the Tek cre system is that it exhibits expression in hematopoietic cells, including macrophages, which could introduce complicating factors in our models related to obesity, IR, and atherosclerosis. The creation of an animal model to investigate the role of EC CD36 in fatty acid uptake, particularly in the context of a pro-atherosclerotic environment, represents a significant outcome of this research. Furthermore, these mice will facilitate the study of EC CD36 signaling pathways activated by excessive dietary fat, which could play a role in EC inflammation, the formation of arterial plaques, and the development of pathological metabolic conditions.

Regarding the uptake of oxLDL, the activation of mitogen-activated protein kinase (MAPK), specifically c-Jun N-terminal kinase 1/2 (JNK1/2) is crucial for the formation of macrophage foam cells through CD36 (258, 259). The connections between CD36, TLRs and Na-K ATPase were revealed to be associated with the initiation of proinflammatory pathways, such as the NF-kB pathway, and the activation of the nucleotide-binding domain, leucine-rich–containing

family, pyrin domain–containing-3 (NLRP3) inflammasome, which contribute to the development of atherosclerosis (258, 259). In light of these findings and considering our model of EC dysfunction (Figure 3), this study also highlights the mechanistic role of EC CD36 in EC activation and FA uptake in HFDs. This diet results in an excess of FAs, potentially leading to the generation and recognition of oxFA by CD36. Surpluses of both FAs and oxFA, which are CD36 ligands, are associated with incomplete beta-oxidation, triggering an inflammatory response. Furthermore, the activation of JNK can disrupt insulin signaling by phosphorylating and deactivating insulin receptor substrate 2 (IRS2), ultimately contributing to the development of IR. In addition, CD36 plays a role in the uptake of FAs.

5.2 Metabolic Impact of EC CD36: Sex-Specific Differences Unveiled in Young Mice

One of the key findings of this study is the significant impact of EC CD36 on metabolic homeostasis in both male and female mice. However, what makes this finding even more intriguing is that although the contribution of EC CD36 to metabolic homeostasis is strong in both sexes, there are notable differences between male and female mice. At 4 weeks of age, both the EC CD36 KO and control mice exhibited similar body weights. Notably, a substantial reduction in the fat mass percentage was observed in both male and female mice with either global or EC CD36 KO compared to their sex-matched controls. This decline in fat mass suggests that the absence of CD36 may affect the efficient uptake or utilization of FAs, leading to decreased fat mass, a trend consistent with studies demonstrating reduced fat mass in CD36 KO mice (134, 150, 260). To understand how the metabolic processes in these mice were functioning, indirect calorimetry was employed, where only male mice showed a greater reliance on carbohydrate metabolism. In addition to the altered metabolic preference, the male mice also displayed reduced locomotor activity and decreased energy expenditure. These findings imply that at this age, male EC CD36 KO mice had distinct metabolic and behavioral differences when compared to the controls. During the early light period, which is the start of the active phase for mice, both the control group and the EC CD36 deficient male mice exhibited a metabolic pattern characterized by a blend of carbohydrate and fat utilization, as indicated by the RER. Interestingly, the male EC CD36 KO mice also consumed more food than the control mice during the same early light period.

As the light period progressed, the EC CD36 KO male mice demonstrated a notable shift towards a greater reliance on carbohydrate metabolism. This suggests that later in the light period, these mice began to prioritize carbohydrates as their primary energy source, possibly because of the deficiency in CD36-mediated FA uptake, the mice may undergo metabolic adaptations to ensure a continuous and adequate energy supply (Figure 45). In the dark phase, which corresponds to the period when mice are typically at their peak activity levels, EC CD36 KO male mice showed a noticeable decrease in their locomotor activity. Furthermore, measurements of oxygen consumption and carbon dioxide production, which serve as indicators of energy expenditure, showed reductions in both the dark and light phases compared with the control group. The reason for these changes may be linked to a shift in the way these mice generate adenosine triphosphate (ATP), which is the primary molecule that cells use for energy. The decrease in ATP generation is likely a result of the anaerobic respiration of carbohydrates. Anaerobic respiration is a less efficient way of producing ATP than aerobic respiration, and it often relies on carbohydrates as the main energy source. During anaerobic respiration, cells use alternative electron acceptors (in addition to oxygen) to complete the electron transport chain, resulting in a lower ATP yield. Taken together, these observations indicate a systemic alteration in the energy metabolism of mice. Specifically, there appears to be a decrease in FA oxidation to produce energy. FA oxidation is known to produce a substantial amount of high-energy molecules, and its decrease may contribute to the overall changes in energy metabolism and activity levels observed in EC CD36 KO male mice during the dark phase.

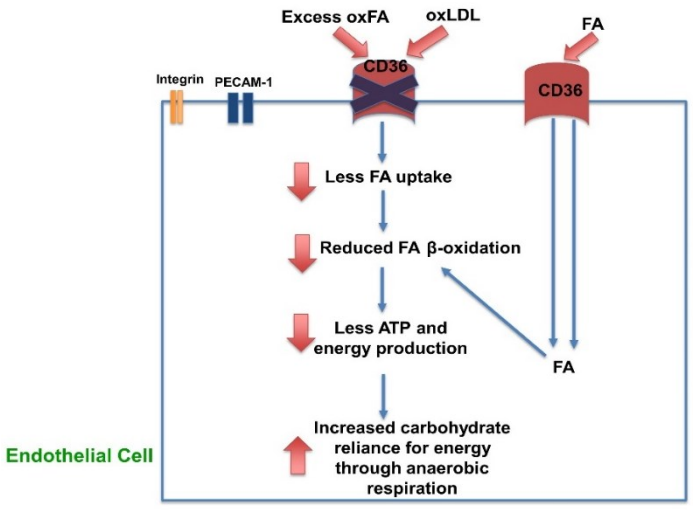

Figure 45: Metabolic adaptations in EC CD36 KO mice. Absence of EC CD36 leads to diminished FA uptake, reducing β-oxidation and ATP production. Consequently, there is an increased reliance on glucose utilization for energy production.

5.3 Limitations of Indirect Calorimetry and Sex-Specific Variations in EC CD36 Deficiency: Implications for Substrate Utilization and Hormonal Influences

Indirect calorimetry has a limitation that it provides information on total energy expenditure but lacks a direct assessment of the specific utilization of substrates, such as carbohydrates and fats. As a result, changes in substrate utilization may not be accurately reflected solely through measurements of oxygen consumption and carbon dioxide production. Furthermore, this study primarily focuses on a single time point (4 weeks of age). Performing longitudinal assessments at various time points could contribute to a more comprehensive comprehension of how metabolic and behavioral differences between sexes evolve over time. Continuing these investigations in older mice will be crucial for gaining insights into whether these initial metabolic patterns endure in both males and females. In addition, it will help elucidate the impact of various dietary interventions on these patterns. The metabolic data in males closely align with previous findings in global CD36 KO mice, indicating an increased preference for carbohydrates as an energy source over fats, particularly in the heart and muscle tissues (133, 134, 261, 262). However, a notable difference emerged when comparing male mice with EC-specific CD36 deficiency to the global CD36 KO mice. In the case of the EC CD36 KO male mice, their body weights were similar with those of the control group, indicating that the absence of CD36 in ECs did not lead to the weight changes typically observed in global CD36 KO mice. Furthermore, an intriguing revelation from the data is the disparity between the sexes. Although this study identified differences in metabolic responses between male and female mice, these distinctions were not observed in the global CD36 KO mice.

Systemic metabolic alterations resulting from decreased FAs uptake were also evident in mice with EC CD36 deficiency generated using the Tek cre mouse. Interestingly, the metabolic effects displayed sex-dependent variations. In male mice, there was a significant reduction in the uptake of oleic acid in crucial tissues such as the heart, muscle, and brown adipose tissue. This has significant implications for their energy metabolism, consistent with the indirect calorimetry

results in the male Tie2e cre EC CD36 KO mice. On the other hand, in the case of female Tek cre EC CD36 KO mice, no such differences in oleic acid uptake were observed within their muscle tissue. **(116)**. This again would be consistent with the absence of differences in indirect calorimetry results between female controls and Tie2e cre EC CD36 KOs. The data we have collected may indicate the presence of sex-specific differences in the expression of CD36 within subsets of ECs, or it could suggest that there are variations in the activity of alternative transporters that play a role in FA uptake.

Moreover, it is important to highlight the potential influence of sex hormones, such as estrogen and testosterone, in this context. With regard to future research, understanding how these hormones impact CD36 expression and FA metabolism could provide valuable insights into the observed sex-specific differences in our study.

5.4 Metabolic Profiling Analysis Reveals Altered Amino Acid and Metabolite Levels in EC CD36 KO Mice: Implications for FA Metabolism, Inflammation and Vitamin K Pathway

Our metabolic profiling analysis data showed that plasma acetylcarnitine levels in male EC CD36 KO mice were elevated compared with the control group. Conversely, the increase in acetylcarnitine levels in male mice lacking EC CD36 implies modifications in FA metabolism. Acetylcarnitine is crucial for beta-oxidation, specifically, the transport of FAs into mitochondria for energy production. In a study by Schroeder *et al.* (263) it was demonstrated that acetylcarnitine plays a pivotal role in the dynamic cycling of acetyl-CoA produced from pyruvate. This cycling finely adjusts the immediate supply of acetyl-CoA derived from carbohydrates to meet the demands of the Krebs cycle; a fundamental cellular process involved in energy production. The increased plasma acetylcarnitine levels in EC CD36 KO mice may indicate an enhanced capacity for this dynamic cycling process. The cycling mechanism of acetylcarnitine also contributes to preventing the static accumulation of acetyl-CoA. Consequently, the elevated plasma acetylcarnitine levels in the KO mice likely signify an adaptive response, enabling effective buffering and utilization of acetyl-CoA to maintain a balanced and controlled energy metabolism in the heart. We observed a decrease in phenylalanyl-glutamine levels in the male EC CD36 KO group compared to the fl/fl CD36 mice. Phenylalanyl-glutamine, a dipeptide composed of

phenylalanine and glutamine, serves as an indicator of potential alterations in amino acid metabolism, likely influenced by the absence of EC CD36. Disruptions in the normal catabolism of phenylalanine, as seen in conditions like phenylketonuria, can result in the accumulation of phenylalanine and its metabolites, including phenylpyruvate, in the body.

According to the study by Lv *et al.* (264), phenylpyruvate can be taken up by macrophages through CD36, promoting a proinflammatory macrophage phenotype. CD36 knockdown in bone marrow-derived macrophages markedly decreased phenylpyruvate uptake. This mechanistic insight provides context for the observed decrease in phenylalanine levels in the male EC CD36 KO group. The interaction between phenylpyruvate and CD36, along with its downstream effects on NLRP3 inflammasome activation and inflammatory responses, establishes a connection in the context of macrophage function and inflammation. The observed decrease in glutamine levels in the male EC CD36 KO group suggests potential disruptions in glutamine metabolism. This alteration could, in turn, affect the regulatory role of glutamine in macrophage activation and the production of pro-inflammatory cytokines. Furthermore, another study demonstrated that mice with CD36 KO subjected to transverse aortic constriction exhibited reduced levels of glutamine.

Female EC CD36 KO mice exhibited elevated plasma threonine levels compared with the control group. Threonine, an essential amino acid, plays a crucial role in lipid metabolism, protein synthesis and changes in its levels may reflect shifts in protein turnover, catabolism, or other metabolic processes. Supplementing a HFD with threonine could potentially reduce lipid deposition through the regulation of the PPARγ signaling pathway (265). PPARγ is essential for adipocyte differentiation, lipid metabolism, and insulin sensitivity. It also governs gene networks related to glucose homeostasis, including the enhancement of glucose transporter type 4 expression (266). In another study, it was found that threonine levels are associated with a reduced risk of developing an atherogenic lipid profile and that there is a negative correlation between threonine levels and the concentrations of LDL as well as TGs (267). Consequently, the elevated threonine levels in EC CD36 KO females may influence metabolic pathways, potentially leading to improvements in glucose clearance and a decrease in TG levels, as observed in these mice.

Female EC CD36 KO mice also demonstrated a decrease in xanthurenic acid levels compared to the fl/fl CD36 group. Xanthurenic acid is a metabolite generated in the kynurenine pathway, which transforms tryptophan into diverse biologically active compounds. Activation of

this pathway is prompted by proinflammatory cytokines in different cell types, including ECs (268). Consequently, the reduced levels of this metabolite in the plasma of female EC CD36 knockout mice suggest a diminished inflammatory response, aligning with the observed characteristics in these mice.

We also observed a decrease in thrombosis time and Hb levels in both global and EC CD36 KO mice suggests a potential connection between the absence of CD36 and the vitamin K pathway. The alignment of thrombosis data with Hb levels indicates that CD36 KO mice experience reduced bleeding and lower Hb, implying an association with factors influenced by the vitamin K pathway. To explore this further, our metabolomic analyses revealed a decrease in menaquinol levels specifically in EC CD36 KO males. Menaquinol, the reduced form of vitamin K2 (menaquinone), is known to play a crucial role in the vitamin K pathway. In this pathway, menaquinol acts as an essential cofactor for the activation of certain vitamin K-dependent proteins. Therefore, the observed decrease in menaquinol levels in EC CD36 KO males suggests a disruption in the vitamin K pathway due to the absence of CD36. As menaquinol is a vital component for the activation of vitamin K-dependent proteins involved in various physiological functions, its reduction may contribute to the observed changes in thrombosis time and Hb levels. This intricate connection underscores the importance of CD36 in maintaining the proper functioning of the vitamin K pathway and its effects on blood clotting and Hb regulation.

5.5 Sex-Specific Metabolic Responses in EC CD36 KO Mice: Influence of Diet Composition Glucose Metabolism and Hormones

When fed a low-fat 4% NC diet, EC CD36 KO male mice displayed lower plasma glucose levels at 4 weeks with no difference in body weight or glucose clearance between the male and female mice and their respective sex-matched controls. The lower plasma glucose levels could be attributed to an enhanced dependence on carbohydrate metabolism. A similar pattern was noted in mice with global CD36 KO. When the mice were subjected to diets that contained a higher fat content than standard chow, several interesting findings emerged. At most of the time points studied, there were no noticeable differences in weight gain between the EC CD36 KO mice and the control group. However, females did display some transient differences in weight gain. In terms

of glucose metabolism, female EC CD36 KO mice consistently demonstrated faster clearance of a bolus of glucose when fed both the 10% and 45% fat diets. Conversely, male EC CD36 KO mice exhibited swifter glucose clearance than the control group, but this effect was only evident when they were fed the 45% fat diet. This metabolic profile corresponds with the understanding that, during episodes of overnutrition, the activation of pro-inflammatory signaling in macrophages, along with signals originating from adipocytes and increased FA uptake in muscle tissues, collectively contribute to the disruption of insulin signaling and the impairment of glucose tolerance (269) (Figure 46).

Enhanced glucose clearance by male EC CD36 KO mice may be attributed to their diminished ability to efficiently use FAs in both the heart and muscle, leading to an increased reliance on glucose as an energy source (Figure 46). A similar scenario may apply to females if they also exhibit decreased FA uptake in muscle. Interestingly, in female EC CD36 KO mice created using Tek cre, there was notable protection against IR, even though they maintained normal FA uptake in muscle (116). This intriguing observation suggests that CD36-dependent inflammation within ECs may play a role in activating systemic inflammatory pathways that ultimately contribute to the development of IR. Unraveling the mechanisms involved in this process represents an important avenue for future study and holds significant implications for understanding the intricate connections between CD36, EC inflammation, and systemic metabolic outcomes.

Furthermore, a recent study (270) has unveiled another dimension to CD36's role, demonstrating its involvement not only in glucose metabolism but also in regulating the circadian clock in the mouse liver. This study identifies CD36 as a potential regulator of the circadian rhythm of glucose metabolism, establishing a novel link between circadian patterns and glucose balance. They showed that the absence of CD36 in the liver disrupts the daily fluctuations in hepatic clock genes and mouse behaviors, further worsening the imbalance in glucose homeostasis. This dual role of CD36 in both circadian regulation and glucose metabolism underscores its importance in maintaining metabolic balance and highlights potential avenues for therapeutic interventions in metabolic disorders.

Moreover, linking CD36 to hormonal influences, estradiol, a type of estrogen, has been found to significantly impact CD36 expression and lipid metabolism. In a study conducted by Liu

et al. (271) the administration of estradiol yielded positive outcomes, including a decrease in body weight and reductions in serum levels of TGs, total and LDL-cholesterol following ovariectomy in rats. Notably, ovariectomy was linked to reduced expression of estrogen receptor 1 (ESR1), CD36, and PPARα. Importantly, the observed changes were reversed with estradiol treatment, indicating a potential inhibitory impact of estradiol on TG synthesis. This reversal suggests a potential enhancement in IR, possibly mediated through the ESR1-CD36-PPARα pathway in skeletal muscles. The collective insights from these studies underscore the intricate interplay involving CD36, hormonal influences, circadian rhythms, and metabolic regulation.

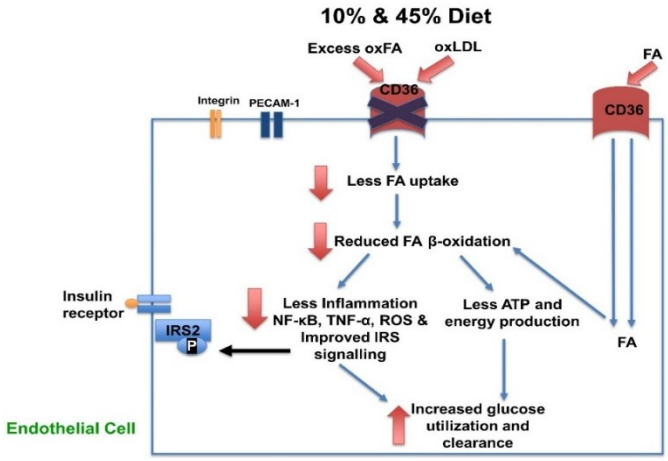

Figure 46: Glucose clearance dynamics in EC CD36 KO mice across varied dietary fat content. Absence of EC CD36 in the presence of HFD induced excess FA and oxFA contribute to diminished FA uptake, leading to decreased β-oxidation and ATP production. This shift results in an elevated dependence on glucose utilization for energy production. Moreover, reduced β-oxidation contributes to lower inflammation, minimizing disruptions in the insulin signaling pathway, thereby enhancing insulin sensitivity and improving glucose clearance.

5.6 Lipid Distribution Dynamics and Weight Regulation in EC CD36 KO Mice: Impact of Dietary Fat Content

When male EC CD36 KO mice and the control group were fed a diet containing 10 kcal% fat, there were no discernible differences in the distribution of cholesterol and triglycerides among

lipoproteins. However, in female mice with EC CD36 deficiency, there was a notable 23% increase in the enrichment of triglycerides, specifically within the LDL/IDL fraction. This suggests that the absence of CD36 in ECs may contribute to alterations in the distribution of specific lipid components (cholesterol, cholesteryl esters and TGs) in female mice, particularly in the LDL/IDL fraction, under conditions of specified dietary fat content.

When male and female EC CD36 KO mice were subjected to a 45% kcal fat diet, there was an observable shift in the distribution of TGs toward LDL/IDL, showing a 23% increase in males and a 40% increase in females. These findings suggest a delayed capacity to break down TG from the VLDL particles in response to HFD. This shift indicates potential alterations in lipid metabolism, particularly in the hydrolysis of VLDL-associated TGs. Furthermore, in the context of global CD36 KO mice, the investigation revealed that the increased levels of plasma free FAs acted as inhibitors of LPL activity. This inhibition consequently led to a notable reduction in the hydrolysis of VLDL particles (272).

The observed scenario suggests a potential mechanism in which the local concentration of free FAs at the EC interface could increase to levels that inhibit optimal hydrolysis. This increase in FA concentration may be attributed to the absence of EC CD36 and the slower uptake of FAs by the surrounding tissues. Consequently, this could impede the efficient hydrolysis of lipoproteins. Another alternative hypothesis posits that EC CD36 may play a crucial role in anchoring the lipoprotein, facilitating effective lipase activity. In the absence of this anchoring mechanism, the lipoprotein may not be optimally positioned for efficient hydrolysis by lipases. To gain a deeper understanding of the underlying mechanism and discern between these possibilities, further experiments are essential. These results collectively highlight the intricate role of CD36, particularly in ECs, in influencing lipid metabolism and the processing of lipoprotein particles, which may have implications for understanding cardiovascular health and metabolic responses to dietary challenges.

Our data indicate a consistent pattern of weight gain across all groups, regardless of the specific diets administered. This similarity in weight gain was also observed in EC CD36 KO mice generated with using Tek cre, where no discernible difference in white adipose tissue FA uptake was noted (116). In the global CD36 KO mouse model, there was an accumulation of TG-rich VLDL. This accumulation was attributed to inefficient hydrolysis of VLDL at both EC and tissue

surfaces (133). A plausible explanation for the lack of weight impact in the EC CD36 KO mice could be linked to the inefficiency of hydrolysis. Even though hydrolysis is inefficient, as the lipoprotein diminishes in size, it may have the ability to enter the subendothelial space and undergo hydrolysis at the level of individual tissues. The FAs liberated from this process are then taken up by adipocytes for storage. This mechanism may contribute to the observed weight neutrality in the EC CD36 KO mice. It may also be that weight gain is influenced by inflammation and since macrophages still express CD36, unlike in the global KO, they become activated, and this increases lipolysis which releases free FAs that can be taken up at the level of the tissues.

5.7 Interplay of EC CD36, Oxidative Stress, and Atherosclerosis Lesion Development: Insights from Diet-Induced Changes

To comprehend the intricate relationship between EC CD36, oxidative stress markers, and atherosclerosis, we initiated our investigation by considering the well-established role of activated endothelium by providing the surface in atherosclerotic lesion initiation (273). We were interested in understanding how atherosclerosis would unfold in the absence of EC CD36. This curiosity arises from the recognition that HFD contributes to the development of atherosclerosis (226), and that this process is, in part, mediated by alterations in shear stress and other pro-inflammatory pathways. CD36 functions as a pivotal receptor for pro-atherosclerotic-modified LDL ligands, often referred to as oxidized phosphatidylcholines (ox PC)-CD36 (81, 274). The recognition of these ligands is a consequence of the scavenger receptor activity of CD36. In macrophages, the interaction with these ligands triggers processes such as the generation of foam cells, the production of ROS, and the secretion of cytokines (81, 227, 274). While ECs do not accumulate lipids to form foam cells, it was considered that the interaction between EC CD36 and ox PC-CD36 might contribute to the initiation phase of atherosclerosis through inflammatory pathways.

To gain further insights into the underlying mechanisms, we explored oxidative stress markers, particularly 3-NT (a marker for peroxynitrite) which serves as an important indicator of inflammation, protein damage by nitration of tyrosine residues and NO production (275). The assessment of 3-NT levels using plasma from these mice revealed that at the 3-week diet time point, 3-NT levels were elevated in EC CD36 KO/LDLR KO mice compared with control mice.

This outcome was unexpected, as our hypothesis predicted lower levels of 3-NT in double KO mice. According to our hypothesis, ECs lacking CD36 were anticipated to exhibit reduced uptake of ox LDL and ox FA. This reduction in uptake was expected to result in less inflammation and decreased production of ROS, subsequently leading to a decrease in the NO production. The unexpected rise in 3-NT levels in EC CD36 KO/LDLR KO mice may result from compensatory mechanisms triggered by CD36 absence in ECs. The lack of CD36 might activate alternative inflammatory pathways, independent of ox LDL and FA uptake, leading to increased peroxynitrite production. This compensatory response may involve other scavenger receptors or intricate interactions between ECs, macrophages, and vascular components, contributing to the observed changes in inflammation and peroxynitrite production. The complex oxidative stress pathways in EC CD36 KO/LDLR KO mice may differ from the predicted reduction in inflammation based solely on CD36 absence. At the 6-week diet time point, there were no differences in 3-NT between the groups. The complexity of these findings suggests that the relationship between EC CD36, oxidative stress markers, and atherosclerosis may involve intricate and dynamic mechanisms that unfold over time.

For comprehensive understanding we performed atherosclerotic lesion analysis after 16 weeks of diet, a significant reduction in the aortic atherosclerosis burden was observed in EC CD36 KO/LDLR KO female mice. The 16-week time point was chosen to facilitate the development of atherosclerosis, because this is a commonly used time period in the scientific literature for *en face* analysis of the aorta. These findings deviate from the results obtained in global CD36 KO/LDLR KO, where protection against atherosclerosis was evident in both males and females (226). This implies a distinctive role of endothelial CD36 in the progression of atherosclerosis.

5.8 Metabolic and Atherogenic Profiles in Male and Female EC CD36 KO/LDLR KO Mice: Implications for Cardiovascular Risk

Female EC CD36 KO/LDLR KO mice displayed no significant differences in plasma cholesterol levels compared with the control group after 16 weeks of diet feeding. Additionally, no difference in weight was observed at 3, 6 or 16 weeks. Notably, the EC CD36 KO/LDLR KO mice demonstrated reduced fasting glucose levels, and GTT revealed a swifter glucose clearance in

comparison to the control mice. This distinctive trait was evident as early as the 3-week time point, coinciding with a decrease in plasma total and free cholesterol as well as TG levels in female EC CD36 KO/LDLR KO mice.

The persistent characteristic of enhanced glucose clearance remained a notable feature in female EC CD36 KO/LDLR KO mice. Nevertheless, discernible differences in cholesterol and TG levels were not identified at 6 and 16-weeks of diet feeding. However, upon lipoprotein analysis, it was found that female EC CD36 KO/LDLR KO mice displayed a 33% elevation in TG within LDL/IDL particles compared to the control group after 16 weeks of diet feeding. In contrast, male EC CD36 KO/LDLR KO mice displayed lipid profiles similar to those of the control group. The atherogenic diet, while sharing a similar fat content measured in kcal%, deviates from the 45 kcal% diet in terms of its fat source (milk fat instead of lard) and sucrose quantity (341 g/kg compared to 206 g/kg). Milk fat and lard exhibit distinct lipid compositions, with milk fat containing a greater proportion of saturated fats and lard featuring a higher proportion of monounsaturated fats. The FA profiles of these fats can affect lipid metabolism, thereby influencing cholesterol levels, atherosclerosis, and other factors related to cardiovascular risk. Additionally, diets rich in sucrose, may contribute to increased TG levels, a factor associated with heightened cardiovascular risk. (276).

In contrast to the 45 kcal% diet scenario, male EC CD36 KO/LDLR KO mice did not exhibit differences in GTT. This may contribute to the absence of protection against atherosclerosis observed in these mice. At 4 weeks of age, male EC CD36 KO mice showed systemic metabolic changes suggesting enhanced carbohydrate utilization, implying a potentially greater ability to resist the adverse effects of excess FAs, similar to that observed in global CD36 KO mice. However, the HFHC diet could have triggered a systemic inflammatory response greater than that in the global CD36 KO model, possibly due to macrophage expression of CD36 and its interaction with CD36 ligands. Further investigation is warranted to unravel the intricate interplay between dietary components, sex or sex hormones, and the metabolic and atherogenic distinctions uncovered in this context.

Atherosclerosis is a chronic inflammatory condition characterized by the gradual development of lesions in vasculature regions prone to atherogenesis. This process is initiated by the activation of the endothelium, which is triggered by the consumption of HFHC diets (12). In

the context of metabolic health, inflammation is implicated in the development of obesity and the emergence of dysfunctional fat. Additionally, it plays a role in inducing IR in the muscle, contributing to the overall risk of various health issues (277). In the case of female EC CD36 KO/LDLR KO mice, systemic metabolic distinctions were observed in comparison with the control group. Surprisingly, despite similar weight gain, these EC CD36 KO/LDLR KO female mice displayed a reduced burden of atherosclerotic lesions. An intriguing aspect for future studies lies in understanding the inflammatory characteristics of the ECs and adipose tissue in this specific genetic context.

5.9 The Diverse Impact of CD36 on ECs: From FA Uptake to Angiogenesis and Cardiac Metabolism

Apart from the impact of EC CD36 on tissue FA uptake, there is a possibility of direct effects of FAs on ECs. In a recent study conducted by Bou Khzam *et al.* (253), a knockdown approach was employed to reduce CD36 expression by approximately 50% in ECs derived from mouse lung and cardiomyocytes. Notably, the study reported no significant differences in terms of survival or proliferation in ECs following this reduction in CD36 expression. In experiments conducted in the presence of additional FAs, primarily oleic acid, it was observed that the knockdown of CD36 mitigated the FA-induced increases in the proliferation and migration of ECs. This assessment was performed using an *in vivo* scratch wound healing assay (253).

Furthermore, when ECs with reduced CD36 expression were treated with oleic acid, there was an approximately 8-fold increase in the expression of AMPK, an enzyme that serves as an indicator of cellular stress in ECs. In addition to the stress response, the cells exhibited a proangiogenic response, indicating a tendency to promote the formation of new blood vessels (253). The noteworthy aspect is that the effect of added oleic acid in the context of reduced (though not entirely absent) CD36 expression could potentially lead to an IR state in ECs. Excessive exposure to FAs and glucose has been demonstrated to reduce AMPK activity, thereby contributing to the development of IR (278) as shown in Figure 47. Similar to the observed phenomenon in individuals with diabetes, this state inhibits vessel formation even in the presence of pro-angiogenic signals.

Building on the role of CD36 in EC function, Bou Khzam *et al*. (253) used Tek cre EC CD36 KO mice and mouse heart ECs to demonstrate the crucial role of CD36 in promoting EC angiogenic migratory function. Despite the injury-induced rise in AMPK activity through phosphorylation, ECs were unable to overcome the anti-angiogenic effects of CD36 inhibition. Furthermore, the elevation of antiangiogenic VEGFβ and VEGFR1 may play a role in impeding the recovery of EC CD36 KO mice, providing support for the notion that increased VEGFβ levels hinder angiogenesis. In conjunction with these findings, various investigations have highlighted CD36's anti-angiogenic effects through thrombospondin-1 signaling, inducing apoptosis in normal ECs (63, 279). Moreover, CD36 has been shown to hinder the vascular endothelial growth factor receptor 2 pathway in ECs within tumor environments (280). These cumulative insights underscore the multifaceted nature of CD36's involvement in angiogenesis and its impact on key regulatory pathways in ECs.

In conditions of chronic cardiac diseases, notable changes frequently occur in energy metabolism, particularly in the heart's preferences for the uptake and utilization of FAs in comparison to glucose. A healthy heart typically relies on fatty acids as its primary source of energy. However, specific cardiac pathologies may induce a transition toward heightened dependence on glucose as an energy substrate. The lack of CD36 in ECs, typically responsible for facilitating the uptake of FAs, may potentially contribute to alterations in FA metabolism within the heart. Experimental models of cardiac disease have revealed that manipulating the presence of CD36 in the sarcolemma, the outer membrane of heart muscle cells can lead to the normalization of myocardial energy metabolism. This manipulation has been associated with improvements in, or restoration of, cardiac contractile function (281). This suggests that CD36 plays a crucial role in the metabolic changes observed in the context of chronic cardiac diseases and could be a potential target for therapeutic interventions aiming to restore normal energy metabolism and cardiac function.

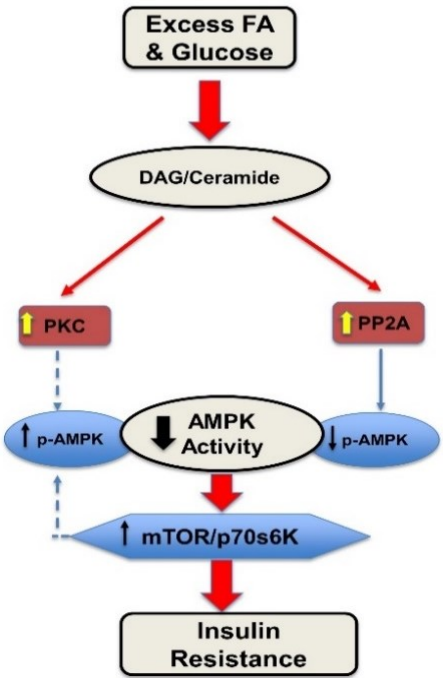

Figure 47: Mechanism showing excessive levels of FAs and glucose result in the suppression of AMPK, promoting IR. Elevated glucose levels lead to an increase in diacylglycerol (DAG), while FA raise both DAG and ceramide levels. This, in turn, enhances the activity of protein kinase C (PKC) and phosphatase (PP2A). PKC has the potential to phosphorylate AMPK, while PP2A dephosphorylates, hindering its functionality. The diminished activity of AMPK facilitates the activation of mTOR/p70S6K, subsequently contributing to IR.

5.10 Future Directions

Considering the future directions of this study, it is imperative to conduct additional research for several compelling reasons. Firstly, it is vital to explore the metabolic patterns in both male and female mice to ascertain the consistency of observed differences as they age. Moreover, recognizing the potential impact of sex hormones, including estrogen and testosterone, is crucial in this context. Therefore, gaining insights into how these hormones influence the expression of CD36 and the metabolism of FAs could provide valuable perspectives on the sex-specific variations identified in our study. This study will use a longitudinal design to examine the metabolic patterns in male and female EC CD36 KO mice over different life stages. Mice will be monitored from a young age to maturity to identify age-dependent changes. Hormonal assessments, including estrogen and testosterone levels, will be conducted to explore their impact on CD36 expression and fatty acid metabolism. Quantification of CD36 expression in ECs using techniques like immunohistochemistry will provide valuable insights. Hormone levels will be measured to understand their influence.

Another intriguing avenue for prospective research involves investigating the inflammatory characteristics of ECs and adipose tissue within this specific genetic context.

Additionally, a thorough analysis of plasma cytokines/chemokines is anticipated to yield deeper mechanistic insights into the protective mechanisms against lesion development. This exploration might also reveal potential distinctions between sexes in the manifestation of these metabolic responses. Additionally, assess the progression of atherosclerotic lesions in major arteries through imaging techniques like histological analysis or non-invasive modalities. Establish correlations between inflammatory markers and the advancement of lesions.

The future work will also encompass an examination of whether the metabolic patterns observed in the early stages persist as the mice age. The inquiry into the longevity of these patterns is essential, considering that the metabolic differences detected in young mice may persist, undergo change, or even disappear as the mice mature. Therefore, studying them longitudinally as they age will furnish valuable insights and contribute to a comprehensive understanding of the dynamics involved.

5.11 Limitations and Conclusion

Although our study yielded insightful results, there are several limitations that warrant consideration. An integral aspect in comprehending the involvement of EC CD36 in cardiovascular disease pertains to its role in the interactions between monocytes/macrophages and the vessel wall. The infiltration of monocytes/macrophages into the subendothelial space is a crucial step in the initiation and progression of atherosclerotic lesions (282). According to our hypothesis, EC CD36 serves as a major receptor for FA and proinflammatory ligands, influencing metabolic phenotypes and contributing to differences in atherosclerosis, suggesting alterations in EC inflammation and FA uptake. Therefore, conducting in vitro transmigration assays and histological analyses to investigate the interaction between EC and monocytes/macrophages is important. These experiments will not only support our hypothesis that proinflammatory ligands induced by a HFD play a role in EC inflammation but also substantiate changes in EC markers of activation. Moreover, since the heart primarily derives most of its energy from FA uptake and oxidation, and EC CD36 is essential for optimal delivery of long-chain fatty acids in cardiomyocytes from the circulation, another potential limitation is the lack of investigation into fatty acid uptake and its potential influence on changes in the heart.

Additionally, while the study provides a plausible explanation for the observed phenomenon, acknowledging the incomplete ruling out of insulin secretion differences highlights a potential gap in the understanding of the underlying mechanisms. Further investigation into insulin secretion may be necessary to comprehensively interpret the observed metabolic changes. The analysis of plasma cytokines/chemokines could have provided more profound mechanistic insights into the protective mechanisms against lesion development and revealed potential variations between sexes in the expression of these metabolic responses.

To summarize, in this study, we present findings that highlight metabolic variations aligned with a diminished capacity to hydrolyze and uptake FAs in the absence of EC CD36. This reduction in FA processing results in decreased FA oxidation and subsequently leads to a decline in energy generation. Our study corroborates previous research, emphasizing the essential role of EC CD36 in facilitating optimal FA uptake by the heart and muscles. The observed alterations in glucose tolerance testing and fasting glucose levels, while not affecting weight, align with the outcome of a prior study (116). Notably, our investigation reveals that the absence of EC CD36 contributes to a significant reduction in aortic atherosclerosis lesions, specifically in female mice. This cumulative evidence underscores the significant impact of EC CD36 on multiple facets of metabolism and cardiovascular health.

To the best of our knowledge, this study marks the first investigation into the effects of the absence of an EC-specific FAs transport protein on atherosclerosis. The obtained data indicate a sex-dependent influence of EC CD36 on lipid metabolism, potentially influencing IR and EC inflammation, thereby contributing to atherogenesis. These findings underscore the crucial role of the endothelium in regulating tissue FA uptake and emphasize the significance of EC CD36 in the development of atherosclerosis. The insights gleaned from this study provide valuable contributions to our understanding of the intricate interplay between EC CD36, lipid metabolism, and atherosclerotic processes.

References

1. Mensah GA, Roth GA, Fuster V. The Global Burden of Cardiovascular Diseases and Risk Factors: 2020 and Beyond. Journal of the American College of Cardiology. 2019;74(20):2529-32.
2. Benjamin EJ, Blaha MJ, Chiuve SE, Cushman M, Das SR, Deo R, et al. Heart Disease and Stroke Statistics-2017 Update: A Report From the American Heart Association. Circulation. 2017;135(10):e146-e603.
3. Tsao CW, Aday AW, Almarzooq ZI, Alonso A, Beaton AZ, Bittencourt MS, et al. Heart Disease and Stroke Statistics-2022 Update: A Report From the American Heart Association. Circulation. 2022;145(8):e153-e639.
4. Roth GA, Mensah GA, Johnson CO, Addolorato G, Ammirati E, Baddour LM, et al. Global Burden of Cardiovascular Diseases and Risk Factors, 1990-2019: Update From the GBD 2019 Study. Journal of the American College of Cardiology. 2020;76(25):2982-3021.
5. Lozano R, Naghavi M, Foreman K, Lim S, Shibuya K, Aboyans V, et al. Global and regional mortality from 235 causes of death for 20 age groups in 1990 and 2010: a systematic analysis for the Global Burden of Disease Study 2010. Lancet. 2012;380(9859):2095-128.
6. Luengo-Fernandez R, Walli-Attaei M, Gray A, Torbica A, Maggioni AP, Huculeci R, et al. Economic burden of cardiovascular diseases in the European Union: a population-based cost study. European heart journal. 2023;44(45):4752-67.
7. Ranjit N, Diez-Roux AV, Shea S, Cushman M, Seeman T, Jackson SA, et al. Psychosocial factors and inflammation in the multi-ethnic study of atherosclerosis. Archives of internal medicine. 2007;167(2):174-81.
8. Hossain E, Ota A, Karnan S, Takahashi M, Mannan SB, Konishi H, et al. Lipopolysaccharide augments the uptake of oxidized LDL by up-regulating lectin-like oxidized LDL receptor-1 in macrophages. Molecular and cellular biochemistry. 2015;400(1-2):29-40.
9. Kunjathoor VV, Febbraio M, Podrez EA, Moore KJ, Andersson L, Koehn S, et al. Scavenger receptors class A-I/II and CD36 are the principal receptors responsible for the uptake of modified low density lipoprotein leading to lipid loading in macrophages. The Journal of biological chemistry. 2002;277(51):49982-8.

10. Park YM. CD36, a scavenger receptor implicated in atherosclerosis. Experimental & molecular medicine. 2014;46(6):e99.
11. Hansson GK, Hermansson A. The immune system in atherosclerosis. Nature immunology. 2011;12(3):204-12.
12. Jebari-Benslaiman S, Galicia-Garcia U, Larrea-Sebal A, Olaetxea JR, Alloza I, Vandenbroeck K, et al. Pathophysiology of Atherosclerosis. International journal of molecular sciences. 2022;23(6).
13. Fruchart JC, Nierman MC, Stroes ES, Kastelein JJ, Duriez P. New risk factors for atherosclerosis and patient risk assessment. Circulation. 2004;109(23 Suppl 1):III15-9.
14. Libby P, Buring JE, Badimon L, Hansson GK, Deanfield J, Bittencourt MS, et al. Atherosclerosis. Nature reviews Disease primers. 2019;5(1):56.
15. Mahmood SS, Levy D, Vasan RS, Wang TJ. The Framingham Heart Study and the epidemiology of cardiovascular disease: a historical perspective. Lancet. 2014;383(9921):999-1008.
16. Rafieian-Kopaei M, Setorki M, Doudi M, Baradaran A, Nasri H. Atherosclerosis: process, indicators, risk factors and new hopes. International journal of preventive medicine. 2014;5(8):927-46.
17. The Lipid Research Clinics Coronary Primary Prevention Trial results. II. The relationship of reduction in incidence of coronary heart disease to cholesterol lowering. Jama. 1984;251(3):365-74.
18. Canner PL, Berge KG, Wenger NK, Stamler J, Friedman L, Prineas RJ, et al. Fifteen year mortality in Coronary Drug Project patients: long-term benefit with niacin. Journal of the American College of Cardiology. 1986;8(6):1245-55.
19. Gimbrone MA, Jr., Garcia-Cardena G. Endothelial Cell Dysfunction and the Pathobiology of Atherosclerosis. Circulation research. 2016;118(4):620-36.
20. Schulz E, Gori T, Munzel T. Oxidative stress and endothelial dysfunction in hypertension. Hypertension research : official journal of the Japanese Society of Hypertension. 2011;34(6):665-73.
21. Deanfield JE, Halcox JP, Rabelink TJ. Endothelial function and dysfunction: testing and clinical relevance. Circulation. 2007;115(10):1285-95.

22. Barton M, Haudenschild CC. Endothelium and atherogenesis: endothelial therapy revisited. Journal of cardiovascular pharmacology. 2001;38 Suppl 2:S23-5.
23. Okumura T, Jamieson GA. Platelet glycocalicin. I. Orientation of glycoproteins of the human platelet surface. The Journal of biological chemistry. 1976;251(19):5944-9.
24. Greenwalt DE, Watt KW, Hasler T, Howard RJ, Patel S. Structural, functional, and antigenic differences between bovine heart endothelial CD36 and human platelet CD36. The Journal of biological chemistry. 1990;265(27):16296-9.
25. Swerlick RA, Lee KH, Wick TM, Lawley TJ. Human dermal microvascular endothelial but not human umbilical vein endothelial cells express CD36 in vivo and in vitro. Journal of immunology. 1992;148(1):78-83.
26. Abumrad NA, el-Maghrabi MR, Amri EZ, Lopez E, Grimaldi PA. Cloning of a rat adipocyte membrane protein implicated in binding or transport of long-chain fatty acids that is induced during preadipocyte differentiation. Homology with human CD36. The Journal of biological chemistry. 1993;268(24):17665-8.
27. Van Nieuwenhoven FA, Verstijnen CP, Abumrad NA, Willemsen PH, Van Eys GJ, Van der Vusse GJ, et al. Putative membrane fatty acid translocase and cytoplasmic fatty acid-binding protein are co-expressed in rat heart and skeletal muscles. Biochemical and biophysical research communications. 1995;207(2):747-52.
28. Zhou J, Febbraio M, Wada T, Zhai Y, Kuruba R, He J, et al. Hepatic fatty acid transporter Cd36 is a common target of LXR, PXR, and PPARgamma in promoting steatosis. Gastroenterology. 2008;134(2):556-67.
29. Silverstein RL, Li W, Park YM, Rahaman SO. Mechanisms of cell signaling by the scavenger receptor CD36: implications in atherosclerosis and thrombosis. Transactions of the American Clinical and Climatological Association. 2010;121:206-20.
30. Calvo D, Dopazo J, Vega MA. The CD36, CLA-1 (CD36L1), and LIMPII (CD36L2) gene family: cellular distribution, chromosomal location, and genetic evolution. Genomics. 1995;25(1):100-6.
31. Glatz JF, Nabben M, Heather LC, Bonen A, Luiken JJ. Regulation of the subcellular trafficking of CD36, a major determinant of cardiac fatty acid utilization. Biochimica et biophysica acta. 2016;1861(10):1461-71.

32. Fernandez-Ruiz E, Armesilla AL, Sanchez-Madrid F, Vega MA. Gene encoding the collagen type I and thrombospondin receptor CD36 is located on chromosome 7q11.2. Genomics. 1993;17(3):759-61.

33. Glatz JFC, Heather LC, Luiken J. CD36 as a gatekeeper of myocardial lipid metabolism and therapeutic target for metabolic disease. Physiological reviews. 2023.

34. Rac ME, Safranow K, Poncyljusz W. Molecular basis of human CD36 gene mutations. Molecular medicine. 2007;13(5-6):288-96.

35. Glatz JFC, Luiken J. Dynamic role of the transmembrane glycoprotein CD36 (SR-B2) in cellular fatty acid uptake and utilization. Journal of lipid research. 2018;59(7):1084-93.

36. Hoosdally SJ, Andress EJ, Wooding C, Martin CA, Linton KJ. The Human Scavenger Receptor CD36: glycosylation status and its role in trafficking and function. The Journal of biological chemistry. 2009;284(24):16277-88.

37. Yang X, Okamura DM, Lu X, Chen Y, Moorhead J, Varghese Z, et al. CD36 in chronic kidney disease: novel insights and therapeutic opportunities. Nature reviews Nephrology. 2017;13(12):769-81.

38. Ding Z, Liu S, Wang X, Theus S, Deng X, Fan Y, et al. PCSK9 regulates expression of scavenger receptors and ox-LDL uptake in macrophages. Cardiovascular research. 2018;114(8):1145-53.

39. Jochen A, Hays J. Purification of the major substrate for palmitoylation in rat adipocytes: N-terminal homology with CD36 and evidence for cell surface acylation. Journal of lipid research. 1993;34(10):1783-92.

40. Pohl J, Ring A, Korkmaz U, Ehehalt R, Stremmel W. FAT/CD36-mediated long-chain fatty acid uptake in adipocytes requires plasma membrane rafts. Molecular biology of the cell. 2005;16(1):24-31.

41. Ring A, Le Lay S, Pohl J, Verkade P, Stremmel W. Caveolin-1 is required for fatty acid translocase (FAT/CD36) localization and function at the plasma membrane of mouse embryonic fibroblasts. Biochimica et biophysica acta. 2006;1761(4):416-23.

42. Calvo D, Gomez-Coronado D, Suarez Y, Lasuncion MA, Vega MA. Human CD36 is a high affinity receptor for the native lipoproteins HDL, LDL, and VLDL. Journal of lipid research. 1998;39(4):777-88.

43. Endemann G, Stanton LW, Madden KS, Bryant CM, White RT, Protter AA. CD36 is a receptor for oxidized low density lipoprotein. The Journal of biological chemistry. 1993;268(16):11811-6.
44. Liu J, Yang P, Zuo G, He S, Tan W, Zhang X, et al. Long-chain fatty acid activates hepatocytes through CD36 mediated oxidative stress. Lipids in health and disease. 2018;17(1):153.
45. Simantov R, Febbraio M, Silverstein RL. The antiangiogenic effect of thrombospondin-2 is mediated by CD36 and modulated by histidine-rich glycoprotein. Matrix biology : journal of the International Society for Matrix Biology. 2005;24(1):27-34.
46. Lee S, Eguchi A, Sakamoto K, Matsumura S, Tsuzuki S, Inoue K, et al. A role of CD36 in the perception of an oxidised phospholipid species in mice. Biomedical research. 2015;36(5):303-11.
47. Oquendo P, Hundt E, Lawler J, Seed B. CD36 directly mediates cytoadherence of Plasmodium falciparum parasitized erythrocytes. Cell. 1989;58(1):95-101.
48. Zhu W, Li W, Silverstein RL. Advanced glycation end products induce a prothrombotic phenotype in mice via interaction with platelet CD36. Blood. 2012;119(25):6136-44.
49. Coraci IS, Husemann J, Berman JW, Hulette C, Dufour JH, Campanella GK, et al. CD36, a class B scavenger receptor, is expressed on microglia in Alzheimer's disease brains and can mediate production of reactive oxygen species in response to beta-amyloid fibrils. The American journal of pathology. 2002;160(1):101-12.
50. Ren Y, Silverstein RL, Allen J, Savill J. CD36 gene transfer confers capacity for phagocytosis of cells undergoing apoptosis. The Journal of experimental medicine. 1995;181(5):1857-62.
51. Hsieh FL, Turner L, Bolla JR, Robinson CV, Lavstsen T, Higgins MK. The structural basis for CD36 binding by the malaria parasite. Nature communications. 2016;7:12837.
52. Neculai D, Schwake M, Ravichandran M, Zunke F, Collins RF, Peters J, et al. Structure of LIMP-2 provides functional insights with implications for SR-BI and CD36. Nature. 2013;504(7478):172-6.
53. Tarhda Z, Semlali O, Kettani A, Moussa A, Abumrad NA, Ibrahimi A. Three Dimensional Structure Prediction of Fatty Acid Binding Site on Human Transmembrane Receptor CD36. Bioinformatics and biology insights. 2013;7:369-73.

54. Samovski D, Sun J, Pietka T, Gross RW, Eckel RH, Su X, et al. Regulation of AMPK activation by CD36 links fatty acid uptake to beta-oxidation. Diabetes. 2015;64(2):353-9.

55. Neels JG, Grimaldi PA. Physiological functions of peroxisome proliferator-activated receptor beta. Physiological reviews. 2014;94(3):795-858.

56. Montaigne D, Butruille L, Staels B. PPAR control of metabolism and cardiovascular functions. Nature reviews Cardiology. 2021;18(12):809-23.

57. Stewart CR, Stuart LM, Wilkinson K, van Gils JM, Deng J, Halle A, et al. CD36 ligands promote sterile inflammation through assembly of a Toll-like receptor 4 and 6 heterodimer. Nature immunology. 2010;11(2):155-61.

58. Kennedy DJ, Chen Y, Huang W, Viterna J, Liu J, Westfall K, et al. CD36 and Na/K-ATPase-alpha1 form a proinflammatory signaling loop in kidney. Hypertension. 2013;61(1):216-24.

59. Pearce SF, Roy P, Nicholson AC, Hajjar DP, Febbraio M, Silverstein RL. Recombinant glutathione S-transferase/CD36 fusion proteins define an oxidized low density lipoprotein-binding domain. The Journal of biological chemistry. 1998;273(52):34875-81.

60. Nassir F, Wilson B, Han X, Gross RW, Abumrad NA. CD36 is important for fatty acid and cholesterol uptake by the proximal but not distal intestine. The Journal of biological chemistry. 2007;282(27):19493-501.

61. Kigerl KA, de Rivero Vaccari JP, Dietrich WD, Popovich PG, Keane RW. Pattern recognition receptors and central nervous system repair. Experimental neurology. 2014;258:5-16.

62. Garcia-Bonilla L, Sciortino R, Shahanoor Z, Racchumi G, Janakiraman M, Montaner J, et al. Role of microglial and endothelial CD36 in post-ischemic inflammasome activation and interleukin-1beta-induced endothelial activation. Brain, behavior, and immunity. 2021;95:489-501.

63. Febbraio M, Hajjar DP, Silverstein RL. CD36: a class B scavenger receptor involved in angiogenesis, atherosclerosis, inflammation, and lipid metabolism. The Journal of clinical investigation. 2001;108(6):785-91.

64. Chen Y, Zhang J, Cui W, Silverstein RL. CD36, a signaling receptor and fatty acid transporter that regulates immune cell metabolism and fate. The Journal of experimental medicine. 2022;219(6).

65. Silverstein RL, Febbraio M. CD36, a scavenger receptor involved in immunity, metabolism, angiogenesis, and behavior. Science signaling. 2009;2(72):re3.

66. Wang H, Franco F, Tsui YC, Xie X, Trefny MP, Zappasodi R, et al. CD36-mediated metabolic adaptation supports regulatory T cell survival and function in tumors. Nature immunology. 2020;21(3):298-308.
67. Muri J, Thut H, Bornkamm GW, Kopf M. B1 and Marginal Zone B Cells but Not Follicular B2 Cells Require Gpx4 to Prevent Lipid Peroxidation and Ferroptosis. Cell reports. 2019;29(9):2731-44 e4.
68. Feng WW, Wilkins O, Bang S, Ung M, Li J, An J, et al. CD36-Mediated Metabolic Rewiring of Breast Cancer Cells Promotes Resistance to HER2-Targeted Therapies. Cell reports. 2019;29(11):3405-20 e5.
69. Karunakaran U, Elumalai S, Moon JS, Won KC. CD36 Signal Transduction in Metabolic Diseases: Novel Insights and Therapeutic Targeting. Cells. 2021;10(7).
70. Zhao L, Li Y, Ding Q, Li Y, Chen Y, Ruan XZ. CD36 Senses Dietary Lipids and Regulates Lipids Homeostasis in the Intestine. Frontiers in physiology. 2021;12:669279.
71. Volkman A, Gowans JL. The Origin of Macrophages from Bone Marrow in the Rat. British journal of experimental pathology. 1965;46(1):62-70.
72. Chen S, Saeed A, Liu Q, Jiang Q, Xu H, Xiao GG, et al. Macrophages in immunoregulation and therapeutics. Signal transduction and targeted therapy. 2023;8(1):207.
73. Wynn TA, Chawla A, Pollard JW. Macrophage biology in development, homeostasis and disease. Nature. 2013;496(7446):445-55.
74. Wynn TA, Vannella KM. Macrophages in Tissue Repair, Regeneration, and Fibrosis. Immunity. 2016;44(3):450-62.
75. von Ehr A, Bode C, Hilgendorf I. Macrophages in Atheromatous Plaque Developmental Stages. Frontiers in cardiovascular medicine. 2022;9:865367.
76. Robbins CS, Hilgendorf I, Weber GF, Theurl I, Iwamoto Y, Figueiredo JL, et al. Local proliferation dominates lesional macrophage accumulation in atherosclerosis. Nature medicine. 2013;19(9):1166-72.
77. Zernecke A, Winkels H, Cochain C, Williams JW, Wolf D, Soehnlein O, et al. Meta-Analysis of Leukocyte Diversity in Atherosclerotic Mouse Aortas. Circulation research. 2020;127(3):402-26.

78. Hashimoto D, Chow A, Noizat C, Teo P, Beasley MB, Leboeuf M, et al. Tissue-resident macrophages self-maintain locally throughout adult life with minimal contribution from circulating monocytes. Immunity. 2013;38(4):792-804.
79. Rahman K, Vengrenyuk Y, Ramsey SA, Vila NR, Girgis NM, Liu J, et al. Inflammatory Ly6Chi monocytes and their conversion to M2 macrophages drive atherosclerosis regression. The Journal of clinical investigation. 2017;127(8):2904-15.
80. Chinetti-Gbaguidi G, Staels B. Macrophage polarization in metabolic disorders: functions and regulation. Current opinion in lipidology. 2011;22(5):365-72.
81. Podrez EA, Febbraio M, Sheibani N, Schmitt D, Silverstein RL, Hajjar DP, et al. Macrophage scavenger receptor CD36 is the major receptor for LDL modified by monocyte-generated reactive nitrogen species. The Journal of clinical investigation. 2000;105(8):1095-108.
82. Febbraio M, Podrez EA, Smith JD, Hajjar DP, Hazen SL, Hoff HF, et al. Targeted disruption of the class B scavenger receptor CD36 protects against atherosclerotic lesion development in mice. The Journal of clinical investigation. 2000;105(8):1049-56.
83. Bobryshev YV, Ivanova EA, Chistiakov DA, Nikiforov NG, Orekhov AN. Macrophages and Their Role in Atherosclerosis: Pathophysiology and Transcriptome Analysis. BioMed research international. 2016;2016:9582430.
84. Chistiakov DA, Bobryshev YV, Nikiforov NG, Elizova NV, Sobenin IA, Orekhov AN. Macrophage phenotypic plasticity in atherosclerosis: The associated features and the peculiarities of the expression of inflammatory genes. International journal of cardiology. 2015;184:436-45.
85. Orecchioni M, Ghosheh Y, Pramod AB, Ley K. Macrophage Polarization: Different Gene Signatures in M1(LPS+) vs. Classically and M2(LPS-) vs. Alternatively Activated Macrophages. Frontiers in immunology. 2019;10:1084.
86. Murray PJ. Macrophage Polarization. Annual review of physiology. 2017;79:541-66.
87. Zhao J, Ling L, Zhu W, Ying T, Yu T, Sun M, et al. M1/M2 re-polarization of kaempferol biomimetic NPs in anti-inflammatory therapy of atherosclerosis. Journal of controlled release : official journal of the Controlled Release Society. 2023;353:1068-83.
88. Arabpour M, Saghazadeh A, Rezaei N. Anti-inflammatory and M2 macrophage polarization-promoting effect of mesenchymal stem cell-derived exosomes. International immunopharmacology. 2021;97:107823.

89. Chen S, Yang J, Wei Y, Wei X. Epigenetic regulation of macrophages: from homeostasis maintenance to host defense. Cellular & molecular immunology. 2020;17(1):36-49.
90. Woo MS, Yang J, Beltran C, Cho S. Cell Surface CD36 Protein in Monocyte/Macrophage Contributes to Phagocytosis during the Resolution Phase of Ischemic Stroke in Mice. The Journal of biological chemistry. 2016;291(45):23654-61.
91. Pennathur S, Pasichnyk K, Bahrami NM, Zeng L, Febbraio M, Yamaguchi I, et al. The macrophage phagocytic receptor CD36 promotes fibrogenic pathways on removal of apoptotic cells during chronic kidney injury. The American journal of pathology. 2015;185(8):2232-45.
92. Raggi F, Pelassa S, Pierobon D, Penco F, Gattorno M, Novelli F, et al. Regulation of Human Macrophage M1-M2 Polarization Balance by Hypoxia and the Triggering Receptor Expressed on Myeloid Cells-1. Frontiers in immunology. 2017;8:1097.
93. Jetten N, Verbruggen S, Gijbels MJ, Post MJ, De Winther MP, Donners MM. Anti-inflammatory M2, but not pro-inflammatory M1 macrophages promote angiogenesis in vivo. Angiogenesis. 2014;17(1):109-18.
94. Shiratori H, Feinweber C, Luckhardt S, Linke B, Resch E, Geisslinger G, et al. THP-1 and human peripheral blood mononuclear cell-derived macrophages differ in their capacity to polarize in vitro. Molecular immunology. 2017;88:58-68.
95. Philipp D, Suhr L, Wahlers T, Choi YH, Paunel-Gorgulu A. Preconditioning of bone marrow-derived mesenchymal stem cells highly strengthens their potential to promote IL-6-dependent M2b polarization. Stem cell research & therapy. 2018;9(1):286.
96. Wang LX, Zhang SX, Wu HJ, Rong XL, Guo J. M2b macrophage polarization and its roles in diseases. Journal of leukocyte biology. 2019;106(2):345-58.
97. Shapouri-Moghaddam A, Mohammadian S, Vazini H, Taghadosi M, Esmaeili SA, Mardani F, et al. Macrophage plasticity, polarization, and function in health and disease. Journal of cellular physiology. 2018;233(9):6425-40.
98. Xie Y, Chen H, Qu P, Qiao X, Guo L, Liu L. Novel insight on the role of Macrophages in atherosclerosis: Focus on polarization, apoptosis and efferocytosis. International immunopharmacology. 2022;113(Pt A):109260.
99. Mushenkova NV, Nikiforov NG, Melnichenko AA, Kalmykov V, Shakhpazyan NK, Orekhova VA, et al. Functional Phenotypes of Intraplaque Macrophages and Their Distinct Roles in Atherosclerosis Development and Atheroinflammation. Biomedicines. 2022;10(2).

100. Kadl A, Meher AK, Sharma PR, Lee MY, Doran AC, Johnstone SR, et al. Identification of a novel macrophage phenotype that develops in response to atherogenic phospholipids via Nrf2. Circulation research. 2010;107(6):737-46.
101. Erbel C, Tyka M, Helmes CM, Akhavanpoor M, Rupp G, Domschke G, et al. CXCL4-induced plaque macrophages can be specifically identified by co-expression of MMP7+S100A8+ in vitro and in vivo. Innate immunity. 2015;21(3):255-65.
102. Gleissner CA, Shaked I, Little KM, Ley K. CXC chemokine ligand 4 induces a unique transcriptome in monocyte-derived macrophages. Journal of immunology. 2010;184(9):4810-8.
103. Gleissner CA, Shaked I, Erbel C, Bockler D, Katus HA, Ley K. CXCL4 downregulates the atheroprotective hemoglobin receptor CD163 in human macrophages. Circulation research. 2010;106(1):203-11.
104. Domschke G, Gleissner CA. CXCL4-induced macrophages in human atherosclerosis. Cytokine. 2019;122:154141.
105. Schonfeld P, Wojtczak L. Short- and medium-chain fatty acids in energy metabolism: the cellular perspective. Journal of lipid research. 2016;57(6):943-54.
106. Sassa T, Kihara A. Metabolism of very long-chain Fatty acids: genes and pathophysiology. Biomolecules & therapeutics. 2014;22(2):83-92.
107. Ghosh-Choudhary S, Liu J, Finkel T. Metabolic Regulation of Cell Fate and Function. Trends in cell biology. 2020;30(3):201-12.
108. Hubert M, Larsson E, Vegesna NVG, Ahnlund M, Johansson AI, Moodie LW, et al. Lipid accumulation controls the balance between surface connection and scission of caveolae. eLife. 2020;9.
109. Jacome-Sosa M, Miao ZF, Peche VS, Morris EF, Narendran R, Pietka KM, et al. CD36 maintains the gastric mucosa and associates with gastric disease. Communications biology. 2021;4(1):1247.
110. Carta G, Murru E, Banni S, Manca C. Palmitic Acid: Physiological Role, Metabolism and Nutritional Implications. Frontiers in physiology. 2017;8:902.
111. Stern JH, Rutkowski JM, Scherer PE. Adiponectin, Leptin, and Fatty Acids in the Maintenance of Metabolic Homeostasis through Adipose Tissue Crosstalk. Cell metabolism. 2016;23(5):770-84.

112. Goodpaster BH, Sparks LM. Metabolic Flexibility in Health and Disease. Cell metabolism. 2017;25(5):1027-36.
113. Abumrad NA, Goldberg IJ. CD36 actions in the heart: Lipids, calcium, inflammation, repair and more? Biochimica et biophysica acta. 2016;1861(10):1442-9.
114. Jang C, Oh SF, Wada S, Rowe GC, Liu L, Chan MC, et al. A branched-chain amino acid metabolite drives vascular fatty acid transport and causes insulin resistance. Nature medicine. 2016;22(4):421-6.
115. Bae H, Hong KY, Lee CK, Jang C, Lee SJ, Choe K, et al. Angiopoietin-2-integrin alpha5beta1 signaling enhances vascular fatty acid transport and prevents ectopic lipid-induced insulin resistance. Nature communications. 2020;11(1):2980.
116. Son NH, Basu D, Samovski D, Pietka TA, Peche VS, Willecke F, et al. Endothelial cell CD36 optimizes tissue fatty acid uptake. The Journal of clinical investigation. 2018;128(10):4329-42.
117. Beigneux AP, Davies BS, Gin P, Weinstein MM, Farber E, Qiao X, et al. Glycosylphosphatidylinositol-anchored high-density lipoprotein-binding protein 1 plays a critical role in the lipolytic processing of chylomicrons. Cell metabolism. 2007;5(4):279-91.
118. Kamp F, Hamilton JA. How fatty acids of different chain length enter and leave cells by free diffusion. Prostaglandins, leukotrienes, and essential fatty acids. 2006;75(3):149-59.
119. Hamilton JA, Kamp F. How are free fatty acids transported in membranes? Is it by proteins or by free diffusion through the lipids? Diabetes. 1999;48(12):2255-69.
120. Van der Vusse GJ, Glatz JF, Van Nieuwenhoven FA, Reneman RS, Bassingthwaighte JB. Transport of long-chain fatty acids across the muscular endothelium. Advances in experimental medicine and biology. 1998;441:181-91.
121. Ghosh A, Murugesan G, Chen K, Zhang L, Wang Q, Febbraio M, et al. Platelet CD36 surface expression levels affect functional responses to oxidized LDL and are associated with inheritance of specific genetic polymorphisms. Blood. 2011;117(23):6355-66.
122. Abumrad NA, Park JH, Park CR. Permeation of long-chain fatty acid into adipocytes. Kinetics, specificity, and evidence for involvement of a membrane protein. The Journal of biological chemistry. 1984;259(14):8945-53.
123. Hamilton JA, Guo W, Kamp F. Mechanism of cellular uptake of long-chain fatty acids: Do we need cellular proteins? Molecular and cellular biochemistry. 2002;239(1-2):17-23.

124. Kampf JP, Kleinfeld AM. Is membrane transport of FFA mediated by lipid, protein, or both? An unknown protein mediates free fatty acid transport across the adipocyte plasma membrane. Physiology. 2007;22:7-14.
125. Bonen A, Chabowski A, Luiken JJ, Glatz JF. Is membrane transport of FFA mediated by lipid, protein, or both? Mechanisms and regulation of protein-mediated cellular fatty acid uptake: molecular, biochemical, and physiological evidence. Physiology. 2007;22:15-29.
126. Kamp F, Hamilton JA, Kamp F, Westerhoff HV, Hamilton JA. Movement of fatty acids, fatty acid analogues, and bile acids across phospholipid bilayers. Biochemistry. 1993;32(41):11074-86.
127. Abumrad NA, Cabodevilla AG, Samovski D, Pietka T, Basu D, Goldberg IJ. Endothelial Cell Receptors in Tissue Lipid Uptake and Metabolism. Circulation research. 2021;128(3):433-50.
128. Cifarelli V, Abumrad NA. Intestinal CD36 and Other Key Proteins of Lipid Utilization: Role in Absorption and Gut Homeostasis. Comprehensive Physiology. 2018;8(2):493-507.
129. Bonen A, Parolin ML, Steinberg GR, Calles-Escandon J, Tandon NN, Glatz JF, et al. Triacylglycerol accumulation in human obesity and type 2 diabetes is associated with increased rates of skeletal muscle fatty acid transport and increased sarcolemmal FAT/CD36. FASEB journal : official publication of the Federation of American Societies for Experimental Biology. 2004;18(10):1144-6.
130. Hao JW, Wang J, Guo H, Zhao YY, Sun HH, Li YF, et al. CD36 facilitates fatty acid uptake by dynamic palmitoylation-regulated endocytosis. Nature communications. 2020;11(1):4765.
131. Bedford PG. Feline central retinal degeneration in the United Kingdom. The Veterinary record. 1983;112(19):456-7.
132. Chmurzynska A. The multigene family of fatty acid-binding proteins (FABPs): function, structure and polymorphism. Journal of applied genetics. 2006;47(1):39-48.
133. Febbraio M, Abumrad NA, Hajjar DP, Sharma K, Cheng W, Pearce SF, et al. A null mutation in murine CD36 reveals an important role in fatty acid and lipoprotein metabolism. The Journal of biological chemistry. 1999;274(27):19055-62.
134. Coburn CT, Knapp FF, Jr., Febbraio M, Beets AL, Silverstein RL, Abumrad NA. Defective uptake and utilization of long chain fatty acids in muscle and adipose tissues of CD36 knockout mice. The Journal of biological chemistry. 2000;275(42):32523-9.

135. Hajri T, Han XX, Bonen A, Abumrad NA. Defective fatty acid uptake modulates insulin responsiveness and metabolic responses to diet in CD36-null mice. The Journal of clinical investigation. 2002;109(10):1381-9.
136. Love-Gregory L, Sherva R, Sun L, Wasson J, Schappe T, Doria A, et al. Variants in the CD36 gene associate with the metabolic syndrome and high-density lipoprotein cholesterol. Human molecular genetics. 2008;17(11):1695-704.
137. Fukuchi K, Nozaki S, Yoshizumi T, Hasegawa S, Uehara T, Nakagawa T, et al. Enhanced myocardial glucose use in patients with a deficiency in long-chain fatty acid transport (CD36 deficiency). Journal of nuclear medicine : official publication, Society of Nuclear Medicine. 1999;40(2):239-43.
138. Harmon CM, Abumrad NA. Binding of sulfosuccinimidyl fatty acids to adipocyte membrane proteins: isolation and amino-terminal sequence of an 88-kD protein implicated in transport of long-chain fatty acids. The Journal of membrane biology. 1993;133(1):43-9.
139. Bartelt A, Bruns OT, Reimer R, Hohenberg H, Ittrich H, Peldschus K, et al. Brown adipose tissue activity controls triglyceride clearance. Nature medicine. 2011;17(2):200-5.
140. Bharadwaj KG, Hiyama Y, Hu Y, Huggins LA, Ramakrishnan R, Abumrad NA, et al. Chylomicron- and VLDL-derived lipids enter the heart through different pathways: in vivo evidence for receptor- and non-receptor-mediated fatty acid uptake. The Journal of biological chemistry. 2010;285(49):37976-86.
141. He C, Weston TA, Jung RS, Heizer P, Larsson M, Hu X, et al. NanoSIMS Analysis of Intravascular Lipolysis and Lipid Movement across Capillaries and into Cardiomyocytes. Cell metabolism. 2018;27(5):1055-66 e3.
142. Shu H, Peng Y, Hang W, Nie J, Zhou N, Wang DW. The role of CD36 in cardiovascular disease. Cardiovascular research. 2022;118(1):115-29.
143. Xu S, Jay A, Brunaldi K, Huang N, Hamilton JA. CD36 enhances fatty acid uptake by increasing the rate of intracellular esterification but not transport across the plasma membrane. Biochemistry. 2013;52(41):7254-61.
144. Glatz JF, Luiken JJ, Bonen A. Membrane fatty acid transporters as regulators of lipid metabolism: implications for metabolic disease. Physiological reviews. 2010;90(1):367-417.
145. Glatz JF, Storch J. Unravelling the significance of cellular fatty acid-binding proteins. Current opinion in lipidology. 2001;12(3):267-74.

146. Glatz JFC, Luiken J. Time for a detente in the war on the mechanism of cellular fatty acid uptake. Journal of lipid research. 2020;61(9):1300-3.
147. Ehehalt R, Fullekrug J, Pohl J, Ring A, Herrmann T, Stremmel W. Translocation of long chain fatty acids across the plasma membrane--lipid rafts and fatty acid transport proteins. Molecular and cellular biochemistry. 2006;284(1-2):135-40.
148. Mattern HM, Raikar LS, Hardin CD. The effect of caveolin-1 (Cav-1) on fatty acid uptake and CD36 localization and lipotoxicity in vascular smooth muscle (VSM) cells. International journal of physiology, pathophysiology and pharmacology. 2009;1(1):1-14.
149. Stenqvist J, Carlsson T, Winder M, Aronsson P. Effects of caveolae depletion and urothelial denudation on purinergic and cholinergic signaling in healthy and cyclophosphamide-induced cystitis in the rat bladder. Autonomic neuroscience : basic & clinical. 2018;213:60-70.
150. Daquinag AC, Gao Z, Fussell C, Immaraj L, Pasqualini R, Arap W, et al. Fatty acid mobilization from adipose tissue is mediated by CD36 posttranslational modifications and intracellular trafficking. JCI insight. 2021;6(17).
151. Peche VS, Pietka TA, Jacome-Sosa M, Samovski D, Palacios H, Chatterjee-Basu G, et al. Endothelial cell CD36 regulates membrane ceramide formation, exosome fatty acid transfer and circulating fatty acid levels. Nature communications. 2023;14(1):4029.
152. Pi X, Xie L, Patterson C. Emerging Roles of Vascular Endothelium in Metabolic Homeostasis. Circulation research. 2018;123(4):477-94.
153. Coppiello G, Collantes M, Sirerol-Piquer MS, Vandenwijngaert S, Schoors S, Swinnen M, et al. Meox2/Tcf15 heterodimers program the heart capillary endothelium for cardiac fatty acid uptake. Circulation. 2015;131(9):815-26.
154. Kalluri AS, Vellarikkal SK, Edelman ER, Nguyen L, Subramanian A, Ellinor PT, et al. Single-Cell Analysis of the Normal Mouse Aorta Reveals Functionally Distinct Endothelial Cell Populations. Circulation. 2019;140(2):147-63.
155. Kanda T, Brown JD, Orasanu G, Vogel S, Gonzalez FJ, Sartoretto J, et al. PPARgamma in the endothelium regulates metabolic responses to high-fat diet in mice. The Journal of clinical investigation. 2009;119(1):110-24.
156. Nagendran J, Pulinilkunnil T, Kienesberger PC, Sung MM, Fung D, Febbraio M, et al. Cardiomyocyte-specific ablation of CD36 improves post-ischemic functional recovery. Journal of molecular and cellular cardiology. 2013;63:180-8.

157. Hwang EH, Taki J, Yasue S, Fujimoto M, Taniguchi M, Matsunari I, et al. Absent myocardial iodine-123-BMIPP uptake and platelet/monocyte CD36 deficiency. Journal of nuclear medicine : official publication, Society of Nuclear Medicine. 1998;39(10):1681-4.
158. Tanaka T, Nakata T, Oka T, Ogawa T, Okamoto F, Kusaka Y, et al. Defect in human myocardial long-chain fatty acid uptake is caused by FAT/CD36 mutations. Journal of lipid research. 2001;42(5):751-9.
159. Hames KC, Vella A, Kemp BJ, Jensen MD. Free fatty acid uptake in humans with CD36 deficiency. Diabetes. 2014;63(11):3606-14.
160. Habets DD, Coumans WA, Voshol PJ, den Boer MA, Febbraio M, Bonen A, et al. AMPK-mediated increase in myocardial long-chain fatty acid uptake critically depends on sarcolemmal CD36. Biochemical and biophysical research communications. 2007;355(1):204-10.
161. Lother A, Bergemann S, Deng L, Moser M, Bode C, Hein L. Cardiac Endothelial Cell Transcriptome. Arteriosclerosis, thrombosis, and vascular biology. 2018;38(3):566-74.
162. Raheel H, Ghaffari S, Khosraviani N, Mintsopoulos V, Auyeung D, Wang C, et al. CD36 mediates albumin transcytosis by dermal but not lung microvascular endothelial cells: role in fatty acid delivery. American journal of physiology Lung cellular and molecular physiology. 2019;316(5):L740-L50.
163. Kasprzak JD, Klosinska M, Drozdz J. Clinical aspects of assessment of endothelial function. Pharmacological reports : PR. 2006;58 Suppl:33-40.
164. Bonetti PO, Lerman LO, Lerman A. Endothelial dysfunction: a marker of atherosclerotic risk. Arteriosclerosis, thrombosis, and vascular biology. 2003;23(2):168-75.
165. Mudau M, Genis A, Lochner A, Strijdom H. Endothelial dysfunction: the early predictor of atherosclerosis. Cardiovascular journal of Africa. 2012;23(4):222-31.
166. Tousoulis D, Simopoulou C, Papageorgiou N, Oikonomou E, Hatzis G, Siasos G, et al. Endothelial dysfunction in conduit arteries and in microcirculation. Novel therapeutic approaches. Pharmacology & therapeutics. 2014;144(3):253-67.
167. Gao X, Belmadani S, Picchi A, Xu X, Potter BJ, Tewari-Singh N, et al. Tumor necrosis factor-alpha induces endothelial dysfunction in Lepr(db) mice. Circulation. 2007;115(2):245-54.
168. Puranik R, Celermajer DS. Smoking and endothelial function. Progress in cardiovascular diseases. 2003;45(6):443-58.

169. Hsueh WA, Lyon CJ, Quinones MJ. Insulin resistance and the endothelium. The American journal of medicine. 2004;117(2):109-17.
170. Fain JN, Bahouth SW, Madan AK. TNFalpha release by the nonfat cells of human adipose tissue. International journal of obesity and related metabolic disorders : journal of the International Association for the Study of Obesity. 2004;28(4):616-22.
171. Katusic ZS. Mechanisms of endothelial dysfunction induced by aging: role of arginase I. Circulation research. 2007;101(7):640-1.
172. Park KH, Park WJ. Endothelial Dysfunction: Clinical Implications in Cardiovascular Disease and Therapeutic Approaches. Journal of Korean medical science. 2015;30(9):1213-25.
173. Cai H, Harrison DG. Endothelial dysfunction in cardiovascular diseases: the role of oxidant stress. Circulation research. 2000;87(10):840-4.
174. Singh VP, Bali A, Singh N, Jaggi AS. Advanced glycation end products and diabetic complications. The Korean journal of physiology & pharmacology : official journal of the Korean Physiological Society and the Korean Society of Pharmacology. 2014;18(1):1-14.
175. Avogaro A, de Kreutzenberg SV, Fadini G. Endothelial dysfunction: causes and consequences in patients with diabetes mellitus. Diabetes research and clinical practice. 2008;82 Suppl 2:S94-S101.
176. Fukushiro R, Ikeda M. [Dermatology and Behcet's disease]. Nihon rinsho Japanese journal of clinical medicine. 1968;26(1):38-46.
177. Mineo C, Deguchi H, Griffin JH, Shaul PW. Endothelial and antithrombotic actions of HDL. Circulation research. 2006;98(11):1352-64.
178. Drexler H, Hornig B. Endothelial dysfunction in human disease. Journal of molecular and cellular cardiology. 1999;31(1):51-60.
179. Yao YS, Li TD, Zeng ZH. Mechanisms underlying direct actions of hyperlipidemia on myocardium: an updated review. Lipids in health and disease. 2020;19(1):23.
180. Antoniades C, Shirodaria C, Leeson P, Antonopoulos A, Warrick N, Van-Assche T, et al. Association of plasma asymmetrical dimethylarginine (ADMA) with elevated vascular superoxide production and endothelial nitric oxide synthase uncoupling: implications for endothelial function in human atherosclerosis. European heart journal. 2009;30(9):1142-50.
181. Nigro P, Abe J, Berk BC. Flow shear stress and atherosclerosis: a matter of site specificity. Antioxidants & redox signaling. 2011;15(5):1405-14.

182. Hahn C, Schwartz MA. Mechanotransduction in vascular physiology and atherogenesis. Nature reviews Molecular cell biology. 2009;10(1):53-62.
183. Chatterjee S, Fisher AB. Mechanotransduction in the endothelium: role of membrane proteins and reactive oxygen species in sensing, transduction, and transmission of the signal with altered blood flow. Antioxidants & redox signaling. 2014;20(6):899-913.
184. Cahill PA, Redmond EM. Vascular endothelium - Gatekeeper of vessel health. Atherosclerosis. 2016;248:97-109.
185. Tabas I, Garcia-Cardena G, Owens GK. Recent insights into the cellular biology of atherosclerosis. The Journal of cell biology. 2015;209(1):13-22.
186. Garcia-Palmieri MR. The endothelium in health and in cardiovascular disease. Puerto Rico health sciences journal. 1997;16(2):136-41.
187. Gimbrone MA, Jr., Garcia-Cardena G. Vascular endothelium, hemodynamics, and the pathobiology of atherosclerosis. Cardiovascular pathology : the official journal of the Society for Cardiovascular Pathology. 2013;22(1):9-15.
188. Chen M, Masaki T, Sawamura T. LOX-1, the receptor for oxidized low-density lipoprotein identified from endothelial cells: implications in endothelial dysfunction and atherosclerosis. Pharmacology & therapeutics. 2002;95(1):89-100.
189. Soldatos G, Cooper ME, Jandeleit-Dahm KA. Advanced-glycation end products in insulin-resistant states. Current hypertension reports. 2005;7(2):96-102.
190. Chiu JJ, Chien S. Effects of disturbed flow on vascular endothelium: pathophysiological basis and clinical perspectives. Physiological reviews. 2011;91(1):327-87.
191. VanderLaan PA, Reardon CA, Getz GS. Site specificity of atherosclerosis: site-selective responses to atherosclerotic modulators. Arteriosclerosis, thrombosis, and vascular biology. 2004;24(1):12-22.
192. Feng S, Bowden N, Fragiadaki M, Souilhol C, Hsiao S, Mahmoud M, et al. Mechanical Activation of Hypoxia-Inducible Factor 1alpha Drives Endothelial Dysfunction at Atheroprone Sites. Arteriosclerosis, thrombosis, and vascular biology. 2017;37(11):2087-101.
193. Chistiakov DA, Melnichenko AA, Grechko AV, Myasoedova VA, Orekhov AN. Potential of anti-inflammatory agents for treatment of atherosclerosis. Experimental and molecular pathology. 2018;104(2):114-24.

194. Ramos CL, Huo Y, Jung U, Ghosh S, Manka DR, Sarembock IJ, et al. Direct demonstration of P-selectin- and VCAM-1-dependent mononuclear cell rolling in early atherosclerotic lesions of apolipoprotein E-deficient mice. Circulation research. 1999;84(11):1237-44.
195. Ley K, Laudanna C, Cybulsky MI, Nourshargh S. Getting to the site of inflammation: the leukocyte adhesion cascade updated. Nature reviews Immunology. 2007;7(9):678-89.
196. Campbell JJ, Qin S, Bacon KB, Mackay CR, Butcher EC. Biology of chemokine and classical chemoattractant receptors: differential requirements for adhesion-triggering versus chemotactic responses in lymphoid cells. The Journal of cell biology. 1996;134(1):255-66.
197. Campbell JJ, Hedrick J, Zlotnik A, Siani MA, Thompson DA, Butcher EC. Chemokines and the arrest of lymphocytes rolling under flow conditions. Science. 1998;279(5349):381-4.
198. Sozzani S, Molino M, Locati M, Luini W, Cerletti C, Vecchi A, et al. Receptor-activated calcium influx in human monocytes exposed to monocyte chemotactic protein-1 and related cytokines. Journal of immunology. 1993;150(4):1544-53.
199. Lin J, Kakkar V, Lu X. Impact of MCP-1 in atherosclerosis. Current pharmaceutical design. 2014;20(28):4580-8.
200. Libby P. Inflammation in atherosclerosis. Nature. 2002;420(6917):868-74.
201. Italiani P, Boraschi D. From Monocytes to M1/M2 Macrophages: Phenotypical vs. Functional Differentiation. Frontiers in immunology. 2014;5:514.
202. Flood C, Gustafsson M, Pitas RE, Arnaboldi L, Walzem RL, Boren J. Molecular mechanism for changes in proteoglycan binding on compositional changes of the core and the surface of low-density lipoprotein-containing human apolipoprotein B100. Arteriosclerosis, thrombosis, and vascular biology. 2004;24(3):564-70.
203. Kawamura M, Heinecke JW, Chait A. Pathophysiological concentrations of glucose promote oxidative modification of low density lipoprotein by a superoxide-dependent pathway. The Journal of clinical investigation. 1994;94(2):771-8.
204. Zamocky M, Jakopitsch C, Furtmuller PG, Dunand C, Obinger C. The peroxidase-cyclooxygenase superfamily: Reconstructed evolution of critical enzymes of the innate immune system. Proteins. 2008;72(2):589-605.
205. Delporte C, Van Antwerpen P, Vanhamme L, Roumeguere T, Zouaoui Boudjeltia K. Low-density lipoprotein modified by myeloperoxidase in inflammatory pathways and clinical studies. Mediators of inflammation. 2013;2013:971579.

206. Harrison JE, Schultz J. Studies on the chlorinating activity of myeloperoxidase. The Journal of biological chemistry. 1976;251(5):1371-4.
207. Hazen SL, Hsu FF, Mueller DM, Crowley JR, Heinecke JW. Human neutrophils employ chlorine gas as an oxidant during phagocytosis. The Journal of clinical investigation. 1996;98(6):1283-9.
208. Carr AC, McCall MR, Frei B. Oxidation of LDL by myeloperoxidase and reactive nitrogen species: reaction pathways and antioxidant protection. Arteriosclerosis, thrombosis, and vascular biology. 2000;20(7):1716-23.
209. Leeuwenburgh C, Hardy MM, Hazen SL, Wagner P, Oh-ishi S, Steinbrecher UP, et al. Reactive nitrogen intermediates promote low density lipoprotein oxidation in human atherosclerotic intima. The Journal of biological chemistry. 1997;272(3):1433-6.
210. Beckmann JS, Ye YZ, Anderson PG, Chen J, Accavitti MA, Tarpey MM, et al. Extensive nitration of protein tyrosines in human atherosclerosis detected by immunohistochemistry. Biological chemistry Hoppe-Seyler. 1994;375(2):81-8.
211. Hazen SL, Zhang R, Shen Z, Wu W, Podrez EA, MacPherson JC, et al. Formation of nitric oxide-derived oxidants by myeloperoxidase in monocytes: pathways for monocyte-mediated protein nitration and lipid peroxidation In vivo. Circulation research. 1999;85(10):950-8.
212. Podrez EA, Schmitt D, Hoff HF, Hazen SL. Myeloperoxidase-generated reactive nitrogen species convert LDL into an atherogenic form in vitro. The Journal of clinical investigation. 1999;103(11):1547-60.
213. Giacona MB, Papapanou PN, Lamster IB, Rong LL, D'Agati VD, Schmidt AM, et al. Porphyromonas gingivalis induces its uptake by human macrophages and promotes foam cell formation in vitro. FEMS microbiology letters. 2004;241(1):95-101.
214. Hajishengallis G, Darveau RP, Curtis MA. The keystone-pathogen hypothesis. Nature reviews Microbiology. 2012;10(10):717-25.
215. Desvarieux M, Demmer RT, Rundek T, Boden-Albala B, Jacobs DR, Jr., Papapanou PN, et al. Relationship between periodontal disease, tooth loss, and carotid artery plaque: the Oral Infections and Vascular Disease Epidemiology Study (INVEST). Stroke. 2003;34(9):2120-5.
216. Brown PM, Kennedy DJ, Morton RE, Febbraio M. CD36/SR-B2-TLR2 Dependent Pathways Enhance Porphyromonas gingivalis Mediated Atherosclerosis in the Ldlr KO Mouse Model. PloS one. 2015;10(5):e0125126.

217. Eskan MA, Benakanakere MR, Rose BG, Zhang P, Zhao J, Stathopoulou P, et al. Interleukin-1beta modulates proinflammatory cytokine production in human epithelial cells. Infection and immunity. 2008;76(5):2080-9.
218. Tedgui A, Mallat Z. Cytokines in atherosclerosis: pathogenic and regulatory pathways. Physiological reviews. 2006;86(2):515-81.
219. Liang DY, Liu F, Chen JX, He XL, Zhou YL, Ge BX, et al. Porphyromonas gingivalis infected macrophages upregulate CD36 expression via ERK/NF-kappaB pathway. Cellular signalling. 2016;28(9):1292-303.
220. Park YM, Febbraio M, Silverstein RL. CD36 modulates migration of mouse and human macrophages in response to oxidized LDL and may contribute to macrophage trapping in the arterial intima. The Journal of clinical investigation. 2009;119(1):136-45.
221. Park YM, Drazba JA, Vasanji A, Egelhoff T, Febbraio M, Silverstein RL. Oxidized LDL/CD36 interaction induces loss of cell polarity and inhibits macrophage locomotion. Molecular biology of the cell. 2012;23(16):3057-68.
222. Guy E, Kuchibhotla S, Silverstein R, Febbraio M. Continued inhibition of atherosclerotic lesion development in long term Western diet fed CD36o /apoEo mice. Atherosclerosis. 2007;192(1):123-30.
223. Jiang Y, Wang M, Huang K, Zhang Z, Shao N, Zhang Y, et al. Oxidized low-density lipoprotein induces secretion of interleukin-1beta by macrophages via reactive oxygen species-dependent NLRP3 inflammasome activation. Biochemical and biophysical research communications. 2012;425(2):121-6.
224. Crowther MA. Pathogenesis of atherosclerosis. Hematology American Society of Hematology Education Program. 2005:436-41.
225. Wali JA, Jarzebska N, Raubenheimer D, Simpson SJ, Rodionov RN, O'Sullivan JF. Cardio-Metabolic Effects of High-Fat Diets and Their Underlying Mechanisms-A Narrative Review. Nutrients. 2020;12(5).
226. Kennedy DJ, Kuchibhotla SD, Guy E, Park YM, Nimako G, Vanegas D, et al. Dietary cholesterol plays a role in CD36-mediated atherogenesis in LDLR-knockout mice. Arteriosclerosis, thrombosis, and vascular biology. 2009;29(10):1481-7.

227. Kennedy DJ, Kuchibhotla S, Westfall KM, Silverstein RL, Morton RE, Febbraio M. A CD36-dependent pathway enhances macrophage and adipose tissue inflammation and impairs insulin signalling. Cardiovascular research. 2011;89(3):604-13.
228. Nicholls HT, Kowalski G, Kennedy DJ, Risis S, Zaffino LA, Watson N, et al. Hematopoietic cell-restricted deletion of CD36 reduces high-fat diet-induced macrophage infiltration and improves insulin signaling in adipose tissue. Diabetes. 2011;60(4):1100-10.
229. Febbraio M, Guy E, Silverstein RL. Stem cell transplantation reveals that absence of macrophage CD36 is protective against atherosclerosis. Arteriosclerosis, thrombosis, and vascular biology. 2004;24(12):2333-8.
230. Dolan JM, Kolega J, Meng H. High wall shear stress and spatial gradients in vascular pathology: a review. Annals of biomedical engineering. 2013;41(7):1411-27.
231. Wong BW, Meredith A, Lin D, McManus BM. The biological role of inflammation in atherosclerosis. The Canadian journal of cardiology. 2012;28(6):631-41.
232. Lacroix S, Rosiers CD, Tardif JC, Nigam A. The role of oxidative stress in postprandial endothelial dysfunction. Nutrition research reviews. 2012;25(2):288-301.
233. Kano A, Wolfgang MJ, Gao Q, Jacoby J, Chai GX, Hansen W, et al. Endothelial cells require STAT3 for protection against endotoxin-induced inflammation. The Journal of experimental medicine. 2003;198(10):1517-25.
234. Yu M, Zhou H, Zhao J, Xiao N, Roychowdhury S, Schmitt D, et al. MyD88-dependent interplay between myeloid and endothelial cells in the initiation and progression of obesity-associated inflammatory diseases. The Journal of experimental medicine. 2014;211(5):887-907.
235. Biswas S, Gao D, Altemus JB, Rekhi UR, Chang E, Febbraio M, et al. Circulating CD36 is increased in hyperlipidemic mice: Cellular sources and triggers of release. Free radical biology & medicine. 2021;168:180-8.
236. Han S, Flattery AM, McLaren D, Raubertas R, Lee SH, Mendoza V, et al. Comparison of lipoprotein separation and lipid analysis methodologies for human and cynomolgus monkey plasma samples. Journal of cardiovascular translational research. 2012;5(1):75-83.
237. Marz W, Siekmeier R, Scharnagl H, Seiffert UB, Gross W. Fast lipoprotein chromatography: new method of analysis for plasma lipoproteins. Clinical chemistry. 1993;39(11 Pt 1):2276-81.

238. Mina AI, LeClair RA, LeClair KB, Cohen DE, Lantier L, Banks AS. CalR: A Web-Based Analysis Tool for Indirect Calorimetry Experiments. Cell metabolism. 2018;28(4):656-66 e1.
239. Wu Y, Li L. Determination of total concentration of chemically labeled metabolites as a means of metabolome sample normalization and sample loading optimization in mass spectrometry-based metabolomics. Analytical chemistry. 2012;84(24):10723-31.
240. Ma Y, Wang W, Zhang J, Lu Y, Wu W, Yan H, et al. Hyperlipidemia and atherosclerotic lesion development in Ldlr-deficient mice on a long-term high-fat diet. PloS one. 2012;7(4):e35835.
241. Huszar D, Varban ML, Rinninger F, Feeley R, Arai T, Fairchild-Huntress V, et al. Increased LDL cholesterol and atherosclerosis in LDL receptor-deficient mice with attenuated expression of scavenger receptor B1. Arteriosclerosis, thrombosis, and vascular biology. 2000;20(4):1068-73.
242. Basso F, Amar MJ, Wagner EM, Vaisman B, Paigen B, Santamarina-Fojo S, et al. Enhanced ABCG1 expression increases atherosclerosis in LDLr-KO mice on a western diet. Biochemical and biophysical research communications. 2006;351(2):398-404.
243. Lalla E, Lamster IB, Hofmann MA, Bucciarelli L, Jerud AP, Tucker S, et al. Oral infection with a periodontal pathogen accelerates early atherosclerosis in apolipoprotein E-null mice. Arteriosclerosis, thrombosis, and vascular biology. 2003;23(8):1405-11.
244. Geloen A, Helin L, Geeraert B, Malaud E, Holvoet P, Marguerie G. CD36 inhibitors reduce postprandial hypertriglyceridemia and protect against diabetic dyslipidemia and atherosclerosis. PloS one. 2012;7(5):e37633.
245. Catunda RQ, Ho KK, Patel S, Febbraio M. A 2-plane micro-computed tomographic alveolar bone measurement approach in mice. Imaging science in dentistry. 2021;51(4):389-98.
246. Moss JW, Ramji DP. Cytokines: roles in atherosclerosis disease progression and potential therapeutic targets. Future medicinal chemistry. 2016;8(11):1317-30.
247. Isoda K, Sawada S, Ishigami N, Matsuki T, Miyazaki K, Kusuhara M, et al. Lack of interleukin-1 receptor antagonist modulates plaque composition in apolipoprotein E-deficient mice. Arteriosclerosis, thrombosis, and vascular biology. 2004;24(6):1068-73.
248. Ringseis R, Eder K. Fatty acids and signalling in endothelial cells. Prostaglandins, leukotrienes, and essential fatty acids. 2010;82(4-6):189-98.

249. Yin Y, Li X, Sha X, Xi H, Li YF, Shao Y, et al. Early hyperlipidemia promotes endothelial activation via a caspase-1-sirtuin 1 pathway. Arteriosclerosis, thrombosis, and vascular biology. 2015;35(4):804-16.

250. McArthur MJ, Atshaves BP, Frolov A, Foxworth WD, Kier AB, Schroeder F. Cellular uptake and intracellular trafficking of long chain fatty acids. Journal of lipid research. 1999;40(8):1371-83.

251. Hajri T, Abumrad NA. Fatty acid transport across membranes: relevance to nutrition and metabolic pathology. Annual review of nutrition. 2002;22:383-415.

252. Glatz JFC, Nabben M, Luiken J. CD36 (SR-B2) as master regulator of cellular fatty acid homeostasis. Current opinion in lipidology. 2022;33(2):103-11.

253. Bou Khzam L, Son NH, Mullick AE, Abumrad NA, Goldberg IJ. Endothelial cell CD36 deficiency prevents normal angiogenesis and vascular repair. American journal of translational research. 2020;12(12):7737-61.

254. Mehrotra D, Wu J, Papangeli I, Chun HJ. Endothelium as a gatekeeper of fatty acid transport. Trends in endocrinology and metabolism: TEM. 2014;25(2):99-106.

255. Rekhi U, Piche JE, Immaraj L, Febbraio M. Neointimal hyperplasia: are fatty acid transport proteins a new therapeutic target? Current opinion in lipidology. 2019;30(5):377-82.

256. Iso T, Maeda K, Hanaoka H, Suga T, Goto K, Syamsunarno MR, et al. Capillary endothelial fatty acid binding proteins 4 and 5 play a critical role in fatty acid uptake in heart and skeletal muscle. Arteriosclerosis, thrombosis, and vascular biology. 2013;33(11):2549-57.

257. Hagberg CE, Falkevall A, Wang X, Larsson E, Huusko J, Nilsson I, et al. Vascular endothelial growth factor B controls endothelial fatty acid uptake. Nature. 2010;464(7290):917-21.

258. Chen K, Febbraio M, Li W, Silverstein RL. A specific CD36-dependent signaling pathway is required for platelet activation by oxidized low-density lipoprotein. Circulation research. 2008;102(12):1512-9.

259. Yang M, Silverstein RL. CD36 signaling in vascular redox stress. Free radical biology & medicine. 2019;136:159-71.

260. Cai L, Wang Z, Ji A, Meyer JM, van der Westhuyzen DR. Scavenger receptor CD36 expression contributes to adipose tissue inflammation and cell death in diet-induced obesity. PloS one. 2012;7(5):e36785.

261. Kuang M, Febbraio M, Wagg C, Lopaschuk GD, Dyck JR. Fatty acid translocase/CD36 deficiency does not energetically or functionally compromise hearts before or after ischemia. Circulation. 2004;109(12):1550-7.
262. Bonen A, Han XX, Habets DD, Febbraio M, Glatz JF, Luiken JJ. A null mutation in skeletal muscle FAT/CD36 reveals its essential role in insulin- and AICAR-stimulated fatty acid metabolism. American journal of physiology Endocrinology and metabolism. 2007;292(6):E1740-9.
263. Schroeder MA, Atherton HJ, Dodd MS, Lee P, Cochlin LE, Radda GK, et al. The cycling of acetyl-coenzyme A through acetylcarnitine buffers cardiac substrate supply: a hyperpolarized 13C magnetic resonance study. Circulation Cardiovascular imaging. 2012;5(2):201-9.
264. Lv D, Cao X, Zhong L, Dong Y, Xu Z, Rong Y, et al. Targeting phenylpyruvate restrains excessive NLRP3 inflammasome activation and pathological inflammation in diabetic wound healing. Cell reports Medicine. 2023;4(8):101129.
265. Ma Q, Zhou X, Sun Y, Hu L, Zhu J, Shao C, et al. Threonine, but Not Lysine and Methionine, Reduces Fat Accumulation by Regulating Lipid Metabolism in Obese Mice. Journal of agricultural and food chemistry. 2020;68(17):4876-83.
266. Ahmadian M, Suh JM, Hah N, Liddle C, Atkins AR, Downes M, et al. PPARgamma signaling and metabolism: the good, the bad and the future. Nature medicine. 2013;19(5):557-66.
267. Wang FH, Liu J, Deng QJ, Qi Y, Wang M, Wang Y, et al. Association between plasma essential amino acids and atherogenic lipid profile in a Chinese population: A cross-sectional study. Atherosclerosis. 2019;286:7-13.
268. Wang Y, Liu H, McKenzie G, Witting PK, Stasch JP, Hahn M, et al. Kynurenine is an endothelium-derived relaxing factor produced during inflammation. Nature medicine. 2010;16(3):279-85.
269. Zatterale F, Longo M, Naderi J, Raciti GA, Desiderio A, Miele C, et al. Chronic Adipose Tissue Inflammation Linking Obesity to Insulin Resistance and Type 2 Diabetes. Frontiers in physiology. 2019;10:1607.
270. Chen M, Zhang Y, Zeng S, Li D, You M, Zhang M, et al. CD36 regulates diurnal glucose metabolism and hepatic clock to maintain glucose homeostasis in mice. iScience. 2023;26(4):106524.

271. Liu Q, Li R, Chen G, Wang J, Hu B, Li C, et al. Inhibitory effect of 17beta-estradiol on triglyceride synthesis in skeletal muscle cells is dependent on ESR1 and not ESR2. Molecular medicine reports. 2019;19(6):5087-96.
272. Goudriaan JR, den Boer MA, Rensen PC, Febbraio M, Kuipers F, Romijn JA, et al. CD36 deficiency in mice impairs lipoprotein lipase-mediated triglyceride clearance. Journal of lipid research. 2005;46(10):2175-81.
273. Botts SR, Fish JE, Howe KL. Dysfunctional Vascular Endothelium as a Driver of Atherosclerosis: Emerging Insights Into Pathogenesis and Treatment. Frontiers in pharmacology. 2021;12:787541.
274. Podrez EA, Poliakov E, Shen Z, Zhang R, Deng Y, Sun M, et al. A novel family of atherogenic oxidized phospholipids promotes macrophage foam cell formation via the scavenger receptor CD36 and is enriched in atherosclerotic lesions. The Journal of biological chemistry. 2002;277(41):38517-23.
275. Bartesaghi S, Radi R. Fundamentals on the biochemistry of peroxynitrite and protein tyrosine nitration. Redox biology. 2018;14:618-25.
276. Rippe JM, Angelopoulos TJ. Relationship between Added Sugars Consumption and Chronic Disease Risk Factors: Current Understanding. Nutrients. 2016;8(11).
277. Ellulu MS, Patimah I, Khaza'ai H, Rahmat A, Abed Y. Obesity and inflammation: the linking mechanism and the complications. Archives of medical science : AMS. 2017;13(4):851-63.
278. Coughlan KA, Valentine RJ, Ruderman NB, Saha AK. Nutrient Excess in AMPK Downregulation and Insulin Resistance. Journal of endocrinology, diabetes & obesity. 2013;1(1):1008.
279. Armstrong LC, Bornstein P. Thrombospondins 1 and 2 function as inhibitors of angiogenesis. Matrix biology : journal of the International Society for Matrix Biology. 2003;22(1):63-71.
280. Wang J, Li Y. CD36 tango in cancer: signaling pathways and functions. Theranostics. 2019;9(17):4893-908.
281. Glatz JFC, Wang F, Nabben M, Luiken J. CD36 as a target for metabolic modulation therapy in cardiac disease. Expert opinion on therapeutic targets. 2021;25(5):393-400.

282. Ley K, Miller YI, Hedrick CC. Monocyte and macrophage dynamics during atherogenesis. Arteriosclerosis, thrombosis, and vascular biology. 2011;31(7):1506-16.